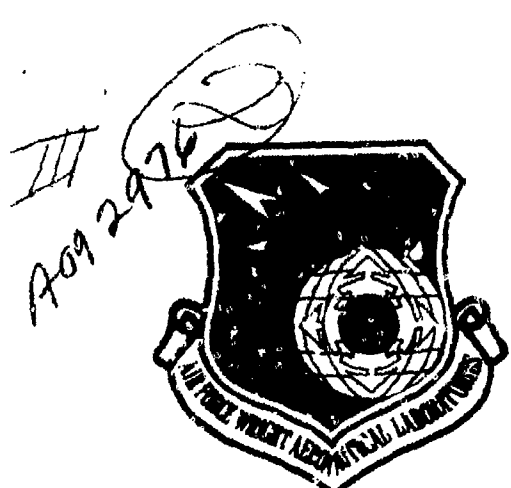


AD A092977

AFWAL-TR-80-3001,  
Volume II

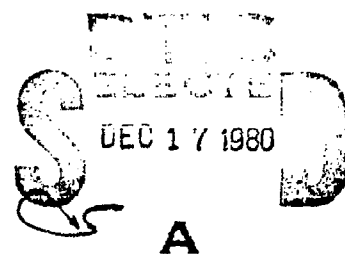


INVESTIGATION OF LASER SHOCK  
PROCESSING

BATTELLE'S COLUMBUS LABORATORIES  
505 KING AVENUE  
COLUMBUS, OHIO 43201

August 1980

TECHNICAL REPORT AFWAL-TR-80-3001, Vol. II  
FINAL REPORT JULY 1978-OCTOBER 1979



Approved for public release; distribution unlimited.

FLIGHT DYNAMICS LABORATORY  
AIR FORCE WRIGHT AERONAUTICAL LABORATORIES  
AIR FORCE SYSTEMS COMMAND  
WRIGHT-PATTERSON AIR FORCE BASE, OHIO 45433

DDC FILE COPY

80 12 17 039

## NOTICES

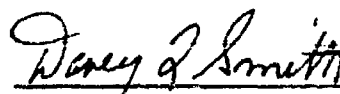
When Government drawings, specifications, or other data are used for any purpose other than in connection with a definitely related Government procurement operation, the United States Government thereby incurs no responsibility nor any obligation whatsoever; and the fact that the Government may have formulated, furnished, or in any way supplied the said drawings, specifications, or other data, is not to be regarded by implication or otherwise as in any manner licensing the holder or any other person or corporation, or conveying any rights or permission to manufacture, use, or sell any patented invention that may in any way be related thereto.

This report has been reviewed by the Information Office (OI) and is releasable to the National Technical Information Service (NTIS). At NTIS, it will be available to the general public, including foreign nations.

This technical report has been reviewed and is approved for publication.



FRANK D. ADAMS  
Project Engineer



DAVEY L. SMITH, Chief  
Structural Integrity Branch  
Structures and Dynamics Division

FOR THE COMMANDER



RALPH L. KUSTER, JR., Colonel, USAF  
Chief, Structures & Dynamics Division

"If your address has changed, if you wish to be removed from our mailing list, or if the addressee is no longer employed by your organization, please notify AFWL/FIBE, WPAFB, OH 45433 to help us maintain a current mailing list."

Copies of this report should not be returned unless return is required by security considerations, contractual obligations, or notice on a specific document.

SECURITY CLASSIFICATION OF THIS PAGE (When Data Entered)

19 REPORT DOCUMENTATION PAGE		READ INSTRUCTIONS BEFORE COMPLETING FORM	
1. REPORT NUMBER	2. GOVT ACCESSION NO.	3. RECIPIENT'S CATALOG NUMBER	
18) AFWAL TR-80-3001	VOL-24D-A092977		
4. TITLE (and Subtitle)		5. TYPE OF REPORT & PERIOD COVERED	
6) Investigation of Laser Shock Processing, Volume II.		9) FINAL REPORT Jul 1978 - Oct 1979	
7. AUTHOR(s)		8. CONTRACT OR GRANT NUMBER(s)	
10) S. C. Ford B. P. Fairand		15) F33615-78-C-3217	
9. PERFORMING ORGANIZATION NAME AND ADDRESS		10. PROGRAM ELEMENT, PROJECT, TASK AREA & WORK UNIT NUMBERS	
Battelle's Columbus Laboratories 505 King Avenue Columbus, Ohio 43201		Project No. 24010128	
11. CONTROLLING OFFICE NAME AND ADDRESS		12. REPORT DATE	
		12) August 1980	
		13. NUMBER OF PAGES	
		124	
14. MONITORING AGENCY NAME & ADDRESS (if different from Controlling Office)		15. SECURITY CLASS. (of this report)	
Flight Dynamics Laboratory (AFWAL/FIBE) AF Wright Aeronautical Laboratories, AFSC Wright-Patterson Air Force Base, Ohio 45433			
		15a. DECLASSIFICATION/DOWNGRADING SCHEDULE	
16. DISTRIBUTION STATEMENT (of this Report)			
Approved for public release; distribution unlimited.			
17. DISTRIBUTION STATEMENT (of the abstract entered in Block 20, if different from Report)			
18. SUPPLEMENTARY NOTES			
19. KEY WORDS (Continue on reverse side if necessary and identify by block number)			
laser shock processing fatigue improvement fastened joints fatigue crack growth			
20. ABSTRACT (Continue on reverse side if necessary and identify by block number)			
The objective of the program was to demonstrate that laser shock processing is a viable method of improving the fatigue and crack growth performance of mechanically fastened joints. It was shown that a decrease in crack growth rate can be achieved under specified conditions. These conditions involve compressive residual stress (induced by the process) which modify the crack shape and reduce the stress intensity factor. 2024-T3 aluminum alloy reacted (continued on next page)			

DD FORM 1 JAN 73 1473 EDITION OF 1 NOV 65 IS OBSOLETE

SECURITY CLASSIFICATION OF THIS PAGE (When Data Entered)

4101080

JOB

20. better to the process than 7075-T6 aluminum. Results were better in thin (.125 inch) than thick (.250 inch) material. Initial design environmental and cost studies indicate that a laser shock processing system for use on a production line is feasible.

## FOREWORD

The research reported herein was conducted by Battelle's Columbus Laboratories for the Air Force Flight Wright Aeronautical Laboratories, Wright-Patterson Air Force Base, Ohio. The work was performed under Contract No. F33615-78-C-3217 Project No. 2401 from July 1978 to October 1979. Dr. Frank D. Adams was the Air Force Program Director.

Contractor personnel contributing to the program were Mr. S. C. Ford, Program Manager and Co-principal Investigator, Dr. B. P. Fairand, Co-principal Investigator, Dr. A. H. Clauer, and Mr. R. D. Galliher. The program was centered in the Structural Materials and Tribology Section of the Transportation and Structures Department. Special thanks are extended to Dr. L. E. Hulbert for his assistance in the preparation of the final manuscript. This report was submitted by the authors on August 13, 1980.

*A*

# TABLE OF CONTENTS

	<u>Page</u>
FOREWORD . . . . .	111
SUMMARY. . . . .	ix
I INTRODUCTION . . . . .	1
1 Background . . . . .	1
2 Program Objective. . . . .	3
3 Program Activities . . . . .	3
4 Conclusions. . . . .	4
5 Recommendations. . . . .	5
6 Description of Report Organization . . . . .	5
II DESCRIPTION OF EXPERIMENTAL PROGRAM. . . . .	7
1 Specimen Configuration . . . . .	7
2 Laser Description. . . . .	12
3 Fatigue Test Description . . . . .	12
4 Residual Stress Measurements . . . . .	19
III DISCUSSION OF EXPERIMENTAL RESULTS . . . . .	25
1 Fatigue Results. . . . .	25
2 Residual Stresses. . . . .	39
3 Metallurgical Studies. . . . .	47
4 Fatigue-Crack Initiation . . . . .	58
5 Fatigue Crack Propagation. . . . .	62
6 Summary of Results . . . . .	63
APPENDIX A . . . . .	67
1 Detailed Listing of Test Results . . . . .	70
APPENDIX B . . . . .	96
1 Pulsed Laser Technology. . . . .	96
2 Laser Shock Processing Systems . . . . .	101
3 Environment Assessment . . . . .	114
REFERENCES . . . . .	124

# LIST OF ILLUSTRATIONS

		<u>Page</u>
Figure 1	The laser shock process. . . . .	2
2	Crack initiation/growth specimen (2 holes) . . . . .	8
3	Precracked crack initiation/growth specimen (2 holes). . .	9
4	Crack initiation/growth specimen (single hole) . . . . .	10
5	Low-load transfer fastened joint specimen. . . . .	11
6	Laser spot configurations. . . . .	13
7	FALSTAFF, Flight 130, flight-by-flight load spectrum . . .	21
8	The location of the numbered sites at which the residual stress measurements were made in the laser-treated region . . . . .	24
9	Matrix I fatigue test results. . . . .	27
10	Matrix II fatigue test results 7075-T6 aluminum specimens. .	30
11	Matrix II fatigue test results of the flight/flight load specimen . . . . .	31
12	Matrix II fatigue test results 2024-T3 aluminum specimens. .	33
13	Matrix IV fatigue test results . . . . .	35
14	Matrix III fatigue test results 40 ksi flight/flight load spectrum . . . . .	37
15	Matrix III fatigue test results 27 ksi flight/flight load spectrum . . . . .	38
16	The location of the numbered sites at which the residual stress measurements were made in the laser-treated region . . . . .	40
17	In-depth residual stress distribution at the sites shown in Figure 16 . . . . .	42
18	The distribution of surface residual stresses across the radius of the laser-shocked region . . . . .	44
19	Possible tensile stress distribution in the midthickness region of the shocked specimens. . . . .	46
20	Fracture surfaces including the crack initiation sites and propagation regions through the laser shocked zone .	49
21	Fracture surface river line patterns and crack front contours. . . . .	52
22	Transmission electron micrographs of the microstructure in specimens after failure . . . . .	57
23	Concentric laser shock spot. . . . .	59
24	Internal residual hoop stress profile for an element in the laser-treated region . . . . .	59

# LIST OF ILLUSTRATIONS (Continued)

		<u>Page</u>
Figure 25	Elemental slice through the compressive residual hoop stress zone . . . . .	60
26	Laser-shock effect on mean stress and stress amplitude . .	61
27	Stress-intensity solution for a center-notched panel of finite width . . . . .	63
28	Crack shape in laser-shocked specimen . . . . .	63
29	Embedded elliptical flaw stress-intensity solution . . . .	64
30	Embedded elliptical flaw aspect ratio effect . . . . .	65
31	Crack-growth rate trace through use of marker bands . . .	66
A-1	Laser spot configurations . . . . .	72
A-2	Matrix I fatigue test results . . . . .	89
A-3	Matrix II fatigue test results 7075-T6 aluminum specimens.	90
A-4	Matrix II fatigue test results 2024-T3 aluminum specimens.	91
A-5	Matrix II fatigue test results flight/flight load spectrum	92
A-6	Matrix III fatigue test results 40 ksi flight/flight load spectrum . . . . .	93
A-7	Matrix III fatigue test results 27 ksi flight/flight load spectrum . . . . .	94
A-8	Matrix IV fatigue test results . . . . .	95
B-1	Peak pressures for different overlays and laser power density conditions . . . . .	97
B-2	Comparison of computed and measured pressures water overlay - aluminum target . . . . .	98
B-3	Laser setup and water flow system . . . . .	100
B-4	30-nsec, 200-J neodymium-glass laser system . . . . .	106
B-5	30-nsec, 200-J iodine laser system . . . . .	108
B-6	Beam transport system . . . . .	113
B-7	Ozone concentration as a function of laser repetition rate (ozone confined to flashlamp enclosures) . . . . .	116
B-8	Ozone concentration as a function of laser repetition rate (uniform dilution in 100 ft. x 50 ft. x 10 ft. volume). . . . .	117
B-9	Toxicity of ozone . . . . .	118
B-10	Concentration of vaporized products as a function of laser repetition rate (material confined in interaction zone) . . . . .	121
B-11	Concentration of vaporized products as a function of laser repetition rate (uniform dilution in room) . . . .	122



# LIST OF TABLES

<u>Table</u>		<u>Page</u>
1	TEST MATRIX I - INVESTIGATION OF SHOCK PARAMETERS . . . . .	14
2	TEST MATRIX II - BASELINE CRACK INITIATION/GROWTH DATA MATRIX . . .	15
3	TEST MATRIX III - LOW-LOAD TRANSFER FASTENED-JOINT FATIGUE EXPERIMENTS . . . . .	17
4	TEST MATRIX IV - HIGH INTENSITY AND PLASTIC OVERLAY EXPERIMENTS . .	18
5	LOADS SELECTION . . . . .	20
6	SUMMARY OF RESIDUAL STRESS RESULTS BEFORE AND AFTER SHOCKING . . .	41
7	FRACTURE SURFACES EXAMINED BY SCANNING ELECTRON MICROSCOPY . . . .	48
8	SPECIMENS EXAMINED BY TRANSMISSION ELECTRON MICROSCOPY . . . . .	56
A-1	TEST MATRIX I - INVESTIGATION OF SHOCK PARAMETERS . . . . .	73
A-2	TEST MATRIX II - BASELINE CRACK INITIATION/GROWTH DATA MATRIX . . .	74
A-3	TEST MATRIX III - LOW-LOAD TRANSFER FASTENED JOINT FATIGUE EXPERIMENTS . . . . .	76
A-4	TEST MATRIX IV - HIGH INTENSITY AND PLASTIC OVERLAY EXPERIMENTS . .	77
A-5	INVESTIGATION OF SHOCK PARAMETERS (CRACK INITIATION/ GROWTH SPECIMENS) . . . . .	78
A-6	BASELINE CRACK INITIATION/GROWTH DATA MATRIX . . . . .	79
A-7	FASTENED JOINT FATIGUE SPECIMENS . . . . .	80
A-8	CRACK INITIATION/GROWTH AND RESIDUAL STRESS SPECIMENS (PROGRAM EXTENSION) . . . . .	81
A-9	INVESTIGATION OF SHOCK PARAMETERS FATIGUE TEST RESULTS, MATRIX I .	83
A-10	BASELINE CRACK INITIATION/GROWTH DATA MATRIX TEST RESULTS, MATRIX II . . . . .	85
A-11	FASTENED JOINT SPECIMEN FATIGUE TEST RESULTS, MATRIX III . . . . .	87
A-12	CRACK INITIATION/GROWTH TEST RESULTS (PROGRAM EXTENSION), MATRIX IV . . . . .	88
B-1	OPERATIONAL PARAMETERS FOR A 5-D-NANOSECOND-PULSEWIDTH, 200-J OUTPUT ENERGY ND-GLASS LASER SYSTEM . . . . .	107
B-2	OPERATIONAL PARAMETERS FOR A 30-NANOSECOND-PULSEWIDTH, 200-J OUTPUT ENERGY IODINE PHOTODISSOCIATION LASER SYSTEM . . . . .	109
B-3	NEODYMIUM-GLASS LASER COST-PER-SHOT ANALYSIS . . . . .	111
B-4	IODINE LASER COST PER SHOT ANALYSIS . . . . .	112

## SUMMARY

The objective of this program was to demonstrate that laser shock processing is a viable tool for increasing time to crack initiation, decreasing crack-growth rates, and improving the fatigue performance of mechanically fastened joints. This program was directed at obtaining crack initiation/growth data for unflawed and precracked specimens made from 7075 and 2024 aluminum alloys in two sheet thicknesses (0.125 and 0.250 inch). Tests were conducted using both constant-amplitude and modified FALSTAFF Flight 130 spectrum loads. In addition, low-load transfer fastened-joint specimens were tested under FALSTAFF loading. A preliminary design, cost, and environmental impact analysis was conducted for simulated production of laser shock systems. Also, fractographic and residual stress work to investigate the failure and mechanistic aspects of the process was complete.

Laser shock processing uses the radiation emitted by a high-power pulsed laser to generate a short-duration (less than 1 millionth of a second) high-amplitude pressure pulse at the surface of the material. It changes the metal's microstructure and stress state, which is the source of the observed improvements in material properties. Generation of the high-amplitude stress wave needed to improve the fatigue properties in aluminum alloys requires covering the surfaces to be shocked with a thin layer of black paint to enhance absorption of the laser radiation and protect the surface from melting and vaporization. A material which is transparent to laser light is placed on top of the black paint. The surface of the black paint is vaporized when it is struck by the laser radiation. The vaporized gas is trapped between the specimen surface and the transparent overlay. During further expansion, by absorbing heat from the laser beam, the pressure increases to extremely high levels causing a pressure pulse to react against the specimen surface and then travel through the metal in the form of a shock wave. The overlay acts to confine the vapor and enhance the amplitude and duration of the pressure pulse acting on the surface. The peak pressures generated at the surface of the aluminum targets are a function of the incident laser power density and the properties of the transparent overlay. The process takes place so rapidly, with vaporization so confined to a small layer, that no significant specimen heating occurs (as opposed to a continuous beam laser). Indeed, the process might well be described as ultra-high energy shot-peening.

Battelle's high power neodymium-glass laser was used in all of the laser shock experiments. This system, which consists of Q-switched oscillator, followed by six amplifier stages, delivers about 200 joules of laser energy. Water was used as the transparent overlay for this program.

Specimens were first laser shocked and then subjected to a constant amplitude or modified FALSTAFF flight spectrum loading. Specimens included plates of .125 or .250 inch thickness and low load transfer fastened joints. Some specimens were fatigued to develop fatigue cracks before being laser shocked.

Two aluminum alloys were investigated in the program (7075 and 2024). The results of the tests showed, in general, that fatigue life was not improved for 7075-T6 in the .250 inch thickness but was improved for the .125 inch thickness. However, the fatigue tests showed that the laser shock treatment significantly reduced crack-growth rate and dramatically increased the fatigue life in 2024-T3. The reason for the unexpected difference in the results for the two alloys appears to be because of the ability of the 2024 alloy to absorb higher levels of plastic strain. Evaluation of the data generated on the program raised several questions concerning the failure mechanisms and causes for differences in the appearance of failed surfaces. As a result, the effort was expanded to provide information on the failure mechanisms from a qualitative evaluation of the fracture surfaces and from residual stress measurements made in laser-shocked specimens. In addition, the effect of a different transparent overlay material and more intense laser shock conditions on enhancement of fatigue properties was investigated.

Because of Battelle's strong interest in the laser shock process and past commitment to its development, additional fastened-joint experiments were conducted at Battelle's expense to determine the improvement in fatigue life of 7075-T651 laser-treated specimens which were tested at a peak stress level less than that employed on the Air Force program. The lower stress level is representative of the stress environment experienced by cargo aircraft (the higher stress level used on the Air Force program may be considered more applicable to fighter aircraft). Results of the Battelle-supported experiments showed that the life of these laser-shocked 7075 specimens tested at the lower stress level was a factor of 2-3 greater than untreated specimens; whereas, the higher stress level tests had shown no improvement due to laser shocking. Some fastened joint tests were conducted with 7075; no data is available for the 2024 alloy.

One of the most revealing aspects of the program was the residual stress measurement results for the 7075 alloy. Extremely high compressive residual stresses are generated at the surface of a laser-shocked specimen. These stresses are balanced by tensile stresses in the midthickness of the specimen. If such tensile stresses occur at the edge of a hole in midthickness, then one would expect crack initiation to occur earlier than in the unshocked specimen which has no tensile residual stresses. Such could be the case for the particular laser shock conditions used in this program. Therefore, equivalent or extended crack-propagation life and time to failure for the shocked specimens implies that the crack-propagation rate for a laser-shocked zone is substantially reduced from that of a nonshocked zone. In fact, the data suggest that the crack-propagation rate is reduced by about one order of magnitude or more.

Study of the fracture surfaces revealed the probable cause for slower crack propagation. Crack initiation occurred near the midthickness of the specimen and grew normally until it approached the outer 30 to 50 thousandths of material thickness. At this position, the crack had to travel through a high compressive residual stress zone and it was very difficult for the crack front to penetrate that zone. As a result, the crack tended to tunnel and grow in an elliptical manner beneath the surface. The result of this forced constriction at the crack front would be to slow the crack propagation rate. By changing the laser shocking conditions to modify the distribution at the residual stresses, it could be possible to inhibit both crack initiation and crack propagation. This could have an even greater impact on the fatigue life after laser shocking.

There are some problem areas where must be dealt with prior to making this process routinely applicable to aerospace structures. A concern is the fact that the crack initiates early and propagates below the surface in a tunneling manner. Since the mechanism of the process is controlled by residual stresses, it is believed that there are a number of ways to retain the positive aspects of the process while preventing crack-growth rate in a subsurface manner. For example, an annular region around the hole could be laser shocked, excluding the edge of the fastener hole, thus leaving no residual tensile stresses at the edge of the hole in the midthickness. Or, one might investigate the feasibility of generating the compressive stresses at the midthickness with surface stresses being in a tension mode. In this case, cracks would initiate at the surface where they could be detected but

penetrate the midthickness only with difficulty, thereby significantly retarding the crack propagation rate. In addition, the possibility of treating the surface of the hole in addition to the surface of the sheet material should be investigated since by inducing beneficial compressive stresses at the surface of the fastener hole, crack initiation could be inhibited along the crack propagation. This could significantly improve fatigue life after laser shocking.

The major findings of the program may be detailed as follows:

- The presence of residual stresses caused by laser shock processing of aluminum alloys is expected to cause early initiation of cracks, but also causes a substantial reduction in crack growth rate due to crack configuration modification.
- The total life to failure is improved by nearly one order of magnitude for 2024 aluminum alloys.
- The total life to failure is not substantially affected by laser shocking for 0.250-inch-thick 7075 specimens.
- The presence of residual stresses provides a reduction in crack growth rate for thinner (0.125 inch) sections of 7075 material compared to thicker (0.250 inch) sections.
- Laser shocked 7075 aluminum specimens subjected to flight-by-flight spectrum loading showed a reduction in crack-growth rate (factor of 2 to 3) as compared to constant-amplitude tests. This is probably due to the number of low load levels in the flight spectrum.
- Low-load-transfer fastened-joint specimens of 7075 aluminum tested at 40 ksi maximum load in flight-by-flight conditions showed no improvement due to shocking but additional tests at a maximum load of 27 ksi showed a factor of 2 to 3 improvement due to shocking.
- An environmental assessment of the laser shocking system indicates that: ozone production will have to be controlled (probably by flowing nitrogen over the flash lamps), vaporized target material will have to be trapped and

carried away, and the sound of laser shocking will have to be absorbed.

- Preliminary design analysis shows a production laser shock processing system to be feasible.
- Cost analysis of preliminary designs of neodymium-glass and iodine lasers suggest a cost/shot range of \$0.065 to \$0.38 depending upon the system selected.

It is concluded that not all aluminum alloys are equally benefited by the laser shock parameters imposed in this program. However, a greater understanding of the mechanism of the laser shock process has been obtained, along with very encouraging results which show a substantial decrease in fatigue-crack-growth rate.

The understanding of the mechanism of the laser shock process provided by the residual stress and fracture studies provides some very positive conclusions concerning the results of this program. Since MIL-A-83444 (Airplane Damage Tolerance Requirements) requires aerospace design engineers to assume that a crack exists in all critically stressed structures, the existence of a process which provides orders of magnitude decrease in crack-growth rate is, indeed, a concept worthy of additional investigation and development. It is, therefore, recommended that investigatory work on this process and its application to aerospace structure be continued.

## I. INTRODUCTION

### 1. d

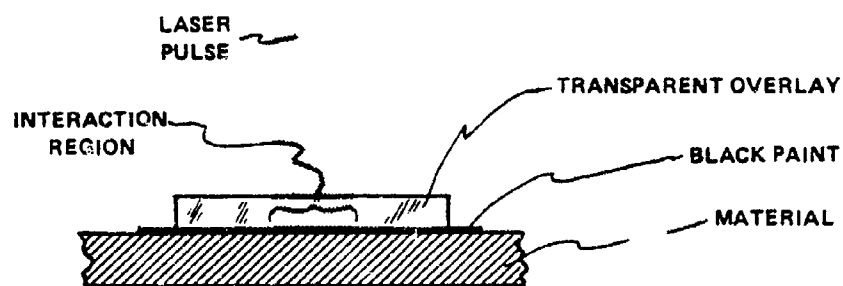
In the early 1970's, Battelle's Columbus Laboratories developed and began reporting upon a process for the improvement of material properties through the imposition of high-intensity, laser-induced shock waves.<sup>(1,2)\*</sup> During this early work it was shown that the yield strength and hardness of aluminum alloys were increased up to 30 percent after laser shocking, and weld zones in aluminum alloys could be strengthened to parent material values.<sup>(1,3)</sup> Metallurgical studies showed that laser-induced plasticity deformed the micro-structure of the treated alloys.<sup>(4)</sup>

The process itself consists of imposing a high energy laser pulse on the surface of a specimen. The specimen is prepared by coating the surface with a sacrificial layer, i.e., black paint, and that layer is subsequently coated with a transparent overlay such as quartz, water, or Mylar tape (see Figure 1). The laser pulse passes through the transparent overlay and is absorbed by the black paint. The black paint is vaporized causing an extremely high pressure near the surface. The vapor is confined by the transparent overlay and the high pressure causes an intense shock wave to travel through the specimen material.

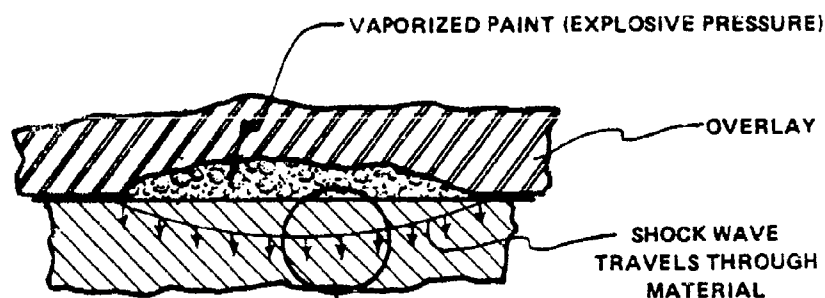
In 1977, investigatory work at Battelle showed that the fatigue life of fastened joint specimens could be improved by the use of this process. These preliminary tests were conducted using medium load transfer specimens wherein the failure mode was that of fretting initiated fatigue. However, laser-shocked specimens withstood considerably more fatigue cycles and required higher loads to generate failures than the unshocked specimens. The failures of the shocked specimens were still fretting fatigue initiated, but the laser shock evidently had significantly inhibited crack initiation or propagation. In addition, some preliminary work was done with sheet-type specimens studying crack initiation/propagation, wherein it appeared that the laser

---

\* References are listed on page 124.



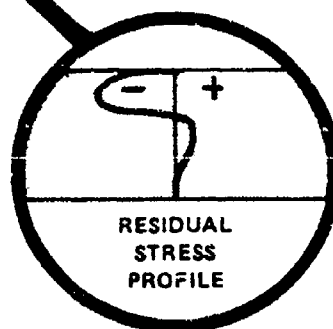
a. Laser shocking setup



HARDNESS INCREASES

YIELD STRENGTH INCREASES

MICROSTRUCTURE SHOWS HIGH DISLOCATION DENSITY



b. Schematic of the vaporization and pressure reactions at the metal surface during laser irradiation

Figure 1. The laser shock process



shock process substantially reduced both of these properties.

As a result of these promising results, the Air Force chose to further investigate this phenomena and contracted with the original developer of the process (Battelle) in the fall of 1978. The program was directed by Dr. Frank D. Adams of the Fatigue, Fracture and Reliability Group, U.S. Air Force Flight Dynamics Laboratory. Because of Battelle's strong interest in the laser shock process and past commitment to its development, additional fastened joint experiments were conducted to support this program.

## 2. Program Objective

The objective of this program was to demonstrate that laser shock processing is a viable tool for increasing time to crack initiation, decreasing crack-growth rates, and improving the fatigue performance of mechanically fastened joints. The program approach involved laser shocking critical areas in various fastened joint and crack initiation/propagation specimens made of 7075-T651 and 2024-T3 aluminum alloys. Laser shocking parameters were also varied to investigate the effects of processing variables on crack initiation/propagation behavior.

## 3. Program Activities

The program basically dealt with two types of activities; namely, experimental and analytical. The experimental program is briefly described as follows:

- Thin plate specimens were exposed to laser shocks from one or both sides and then fatigue tested using constant or variable spectrum loads at one of several stress levels.
- Two types of specimens were used. They were either dog-bone fastened joint specimens or sheet type crack initiation/propagation specimens.
- The crack initiation/propagation specimens were tested either in the unflawed or precracked conditions.
- Specimens of two differing sheet thickness were studied to evaluate thickness effects.

- Two aluminum alloys were tested; 7075-T6 and 2024-T3.
- Residual stresses in several specimens were measured experimentally.
- Post-test, fractographic analyses were made of selected failure surfaces.
- Laser spot size and power variations were investigated.

The analytical portion of the program contained the following tasks:

- Crack initiation/growth studies were conducted for various residual stress states.
- Laser safety and environmental considerations were studied.
- Laser system and cost analyses were conducted.

#### 4. Conclusions

The following conclusions can be drawn from the investigation reported herein:

- The presence of residual stresses caused by laser shock processing of aluminum alloys is expected to cause early initiation of cracks, but also causes a substantial reduction in crack growth rate due to crack configuration modification.
- The total life to failure is improved by nearly one order of magnitude for 2024 aluminum alloys.
- The total life to failure is not substantially affected by laser shocking for 0.250-inch-thick 7075 specimens.
- The presence of residual stresses provides a reduction in crack growth rate for thinner (0.125 inch) sections of 7075 material compared to thicker (0.250 inch) sections.
- Laser shocked 7075 aluminum specimens subjected to flight-by-flight spectrum loading showed a reduction in crack-growth rate (factor of 2 to 3) as compared to constant-amplitude tests. This is probably due to the number of low load levels in the flight spectrum.
- Low-load-transfer fastened-joint specimens of 7075 aluminum tested at 40 ksi maximum load in flight-by-flight conditions showed no improvement due to shocking but additional tests

at a maximum load of 27 ksi showed a factor of 2 to 3 improvement due to shocking.

- An environmental assessment of the laser shocking system indicates that: ozone production will have to be controlled (probably by flowing nitrogen over the flash lamps), vaporized target material will have to be trapped and carried away, and the sound of laser shocking will have to be absorbed.
- Preliminary design analysis shows a production laser shock processing system to be feasible.
- Cost analysis of preliminary designs of neodymium-glass and iodine lasers suggest a cost/shot range of \$0.065 to \$0.38 depending upon the system selected.

## 5. Recommendations

As is apparent from the above, a greater understanding of the mechanism of the laser shock process has been obtained along with positive results which in a number of instances showed a substantial decrease in fatigue crack growth rate. It is, therefore, recommended that investigatory work on this process for applicable aerospace structures be continued. In particular, study should be directed towards the improvement of laser shock geometries with the objective of providing controlled and more beneficial residual stresses. In addition, efforts should be directed towards developing a more production-oriented transparent overlay and enhancing power density capabilities in order to provide greater enhancement for 7075 aluminum alloys.

## 6. Description of Report Organization

The report is organized in three major sections. This introduction is followed by the description of the experimental program which includes specimen configurations, laser setup, fatigue test descriptions and residual stress measurements. The descriptive section is followed by a discussion of results of the fatigue results, residual stress measurements, metallurgical studies, fatigue-crack-initiation and fatigue-crack-propagation analyses, and

a summary. These sections are followed by two appendices. The first deals with detailed test results and contains an introduction, a discussion of laser shock parameters, and fatigue test results. The second appendix is a detailed presentation of the laser shock process. It contains a discussion of the process itself, an analysis of processing systems, and an environmental assessment.

## II. DESCRIPTION OF EXPERIMENTAL PROGRAM

### 1. Specimen Configurations

Battelle's fatigue test laboratory tested 110 fatigue specimens using closed-loop electrohydraulic servo-controlled fatigue machines and, where appropriate, computer-generated and controlled flight-by-flight spectra loads. Specimens were prepared from 7075-T651 and 2024-T3 aluminum alloys in order to provide a direct comparison to previous Air Force-funded investigation.<sup>(5)</sup> Specimens consisted of 72 circular notched crack initiation/growth specimens and 29 low-load transfer fastened joint specimens.

#### a. Circular Notched Crack Initiation/Growth Specimens

Specimen configurations for the circular notched crack initiation/growth specimens are presented in Figures 2, 3, and 4. A majority of the specimens were of the double initial flaw design allowing crack initiation and crack growth data to be obtained for two flaws simultaneously.

#### b. Low-Load Transfer Fastened Joint Specimens

The low-load transfer fastened joint specimens presented in Figure 5 were made in accordance with Figure 6, MIL-STD-1312, Test Method 21, using the nominal fastener diameter size of 1/4 inch. Each specimen consisted of two dogbone specimens made out of 7075-T651 aluminum and were supplied by the Air Force. The two pieces were ray surface primed, drilled and reamed, then assembled using flush shear head steel HiLok fasteners in  $0.001 \pm 0.0005$ -inch interference.

#### c. Residual Stress Specimens

Specimens for residual stress measurements were cut from 0.25-inch thick 7075-T651 material. They were nominally 4 x 4-inch squares.

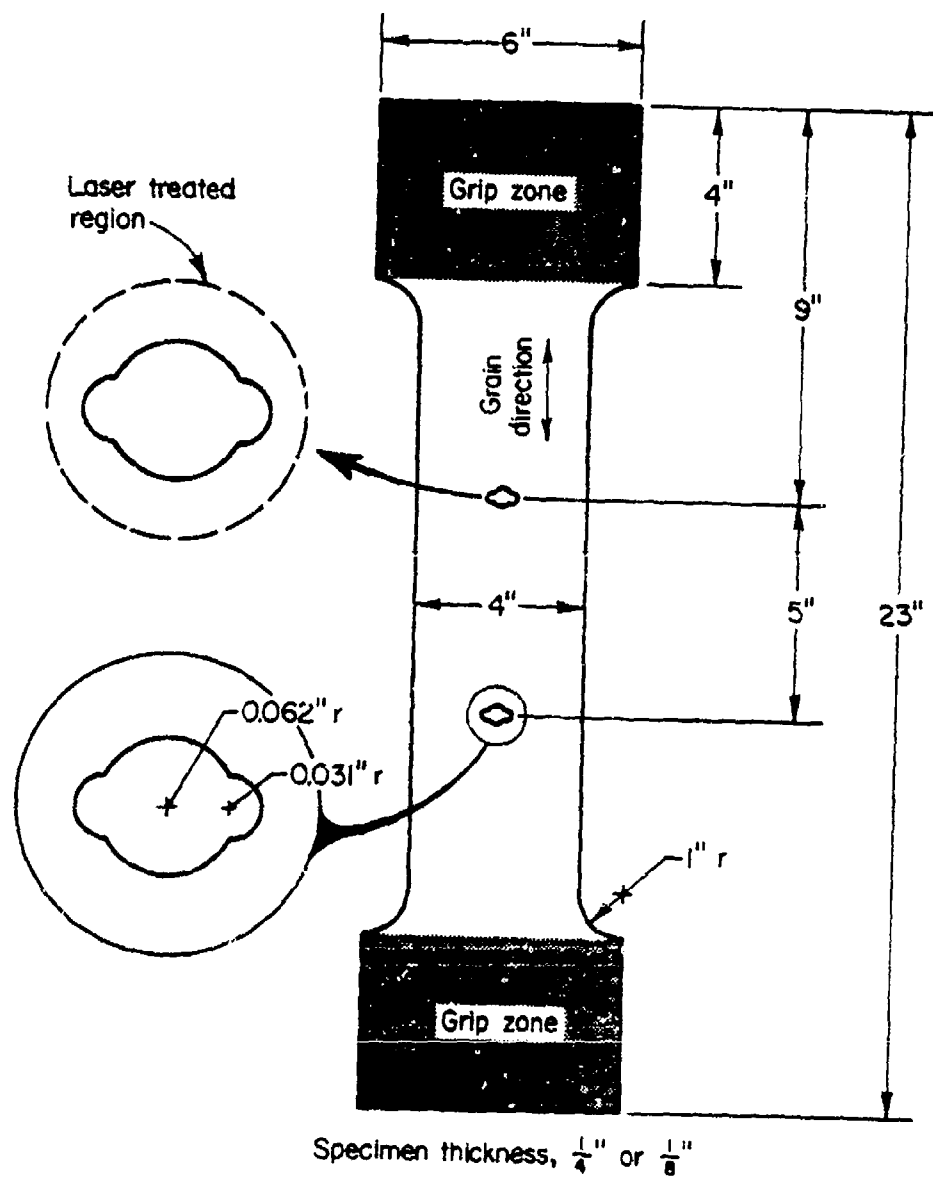
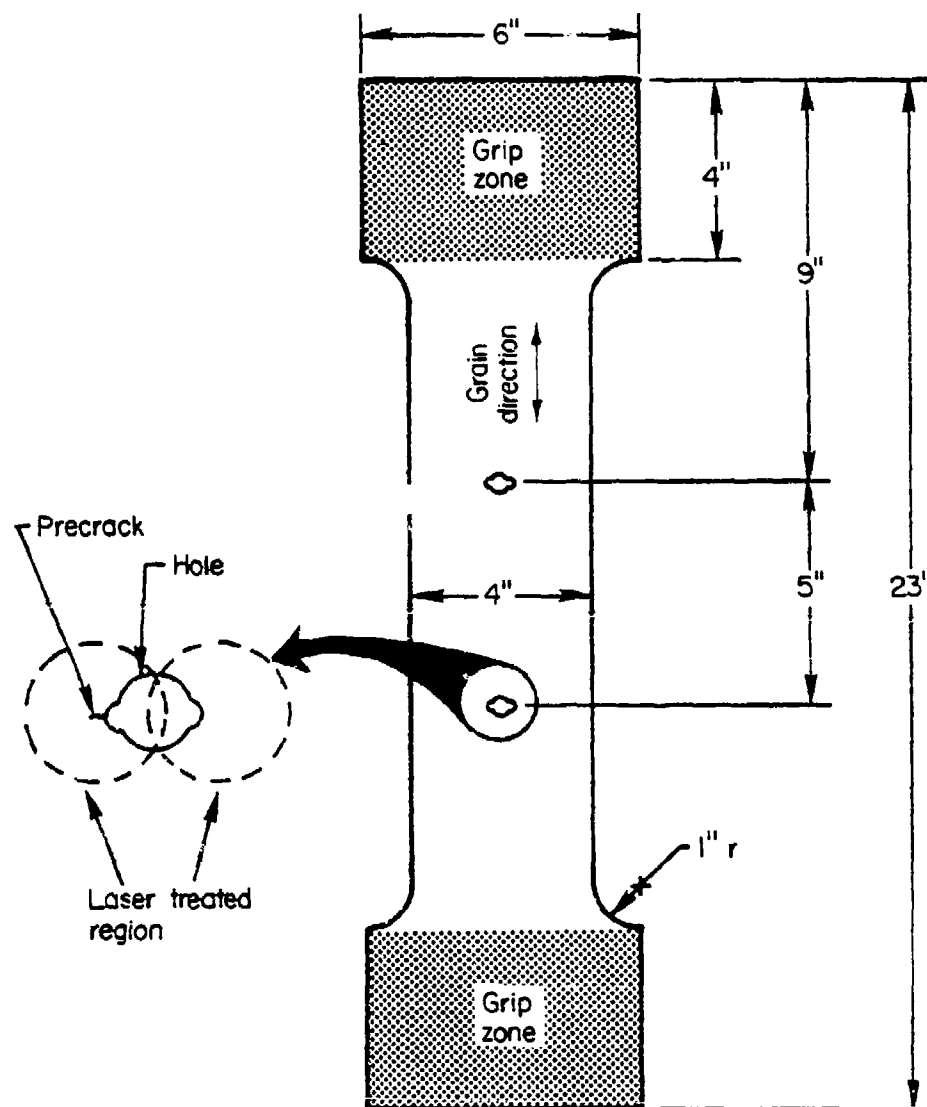


Figure 2. Crack initiation/growth specimen (2 holes)



Specimen thickness,  $\frac{1}{4}$ " or  $\frac{1}{8}$ "

Figure 3. Precracked crack initiation/growth specimen  
(2 holes)

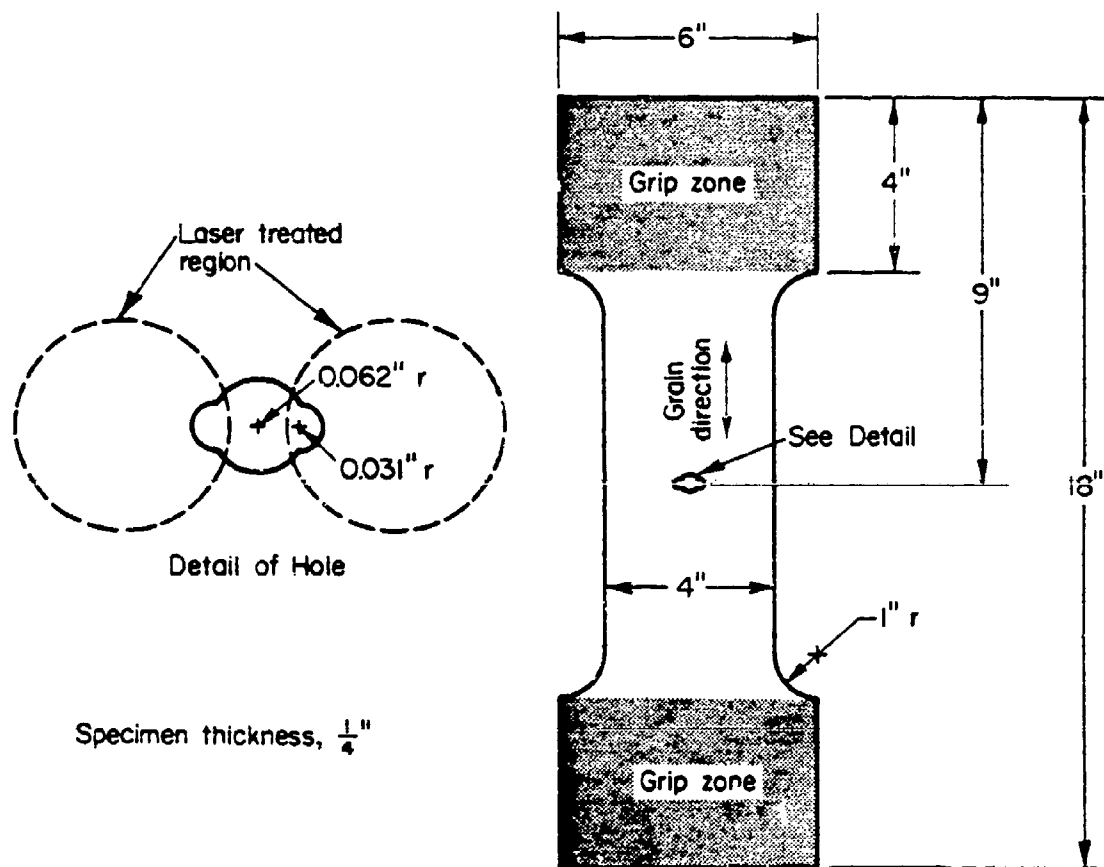


Figure 4. Crack initiation/growth specimen (single hole)





## 2. Laser Description

Battelle's high-power neodymium-glass laser was used in all of the laser shock experiments. The system, which consists of a Q-switched oscillator followed by six amplifier stages, delivers up to about 200 joules of laser energy. Energy density was varied from 50 to 150 joules per square centimeter and pulse width was varied from 13 to 24 nanoseconds. Laser spot size varied from 0.37 to 0.45 inch diameter and spot placement is shown in Figure 6.

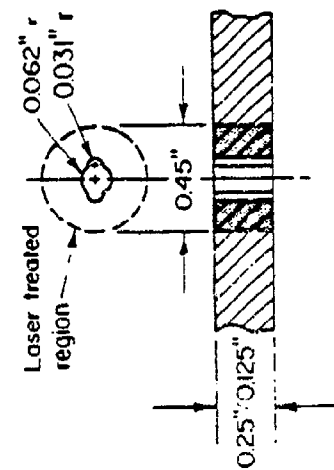
## 3. Fatigue Test Description

The fatigue test program was designed to evaluate the effect of a number of variables upon the crack initiation/growth process in sheet and fastened joint type specimens. Initial tests were devoted to the selection of a baseline stress level and investigation of parameters such as power level, sheet thickness effect, hole drilling effects, and the effect of shocking one or both sides of the specimen. Subsequent tests provided data to evaluate constant amplitude stress level, spectrum load, specimen material, and precracking effects on crack initiation/growth.

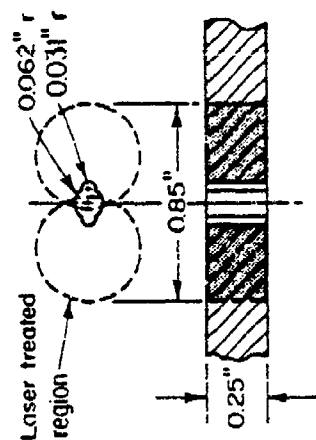
Low-load transfer fastened joint specimens were tested in the shocked and unshocked conditions with properly prepared, as well as flawed, holes. In addition, a series of tests were conducted to investigate increased laser power density and a new plastic overlay. All of the experimental conditions are detailed in Test Matrices I through IV, contained in Tables 1 through 4.

Specimens 2\*, 3\*, 25\* through 28\*, 101 through 104, 7-973, 7-975, 7-926A, and 1-EXT through 12-EXT were added to the original test plan during the course of the program. Specimens 20A and 21A were so designated to avoid duplication of numbers in test Matrices I and II.

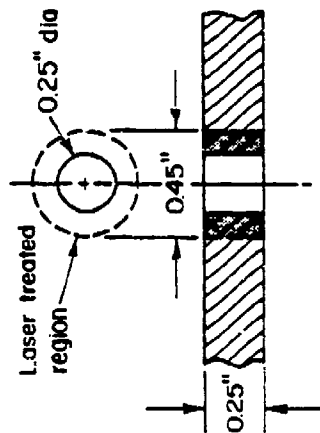
A variety of cyclic loading conditions were tested to investigate whether the type of stress history has an effect on fatigue initiation or crack growth.



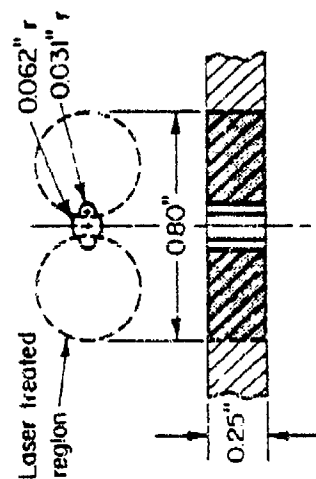
a. Crack propagation specimen with a 0.45" diameter centered laser spot



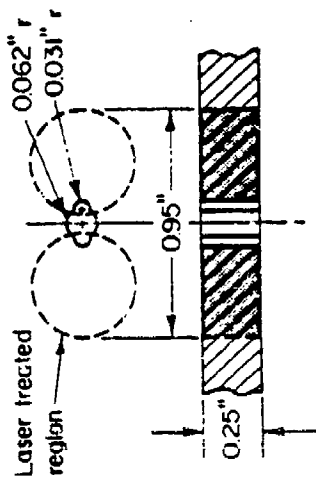
b. Crack propagation specimen with precrack and two 0.45" diameter off-centered laser spots



c. Low-load transfer fastened joint specimen with a 0.45" diameter centered laser spot



d. Crack propagation specimen with two 0.37" diameter off-centered laser spots



e. Crack propagation specimen with two 0.45" diameter off-centered laser spots

Figure 6. Laser spot configurations

TABLE 1. TEST MATRIX I - INVESTIGATION OF SHOCK PARAMETERS

Specimen Number	Sheet Thickness, t	Laser Parameter	Shock Both Sides of Specimen?	Special Conditions	Reason
1	0.25	$\phi_1$	Yes	None	Define working stress that will propagate cracks
2, 3, 2*, 3*	0.25	$\phi_1$	Yes	None	Baseline
4, 5	0.25	$\phi_2$	Yes	None	Evaluate effect of increased laser power density
6, 7	0.125	$\phi_2$	Yes	None	Determine if there is a thickness effect
8, 9	0.25	$\phi_*$	Yes	Radius Hole Edge	Evaluate through-thickness effect with optimum shock parameter
10, 11	0.25	$\phi_*$	Yes	Drill Before Shock	Evaluate drill sequence effects
12, 13	0.25	$\phi_*$	Yes	Drill Before Shock and Radius Hole Edge	Evaluate through thickness and drill sequence effects
14, 15	0.25	$\phi_*$	No	Drill Before Shock	Evaluate effect of shocking one side only (thickness effect)
16, 17	0.125	$\phi_*$	No	Drill Before Shock	Confirm Experiments 14 and 15 (thickness effects)
18, 19	0.125	$\phi_*$	No	Drill After Shock	Confirm thickness and drill sequence effects
20, 21	0.125	$\phi_*$	No	Use Back-up Plate on Back Side	To determine if back-up plate will reflect shock wave

Note 1.  $\phi_*$  is optimum laser power density -- selected after Experiment Number 7.

Note 2. All specimens to be made of 7075-T651 aluminum alloy.

Note 3. Specimen 1 was tested at a maximum stress of 13 ksi. Specimens 2 and 3 were tested at a maximum stress of 14 ksi, 2\*, 3\* and all of the following specimens were tested at a maximum stress of 15 ksi. See the section on Fatigue Test Description for an explanation of specimen numbering.

TABLE 2. TEST MATRIX II - BASELINE CRACK INITIATION/GROWTH DATA MATRIX

Specimen Number	Sheet Thickness, $t$	Laser Parameter	Shock Both Sides of Specimen?	Special Conditions	Reason
20A, 21A, 22	0.25	No Shock	--	Constant Amplitude 7075-T651 ( $\sigma_1$ )	Baseline
23, 24 <sup>a</sup>	0.25	$\phi_*$	Yes	Constant Amplitude 7075-T651 ( $\sigma_1$ )	Direct comparison of laser shock effect
25, 26	0.25	$\phi_*$	Yes	Constant Amplitude 7075-T651 ( $\sigma_2$ )	Evaluate stress effect
25*, 26*	0.25	No Shock	--	Constant Amplitude 7075-T651 ( $\sigma_2$ )	Baseline
27, 28	0.25	$\phi_*$	Yes	Constant Amplitude 7075-T651 ( $\sigma_3$ )	Evaluate stress effect
27*, 28*	0.25	No Shock	--	Constant Amplitude 7075-T651 ( $\sigma_3$ )	Baseline
29, 30	0.25	No Shock	--	Constant Amplitude 2024-T3 ( $\sigma_1$ )	Baseline
31, 32	0.25	$\phi_*$	Yes	Constant Amplitude 2024-T3 ( $\sigma_1$ )	Direct comparison of laser shock effect
33, 34	0.25	$\phi_*$	Yes	Constant Amplitude 2024-T3 ( $\sigma_3$ )	Evaluate stress effect
35, 36	0.25	No Shock	--	Flight/Flight 7075-T651 ( $\sigma_4$ Mean)	Baseline
37-38	0.25	$\phi_*$	Yes	Flight/Flight 7075-T651 ( $\sigma_4$ Mean)	Direct comparison of shock effect

<sup>a</sup> Specimens 4 and 5 are the same as Specimens 23 and 24.

Table 2. (Concluded)

Specimen Number	Sheet Thickness, t	Laser Parameter	Shock Both Sides of Specimen	Special Conditions	Reason
39,40	0.25	$\phi^*$	Yes	Flight/Flight 7075-T651 ( $\sigma_5$ Mean)	Evaluate mean stress effect
41,42	0.25	$\phi^*$	Yes	Constant Amplitude Precrack 7075-T651 ( $\sigma_1$ )	Direct comparison to Experiments 20-24 for repair capability
43,44	0.25	No Shock	Yes	Constant Amplitude Precrack 7075-T651 ( $\sigma_3$ )	Direct comparison to Experiments 27 and 28 for repair capability
45,46	0.25	$\phi^*$	Yes	Flight/Flight Precrack 7075-T651 ( $\sigma_4$ Mean)	Direct comparison to Experiments 35-38 for repair capability
47,48	0.25	$\phi^*$	Yes	Flight/Flight Precrack 7075-T651 ( $\sigma_5$ Mean)	Direct comparison to Experiments 39-40 for stress effect
49,50	0.25	$\phi^*$	Yes	Constant Amplitude Precrack 2024-T3 ( $\sigma_1$ )	Direct comparison to Experiments 29-32 for repair capability
51,52	0.25	$\phi^*$	Yes	Constant Amplitude Precrack 2024-T3 ( $\sigma_3$ )	Direct comparison to Experiments 33-34 for repair capability

TABLE 3. TEST MATRIX III - LOW-LOAD TRANSFER  
FASTENED-JOINT FATIGUE EXPERIMENTS

Specimen Number	Laser Shocked	Hole Condition	Stress
53-59	No	As Drilled/Reamed	$\sigma_4$ (40 ksi) <sup>a</sup>
60-62	No	Flawed	$\sigma_4$ (40 ksi) <sup>a</sup>
63-69	Yes	As Drilled/Reamed	$\sigma_4$ (40 ksi) <sup>a</sup>
70-72	Yes	Flawed	$\sigma_4$ (40 ksi) <sup>a</sup>
101-102	No	As Drilled/Reamed	$\sigma_6$ (27 ksi) <sup>b</sup>
103-104			
7-973, 7-975 7-926A	Yes	As Drilled/Reamed	$\sigma_6$ (27 ksi) <sup>b</sup>

<sup>a</sup>FALSTAFF Flight 130 modified variable amplitude.

<sup>b</sup>40 ksi FALSTAFF Flight 130 modified, proportionally  
reduced to 27 ksi maximum.

NOTE: All specimens are 7075-T651 aluminum.

TABLE 4. TEST MATRIX IV - HIGH INTENSITY AND  
PLASTIC OVERLAY EXPERIMENTS

Specimen Number	Laser Power Density	Overlay	Test Conditions
3-EXT, 4-EXT	$\phi_3^a$	Water	15 ksi Constant Amplitude
1-EXT, 2-EXT	$\phi_3$	Water	15 ksi Constant Amplitude (Drilled Before Laser Shocking)
9-EXT, 10-EXT	$\phi_3$	Water	15 ksi Constant Amplitude (Precrack)
5-EXT, 6-EXT	$\phi_3$	Water	17 ksi Constant Amplitude
7-EXT, 8-EXT	$\phi_3$	Plastic	15 ksi Constant Amplitude
11-EXT, 12-EXT	$\phi_{*}^b$	Plastic	15 ksi Constant Amplitude

<sup>a</sup> $\phi_3 > \phi_{*}$ .

<sup>b</sup>Tests conducted to compare with  $\phi_{*}$ -Water Overlay Experiments

NOTE: Material 7075-T651 aluminum.



a. Circular Notched Crack  
Initiation/Growth Specimens

A majority of the circular notched crack initiation/growth specimens were cycled by a constant amplitude stress with a stress ratio of +0.1. Initial specimens were 7075-T651 aluminum, cycled at a constant-amplitude stress of 13 ksi. These initial results indicated fatigue lives were close to an endurance limit. The minimum fatigue stress from these initial results was later limited to 15 ksi. Two other constant amplitude stress levels were run at 17 ksi and 24 ksi. A summary of the load section is presented in Table 5.

In addition to the constant amplitude tests, flight-by-flight loading representative of an aircraft flight spectrum was applied to a number of specimens. This variable amplitude load history was supplied by the Air Force and defined in the evaluation of fatigue-rated fastener systems program. Designated FALSTAFF Flight 130 (extracted from the European standard fighter stress spectrum and modified by the Air force), the maximum stress level was specified at 40 ksi. Specimens were also tested by modifying the above spectrum, proportionally reducing the entire load history to a 35 ksi and a 27 ksi maximum stress. These three load selections are presented in Table 5. A graphic display of the FALSTAFF spectrum is shown in Figure 7. A summary of crack initiation/growth experiment conditions are in Tables 1, 2, and 4.

b. Low-load Transfer Fastened  
Joint Specimens

All low-load transfer fastened joint specimens were cycled applying the flight-by-flight FALSTAFF load spectrum. Specimens were tested at the 40 ksi maximum stress level or by modifying the FALSTAFF spectrum to a 27 ksi maximum stress level. A summary of the low-load transfer fastened joint fatigue experiment conditions is presented in Table 3.

4. Residual Stress Measurements

Two specimens, 4 x 4 inches square, were cut from 7075-T6 0.25-inch-thick plate. The 4-inch dimension was equal to the width of the crack propagation specimens and would avoid possible effects from the interaction of the stress waves with edges other than that of the hole.

TABLE 5. LOADS SELECTION

Load	Applicable Matrix
$\sigma_1 = 15 \text{ ksi}$	I, II
$\sigma_2 = 17 \text{ ksi}$	II
$\sigma_3 = 24 \text{ ksi}$	II
$\sigma_4 = 40 \text{ ksi (max.)}^a$	II, III
$\sigma_5 = 35 \text{ ksi (max.)}^a$	II
$\sigma_6 = 27.7 \text{ ksi (max.)}^a$	III

<sup>a</sup>FALSTAFF Flight 130 modified.

NOTE: Constant amplitude loads of  $\sigma_1$ ,  $\sigma_2$ , and  $\sigma_3$  were run at a stress ratio of +0.1.

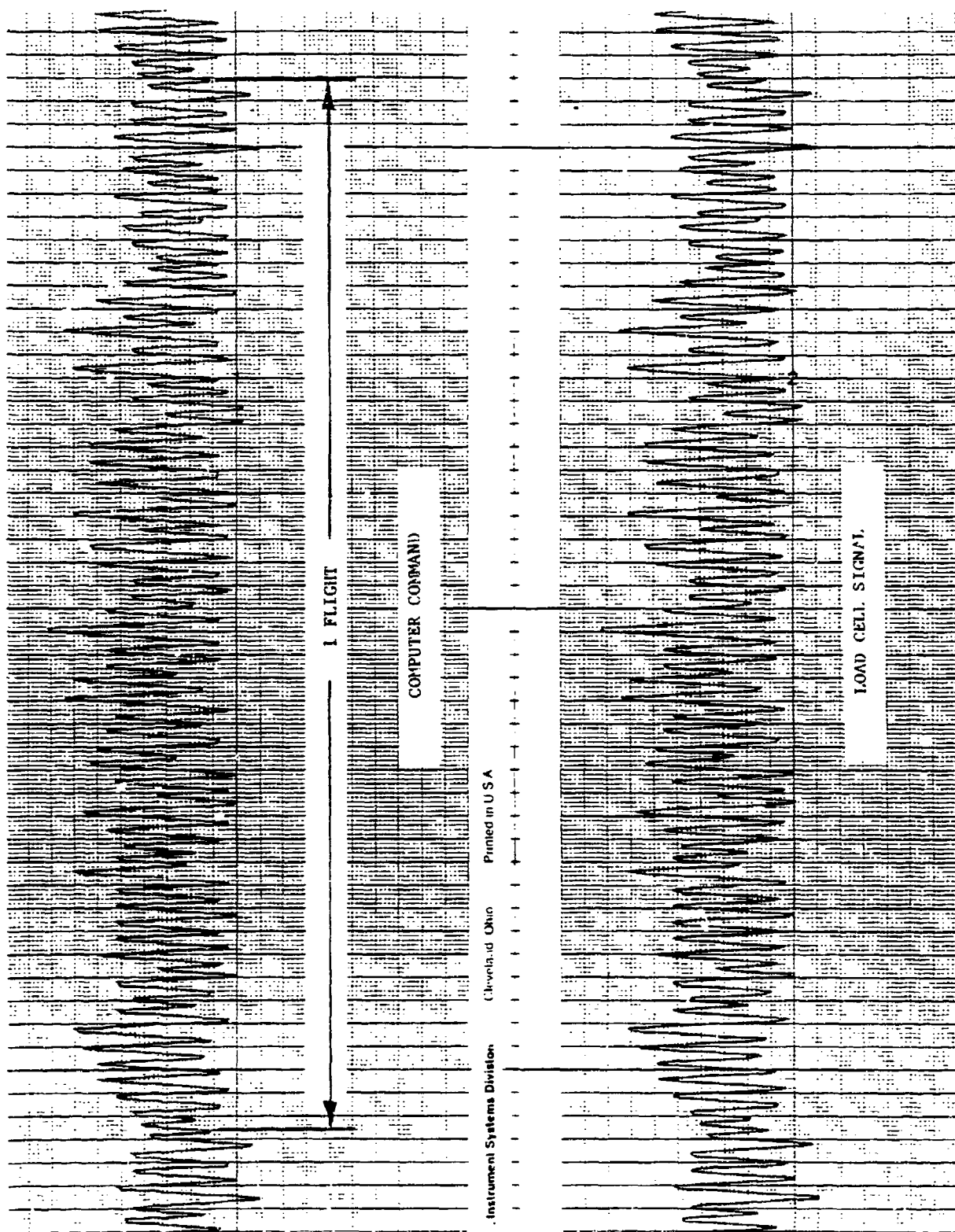


Figure 7. FALSTAFF, Flight 130, flight-by-flight load spectrum

The hole drilled before shock was machined identically to those made in the crack propagation specimens. The hole drilled after shock was drilled and reamed identically to those made in the fastener specimens. A hole size of 0.1875 inch, rather than 0.25 inch diameter was selected to provide more area between the edge of the hole and the edge of the laser-treated region for the residual stress measurements. This would allow an assessment of the extent of relaxation of residual stresses away from the hole after drilling.

The laser shocking conditions for these residual stress specimens were similar to those used in the initial phase of the program. The power density level was  $\phi_*$  (the level selected for the majority of experiments), and the laser-treated zone was 0.45 inch in diameter and located concentric to the drilled hole.

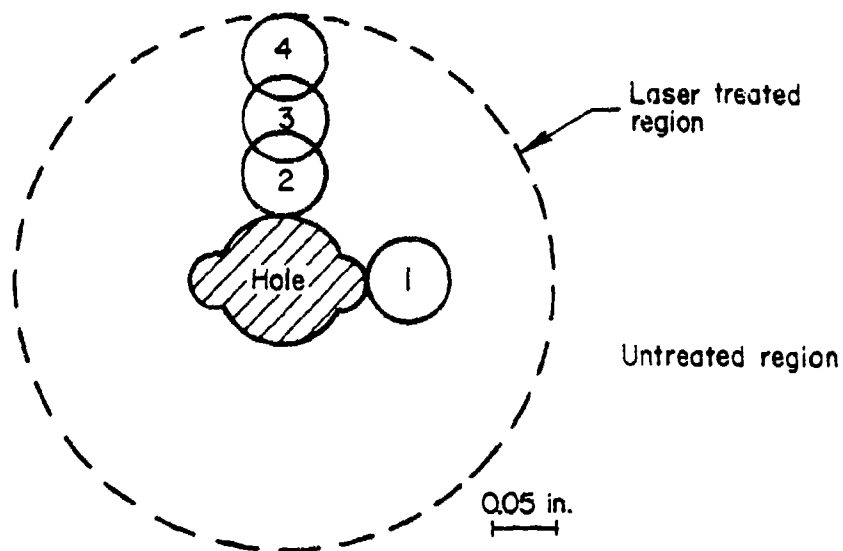
The residual stresses were measured by X-ray diffraction procedures\*<sup>(6)</sup> using the two-angle method and Cr-K $\alpha$  radiation from the [311] crystallographic planes of the specimens. The in-depth profiles were made by consecutively removing 0.005 or 0.010 inch from the surface between sets of readings. The material was removed by electropolishing in a methanol-nitric electrolyte to avoid inducing additional residual stresses into the surface. The inside surfaces of the holes were lacquered to avoid enlarging the holes but preferential attack did occur at the edge of the hole, limiting the number of readings that could be made at these sites. Corrections for penetration of the radiation below the surface and for stress relaxation caused by the material removed in the serial electropolishing of the surface for the in-depth stress profile were applied. Because of the relatively large grain size of this material, the specimen was rocked through an angle of approximately three degrees to obtain sufficient reflecting grains for reliable measurements. The larger grain size also required a large X-ray spot size. A spot size of 0.080 inch square was used here. The elastic constants for the crystallographic direction normal to the [311] planes were measured on a 7075-T6 aluminum alloy specimen in four-point bending.<sup>(7)</sup> The error in the residual stresses are estimated to be  $\pm 4$  ksi at the most, including both random and systematic errors.

---

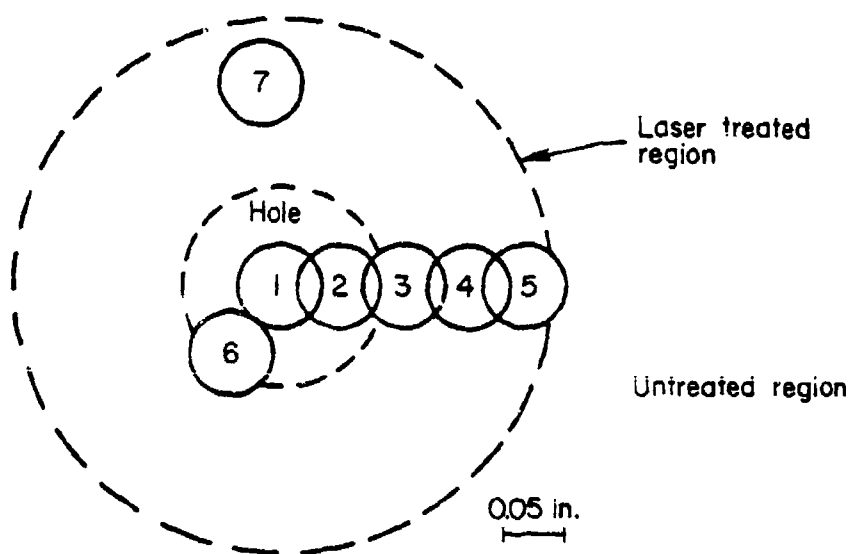
\* The residual stress measurements were made at Lambda Research, Inc., Cincinnati, Ohio.

The locations of the residual stress measurements relative to the laser-treated zone and location of the drilled hole are shown in Figure 8. For the hole drilled before shock, Figure 8a, two measurements were made at separate sites at the edge of the hole. One at Site 1 where the cracks would initiate in the crack propagation specimens, and another at Site 2 on the larger diameter circle to determine whether the local radius of the hole had any effect on the residual stress level. In addition, Site 3 represented a site intermediate between the hole rim and the laser-treated zone edge at Site 4.

The specimen used for the hole drilled after shock initially had five sites (Figure 8b) spaced along the radius from the center of the laser-treated zones to just inside the edge of the zone. Of these sites, Site 4 is intermediate between the hole edge, Site 3, and treated zone edge, Site 5. Sites 6 and 7 are located on small bumps which sometimes appear on the laser-shocked surface. It was decided to make measurements at these bumps to determine if there was a stress difference when compared to Sites 2 and 4.



a. Hole drilled before laser shocking



b. Hole drilled after shock

Figure 8. The location of the numbered sites at which the residual stress measurements were made in the laser-treated region

### III. DISCUSSION OF EXPERIMENTAL RESULTS

Since no previous knowledge existed on the effects of laser shocking on the initiation and propagation of fatigue cracks from holes, it was necessary to investigate a large variety of test conditions. The previous section describes in detail the different parameter values that were investigated. The complexity of the test program, coupled with the usual scatter in fatigue life of aluminum specimens, made it difficult to interpret the results or to describe them simply. However, on the basis of examining the fracture surface of a number of the cracked specimens and on the basis of some measurements of residual stresses in laser-shocked specimens, it is believed that the major effect of laser shocking on fatigue life is a result of the residual stress state induced in the specimen.

In Subsection 1, we will first describe the fatigue results obtained for each specimen tested and attempt to interpret these results in terms of the test conditions and our understanding of the residual stress state of the specimen.

Subsection 2 will describe the measurements that were made of the residual stresses in laser-shocked and unshocked 7075 specimens. On the basis of these residual stress measurements and measurements of the crack growth traces in fatigue specimens, an interpretation is given of the behavior of fatigue crack initiation and propagation in the laser-shocked specimens.

#### 1. Fatigue Results

Tables 1 through 4 presented in the previous section, Description of Experimental Program, give the test conditions for all of the specimens used in this program. Test Matrix I was used to develop insights concerning the variables of laser shocking, including laser power parameters, sheet thickness, and special hole conditions or shocking configurations. Test Matrix II provided data for different materials, stress states, and hole quality conditions. Test Matrix III defined the tests for fastened joint specimens, and Test Matrix IV dealt with the effects of increased laser power and a plastic overlay.

a. Test Matrix I - Investigation  
of Shock Parameters

The test matrix for this section treated only 7075 aluminum. Test conditions were given in Table 1. These were the initial experiments carried out in this program to ascertain the appropriate specimen preparation and laser shocking conditions to use on the rest of the program. The conditions sought were those causing the largest increase of fatigue life after laser shocking compared to the unshocked condition.

The results are shown in bar form in Figure 9. The tabulated results are given in Table A-9 in Appendix A. The specimen numbers corresponding to those in Table 1 are shown on each bar. The designations A and B refer to each of the two holes present in each specimen. The laser power levels are also indicated in the figure. All specimens were shocked on both sides unless otherwise noted. The three crack propagation milestones indicated on the figure are the cycles to grow to 0.25 inch, the cycles to grow to 0.45 inch, and cycles to failure. The first milestone (0.25 inch) included the initial 0.186 flaw size. It was used to define the crack initiation phase. The second milestone (0.45 inch) was chosen since it was the characteristic diameter of a laser spot.

Although the crack initiation results for unshocked specimens exhibited a straightforward process of crack initiation and growth, it will be seen later that crack initiation and propagation in the laser-shocked specimens was more complicated. In the shocked specimens, tunneling of the crack before it breaks through to the surface made the interpretation of the 0.25 inch crack length data very difficult. These data represent the first visible sign of a crack of 0.25 inch length of the specimen surface. They are included here for the sake of completeness.

A more meaningful parameter is the number of cycles to reach 0.45 inch, or the edge of the laser shocked zone. This number represents the total number of cycles to initiate and propagate a crack through the laser-shocked zone. It will be shown later that once the crack has extended beyond the laser-shocked zone, it rapidly expands so the surface intersection of the crack does not lag too far behind the interior of the crack front.

Once the crack has extended beyond the laser-shocked zone, it should propagate at the same rate as a similar crack in an unshocked specimen. Therefore,



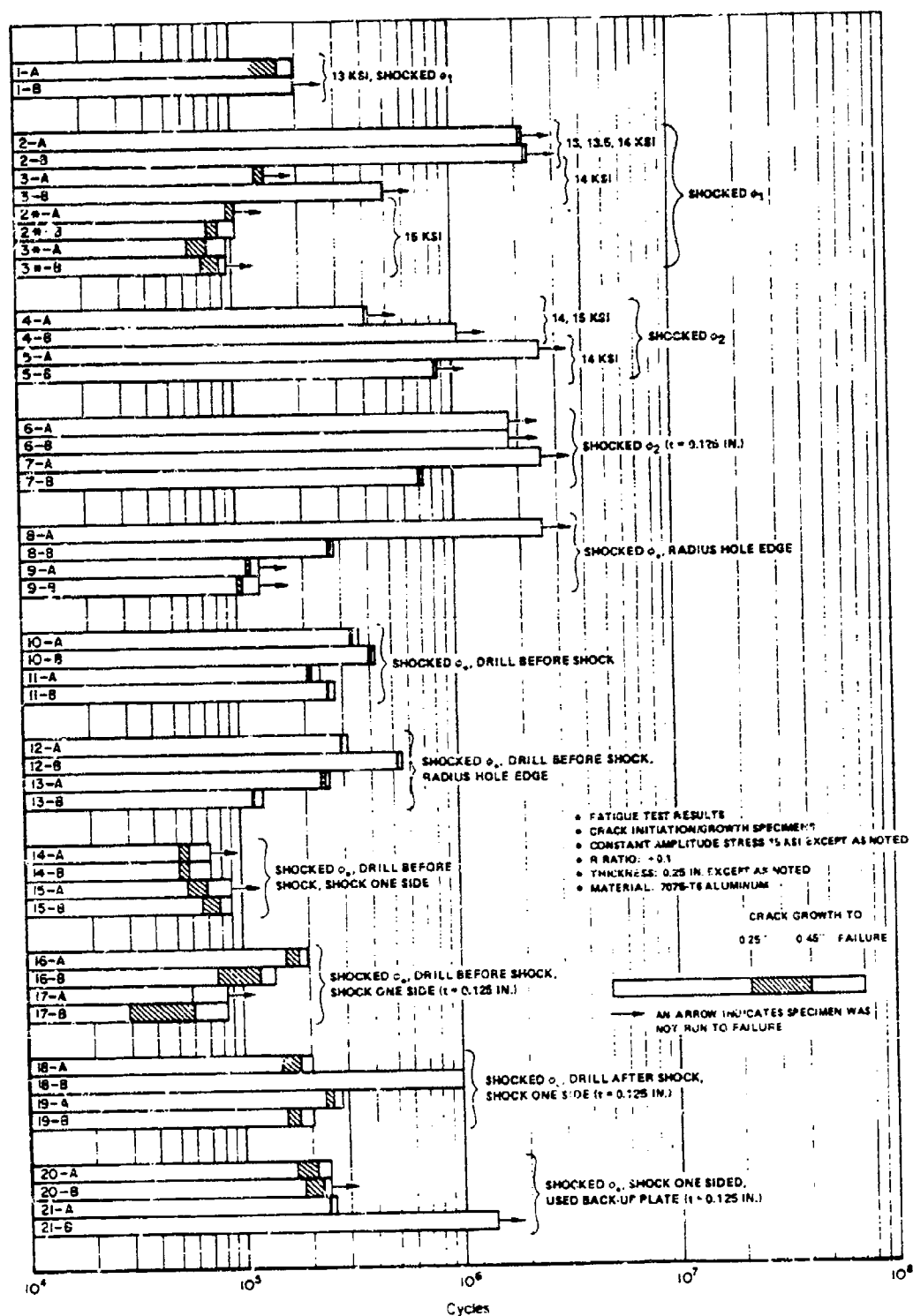


Figure 9. Matrix I fatigue test results

in some instances, the specimens were not tested to failure since the cycles to reach 0.45 inch can be used for comparison of laser shock effects. In addition, since some specimens generated cracks in only one of the two holes, comparisons are made using the hole in which the crack first appeared and propagated.

Figure 9 shows that Specimens 1 through 3\* exhibited a decrease in life to crack initiation as a function of increasing cyclic stress. These specimens were shocked at a power density of  $\phi_1$  and tested at cyclic stresses of 13, 13.5, 14, and 15 ksi. One exception to the trend is Specimen 1 which was short in life and was later examined by transmission and scanning electron microscopy with no explanation found for the anomaly.

The fatigue life of the thinner (0.125 inch thick) Specimens 6 and 7, shocked on both sides, is longer than that of all the thicker (0.25 inch thick) specimens tested at 15 ksi (Specimens 8 to 13). Therefore, thinner specimens shocked on both sides by the split beam appear to have longer fatigue life than identically shocked thicker specimens.

Drilling before or after laser shocking, and radiusing the hole edge, appears to have no effect on the relative fatigue life (Specimens 10 to 13). Laser shocking one side only is not as effective as laser shocking both sides simultaneously (Specimens 14 and 15 compared to Specimens 10 to 13 and Specimens 16 to 19 compared to Specimens 6 and 7). In addition, use of a back-up plate has no discernable effect compared to no backup plate (Specimens 16 to 21).

Radiusing the hole edge was investigated to see what effect laser shocking would have on edge-initiated cracks. Later it is shown that crack initiation usually occurs in the middle portion of the specimen thickness along the hole surface. Because laser shocking in itself evidently inhibited crack initiation at the hole edges, radiusing of the holes had no effect.

From this series of experiments, it was decided that the remainder of the specimens would be shocked at the power density  $\phi_2$  (hereafter called  $\phi_*$ ) with the hole drilled prior to laser shocking.

#### b. Matrix II - Baseline Crack Initiation/ Growth Data

The test matrix for this section is given in Table 2 in the previous section. This series of experiments was conducted to investigate the effect

of stress amplitude and precracking at constant stress amplitude on 7075 and 2024 aluminum. In addition, flight-by-flight testing of 7075 was investigated.

The results of increasing stress amplitude are shown in Figure 10. The tabulated results are given in Table A-10 in Appendix A. The unshocked baseline fatigue properties at 15 ksi are at the top of the figure (Specimens 20A to 22). There is only marginal improvement, if any, after laser shocking (Specimens 23 and 24) for these 0.25 inch thick specimens. At 17 and 24 ksi maximum stress, laser shocking provides no improvement (Specimens 25\* to 26 and 27\* to 28).

Precracking to the number of cycles shown by the gray-shaded amount followed by laser shocking also showed no laser shock benefits on total life in 7075 (compare Specimens 41 and 42 to Specimens 20A to 22 and 43 to 44 to 27 and 28). A "crack initiation" life is reported for the precracked specimens even though a crack was initiated before testing, because the initial crack had not grown to 0.25 inch before laser shocking.

However, the number of cycles required to propagate the crack from 0.25 inch to 0.45 inch is significantly greater for the precracked and shocked specimens cycled at 15 ksi than for unshocked specimens (compare slash-shaded regions in Specimens 41 and 42 to regions in 20 to 22). Comparison of Specimens 27 and 28 to Specimen 44 shows less effect at 24 ksi. The most logical explanation of this effect is that the precracked specimens were shocked with two separate laser shots, one on each side of the flaw (Figure 6b). Specimens 20 to 22 were shocked in a single shot centered at the center of the hole (Figure 6a). Thus the length of laser shocked region beyond the 0.25 inch crack position was increased from 0.10 inch to 0.30 inch. With the greater shocked distance to traverse, the crack propagation rate is considerably retarded. As noted, the higher stress amplitude overcomes this retardation. As explained in a later section this is an apparent result of the cyclic stress relieving the residual stresses because of plastic flow at the higher stress amplitude.

The flight-by-flight spectrum testing of the 7075-T6 specimens showed some interesting results (Figure 11). At the 40 ksi maximum stress level, laser shocking produced a slight improvement in fatigue life (Specimens 35 to 38). For specimens that were precracked followed by laser shocking, the total fatigue life is less than for nonprecracked specimens in terms of the number of cycles to reach 0.45 inch (Specimens 37 and 38 compared to 45 and 46 and Specimens 39 and 40 compared to 47 and 48). Note, however, that the cycles

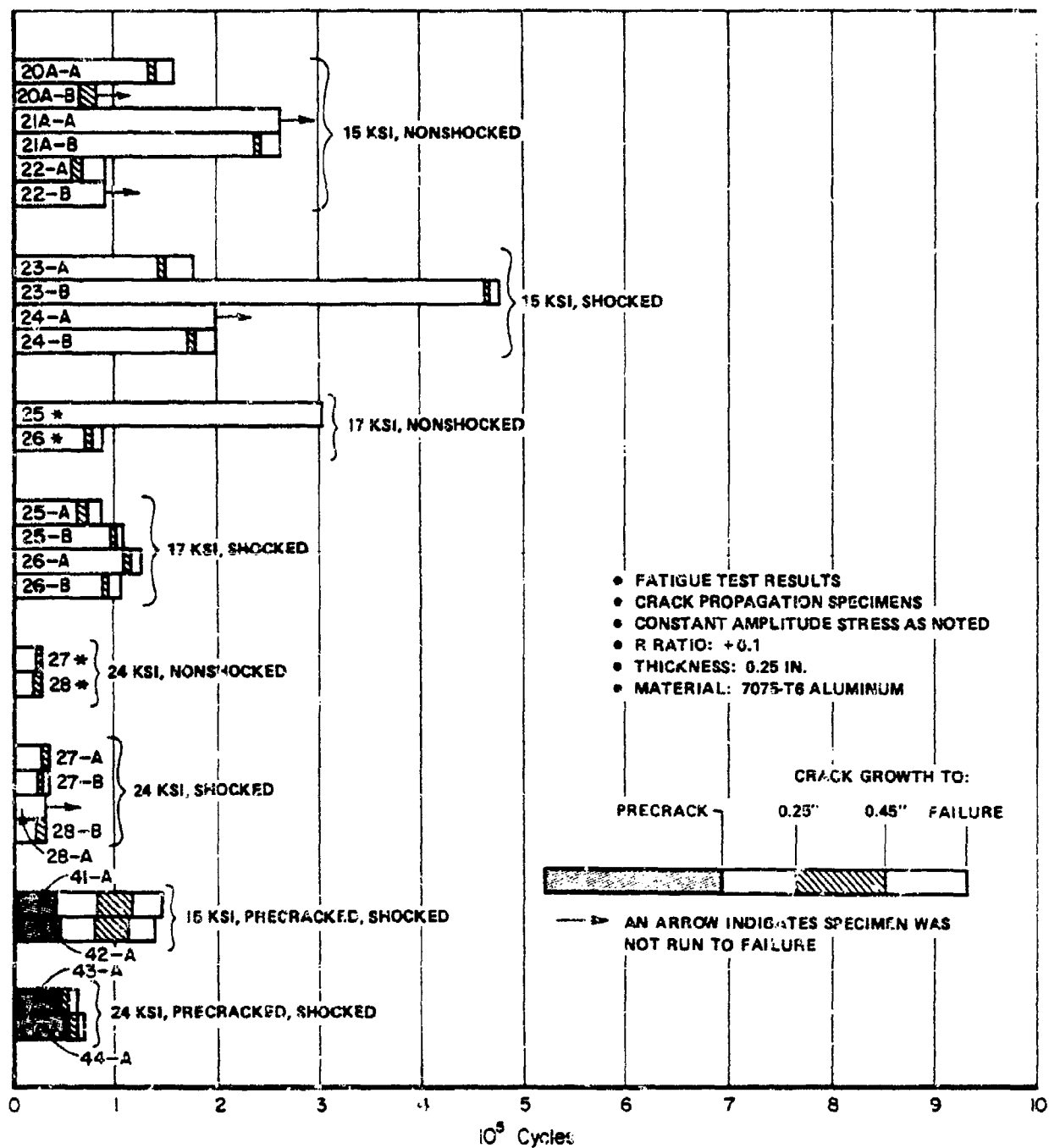


Figure 10. Matrix II fatigue test results 7075-T6 aluminum specimens

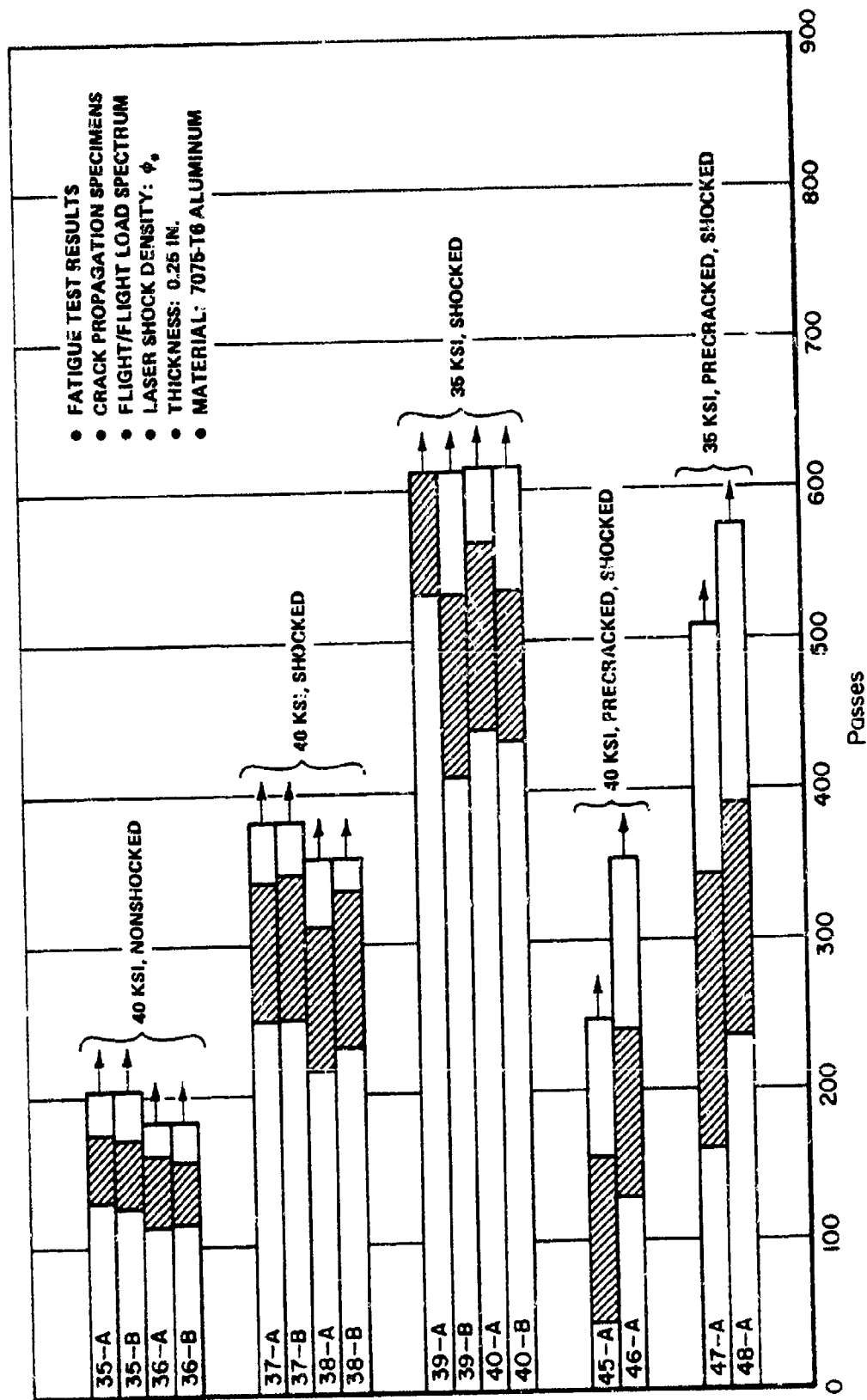


Figure 11. Matrix II fatigue test results of the flight/flight load spectrum

to propagate a crack from 0.25 to 0.45 inch are slightly greater in the pre-cracked specimens (shaded regions).

The constant stress amplitude results for the 2024 specimens are shown in Figure 12. In this alloy, there is a significant increase in fatigue life after laser shocking (Specimens 29 through 32). Laser shocking after precracking also significantly increases the fatigue life. The greatly increased crack propagation life in the laser-shocked zone (the shaded region) in the precracked specimen suggests that the crack propagation rate is slowed significantly by laser shocking together with the effect of having a larger shocked region ahead of the crack.

Part of the increase in the crack propagation period (which actually includes all the life from the top of the dark shaded region on out) is attributable to the longer laser-shocked region in the precracked specimens as mentioned earlier. (Compare the laser-shocked region of Figure 6b with Figure 6a.) Because we don't know when crack initiation actually occurred in Specimens 31 and 32 which were not precracked, we cannot make any direct assessment of the cycles to propagate through the laser-shocked zone for both laser shocking configurations; however, a comparison of life to propagate from 0.25 inch to 0.45 inch does give a relative indication of crack growth behavior. It is also possible that a larger laser-shocked zone in front of the crack will increase fatigue life. At 24 ksi stress amplitude, there is only a marginal increase, if any, after precracking and laser shocking (Specimens 33 and 34 compared to 51 and 52).

In summary, at constant stress amplitude, laser shocking of 2024 showed a significant increase in fatigue life; whereas, 0.25-inch-thick specimens of 7075 did not show any. This occurred even though 15 ksi is a larger fraction of the yield strength of 2024 than it is of 7075. This difference in fatigue response to laser shocking might be related to the yield and flow behavior of the alloy. The lower strength of the 2024 alloy may allow a larger shock induced plastic strain effect in it than is reached in the 7075 alloy with the concomitant increase in relative fatigue life improvement.

#### c. Matrix IV - High Intensity and Plastic Overlay Experiments

These experiments were designed to briefly investigate the effect of a still higher power density, i.e., a more intense laser beam, and the

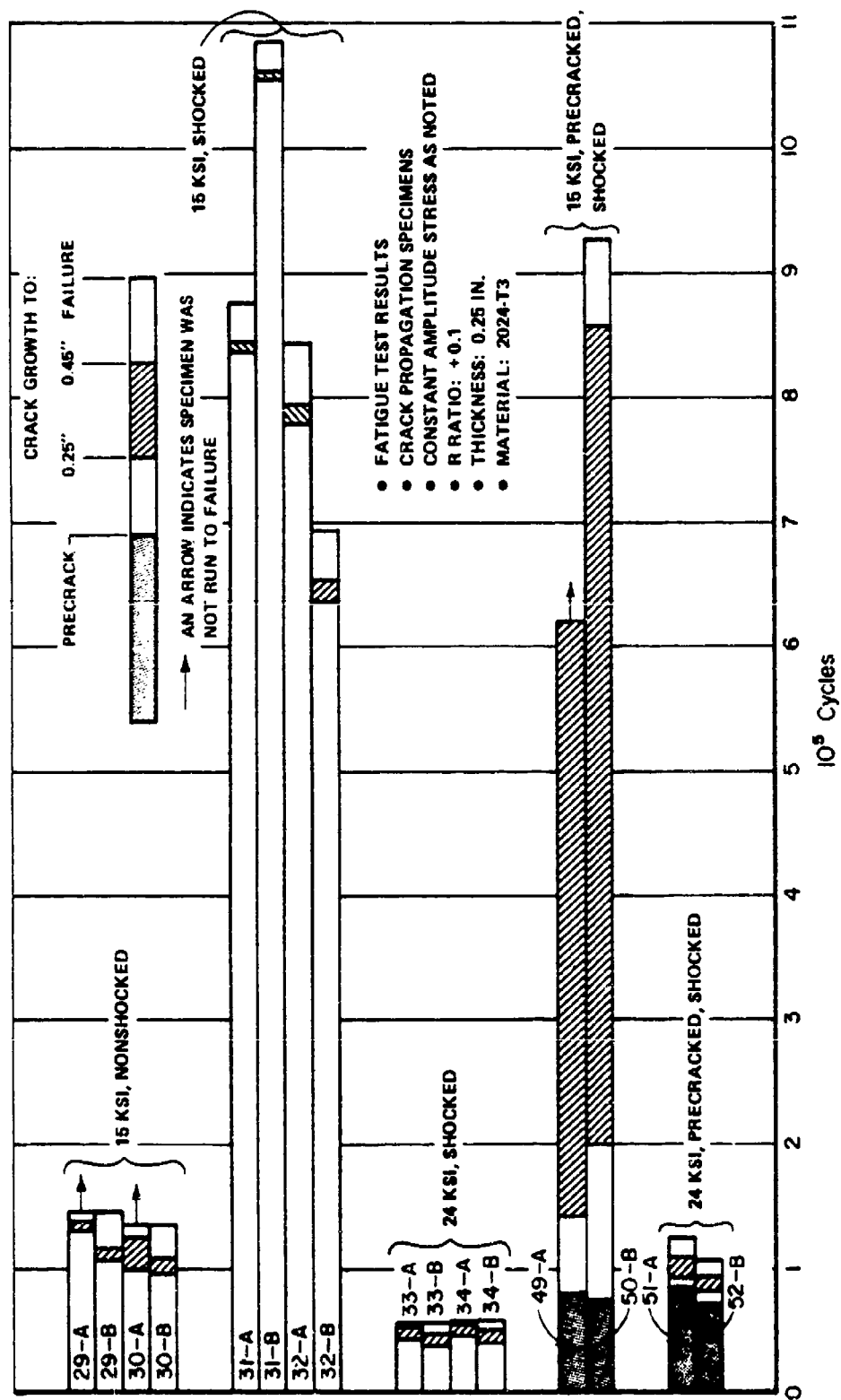


Figure 12. Matrix II fatigue test results 2024-T3 aluminum specimens

potential benefits of a plastic overlay. A more intense laser beam could produce a more intense shock wave in the specimens. Plastic could be a useful production line transparent overlay.

The results of these experiments are shown in Figure 13. The results are tabulated in Table A-12 in Appendix A. For reference, the baseline unshocked data at 15 ksi with a water overlay is included at the top of Figure 13. (Specimens 20A to 22). However, the material for Matrix IV Specimens 1 through 12 is not from the same 7075 lot as that in the test matrices I and II. Therefore, the comparison of the shocked specimens to this baseline is not strictly valid. The higher power density,  $\phi_3$ , produced no substantial decrease in crack growth rate or increase in fatigue life compared to the unshocked conditions (Specimens 1 to 4 compared to 20A to 22). The 17 ksi stress amplitude specimens shocked at  $\phi_3$  also have a lower fatigue life than specimens shocked at  $\phi_*$  (compare Specimens 5 and 6, Figure 13 with Specimens 25 and 26, Figure 10). The plastic overlay gave results comparable to the water overlay (Specimens 7 and 8 compared to Specimens 3 and 4).

Considering that the shocked and unshocked conditions represent different lots of material, these results probably indicate that shocking at  $\phi_3$  has no effect on fatigue life similar to the results at  $\phi_*$  presented in Figures 9 and 10. An attempt to laser shock a precracked specimen at  $\phi_3$  was disrupted by exceptionally long precracking cycles as shown in Figure 13. After laser shocking, the life to failure was similar to non-precracked specimens; however, the crack growth period did appear to be extended somewhat. (Compare the life of Specimens 9 and 10 after precracking to the total life of Specimens 1 and 2.)

To determine whether the higher power density,  $\phi_3$ , was actually degrading the fatigue properties, two specimens were laser shocked at the original power density  $\phi_*$  with a plastic overlay (Specimens 11 and 12). These results were inconclusive, but the short life of Specimen 11 suggested that the higher power density may not have degraded the fatigue properties. Specimen 12 had an initiation life longer than the total cycles tested, but shorter than that of Specimen 9 precracked in the unshocked condition. Thus, Specimen 12's long life may have nothing to do with its having been laser shocked.

In summary, the higher power density  $\phi_3$  did not appear to improve the fatigue life over that given by  $\phi_*$  for 7075 material. It is very possible



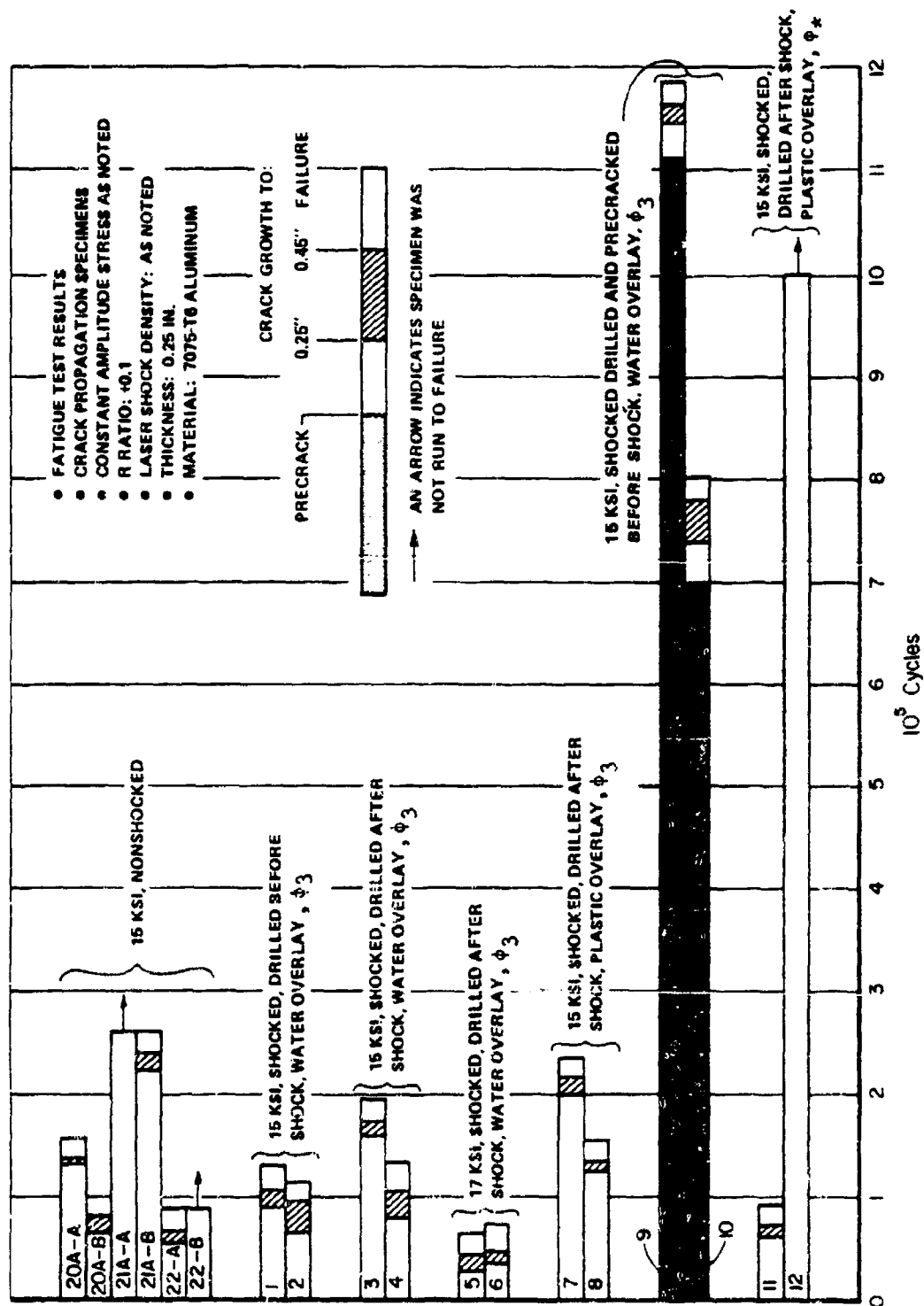


Figure 13. Matrix IV fatigue test results

that some other effect would have been observed at  $\phi_3$  if 2024 had been tested since it did show an increase in fatigue life after shocking at  $\phi_*$ .

d. Matrix III - Low Load Transfer--Fastened  
Joint Fatigue Experiments

This test matrix was set up to investigate the effect of laser shocking on the life of fastened joints of 7075 aluminum. These experiments included fretting fatigue effects. The results for the flight-by-flight loading spectrum at 40 ksi maximum stress is shown in Figure 14 and tabulated in Table A-11 in Appendix A. The flawed condition referred to in Figure 14 consisted of placing a 0.005-inch-deep axial scratch in the fastener hole, normal to the line of load application. Figure 14 shows no effect of laser shocking for either as-drilled or flawed holes.

To investigate the possibility that an improvement of life could be present at lower stress levels, additional specimens were tested at 27 ksi maximum stress (Figure 15). At this stress level, there is clearly an increase in fatigue life after laser shocking.

There are two possible reasons why these load transfer joints did not show a longer fatigue life of the higher operating stress. One has already been mentioned--the higher stress levels, 40 and 27 ksi, compared to that used in the early Battelle experiments (12 ksi). Another possible reason is that the laser-shocked zone is smaller in these specimens. In the early Battelle work, a smaller diameter fastener, (0.1875 inch diameter) was used creating a laser-shocked zone approximated by Figure 6a. In the low-load transfer specimens for this program, larger fasteners (0.250 inch diameter) were used, giving a much shorter laser-shocked zone approximated by Figure 6c. Since this zone is significantly shorter than the specimen thickness and hole radius, substantial relaxation of the residual stress field could occur. This effect combined with the shorter crack distance through laser-shocked material could have minimized any laser shocking benefits which might occur.

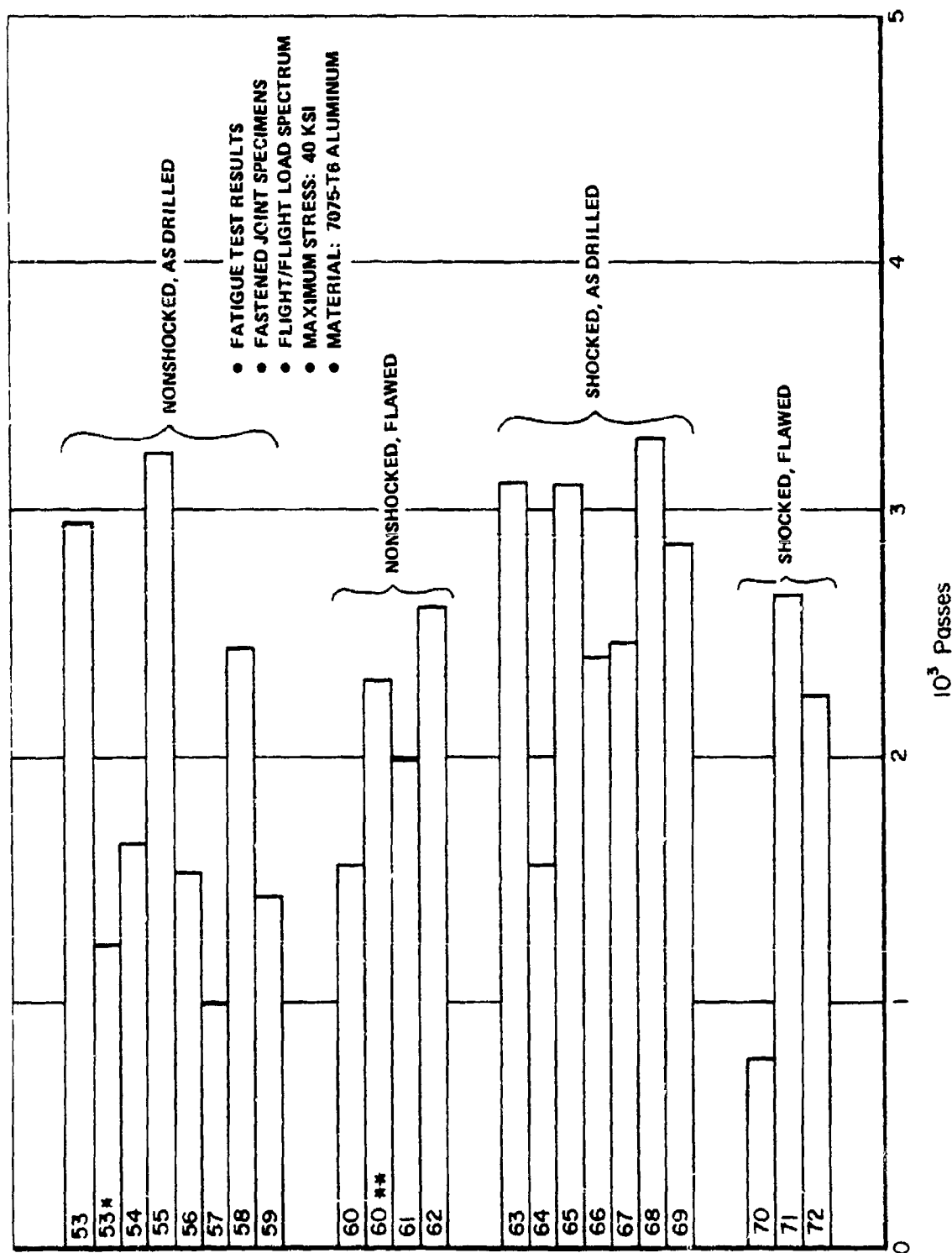


Figure 14. Matrix III fatigue test results 40 ksi flight/flight load spectrum

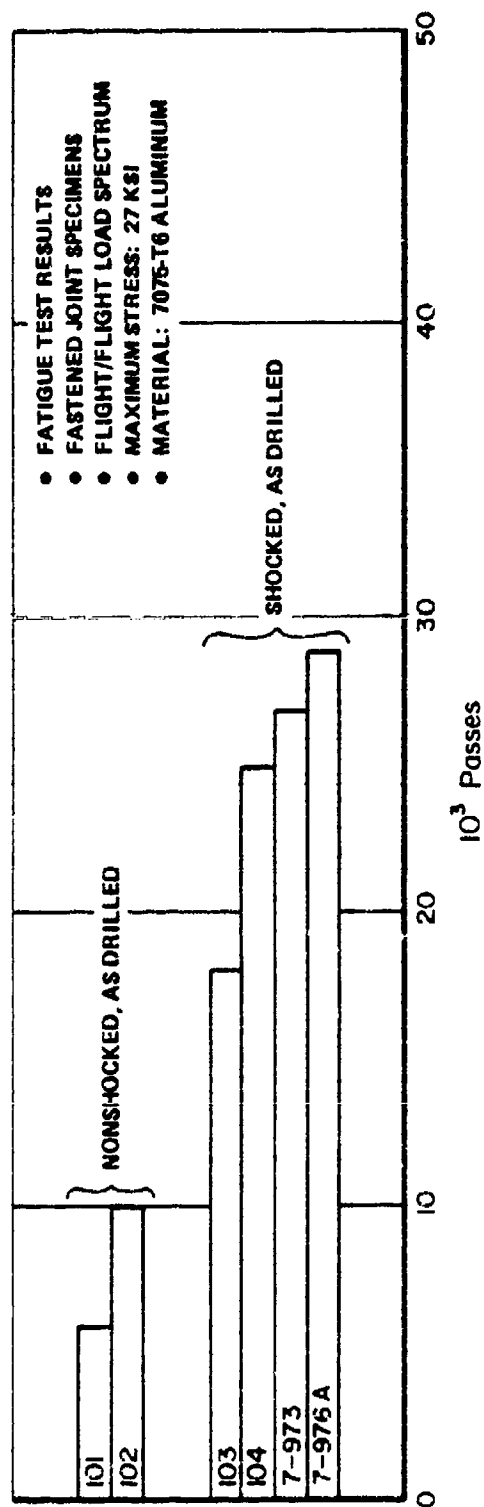


Figure 15. Matrix III fatigue test results 27 ksi flight/flight load spectrum

## 2. Residual Stresses

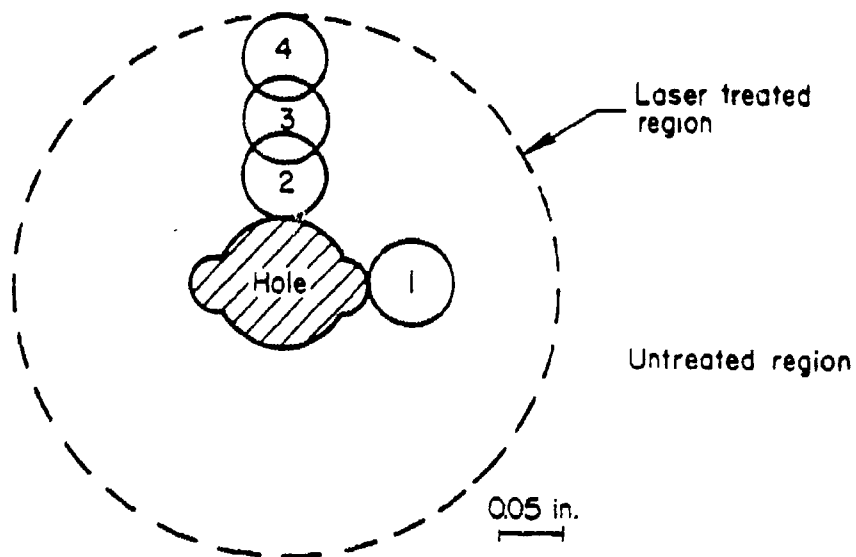
It is believed that a principal contributing factor to the enhanced fatigue life after laser shocking is the presence of compressive residual surface stresses. These compressive residual stresses result from the shock-induced plastic strain which is presumed to be largest at the specimen surface and to decrease in magnitude below the irradiated surface. This is similar to the effect of shot peening.

To determine the size, magnitude, and depth of the residual stresses caused by laser shocking, two specimens were laser shocked and residual stresses were measured by X-ray diffraction procedures. In one of these, a hole of the same shape used in the crack propagation specimens was drilled before laser shocking (Figure 16a). In the other, a round hole similar to that used for inserting fasteners was drilled after laser shocking.

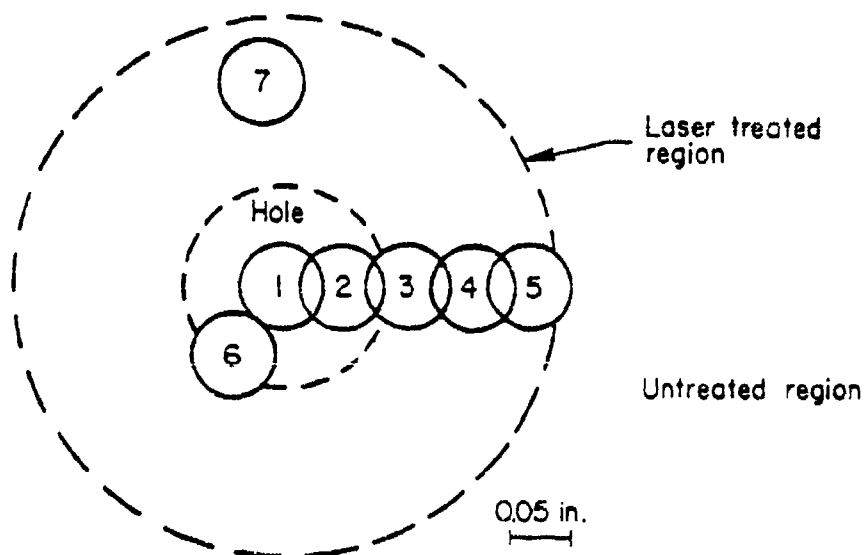
The results of all the residual stress measurements are given in Table 6. The results of the in-depth measurements are plotted in Figure 17 for the sites at which in-depth measurements are made. The compressive residual stresses are plotted as negative stresses.

The residual surface stress on an unshocked surface begins at about -22 ksi and decreases to -8 ksi 0.005-inch below the surface (Table 6, Figure 16). These stresses are probably quenching stresses developed during rapid quenching of the roller plate from the solution treatment temperature. It would be expected that the surface stresses due to rolling the plate would have been mostly relieved at the solution treatment temperatures.

The residual stresses in the laser-treated zone around the hole drilled before shocking are shown in Figure 17a. The points for Sites 1 and 2 at the edge of the hole include readings only to 0.005 inch deep because the electrolytic polishing undercut this region and prohibited accurate measurements at lower depths. While Site 1 shows a small decrease in residual stress below the surface, Site 2 shows an increase which is consistent with the increase also shown at Site 3. The residual stress pattern at Site 3 has a shape similar to those shown by shot-peened surfaces, an increase in compressive residual stress below the surface to a maximum just under the surface followed by a gradual decrease farther from the surface. Eventually, the residual stress will become a tensile stress at greater depths as is the case with



a. Hole drilled before laser shocking



b. Hole drilled after shock

Figure 16. The location of the numbered sites at which the residual stress measurements were made in the laser-treated region

TABLE 6. SUMMARY OF RESIDUAL STRESS RESULTS BEFORE AND AFTER SHOCKING

Depth Below Irradiated Surface, inch	Designation of Measurement Site <sup>a</sup>							Not Shocked <sup>d</sup> ksi ksi	
	1	2	3	3 (Opposite Surface)	4	5	6		
	ksi	ksi	ksi	ksi	ksi	ksi	ksi	ksi	ksi
Hole Drilled Before Laser Shocking (Figure 16a) - All Stresses are Tangential Stresses									
On surface	-51.4 <sup>b</sup>	-45.1 <sup>b</sup>	-45.6		-66.5				
-0.005	-46.5	-75.2	-88.2		-1.2				
-0.010			-42.4		-12.6				
-0.017			-17.1		+7.2				
-0.025			-11.8		-31.7 <sup>c</sup>				
-0.035			-9.9		+2.9				
Hole Drilled After Laser Shocking (Figure 16b) Before Drilling Hole									
On surface, radial	-69.4	-79.6	-85.6		-68.7	-44.1 <sup>e</sup>			
On surface, tangential	-52.8	-69.4	-71.4	-71.1		+22.0 <sup>e</sup>	-34.5	-62.2	
						+22.7			
						+25.5			
After Drilling Hole - All Stresses are Tangential Stresses									
On surface			-78.8	-59.9	-66.3	-14.8	-44.0	-23.1	-20.8
-0.006			-60.7		-58.4	-15.7	-56.6	-8.2	
-0.011			-58.6		-53.8	-19.6	-34.9		
-0.015			-36.2		-41.9	-6.8			
-0.025			-12.4			-22.7			
-0.035			+11.6			-27.9			

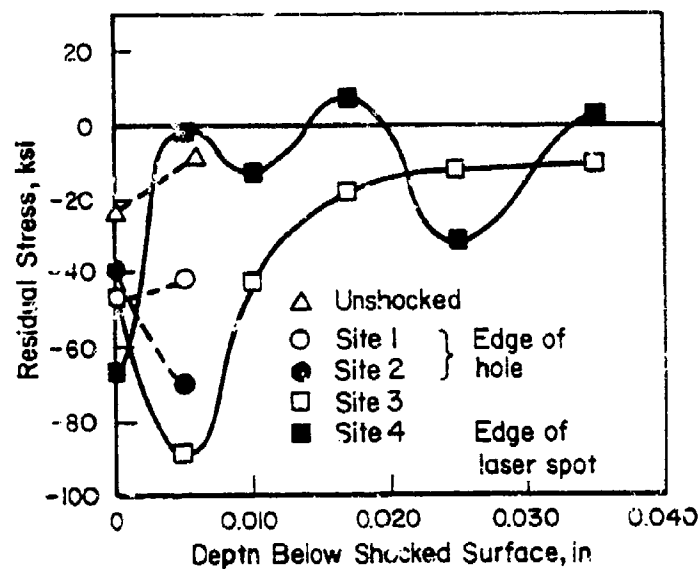
<sup>a</sup>The measurement sites refer to those shown in Figure 16.

<sup>b</sup>These stresses are too high by approximately 6 ksi because they cannot be corrected for the material removed.

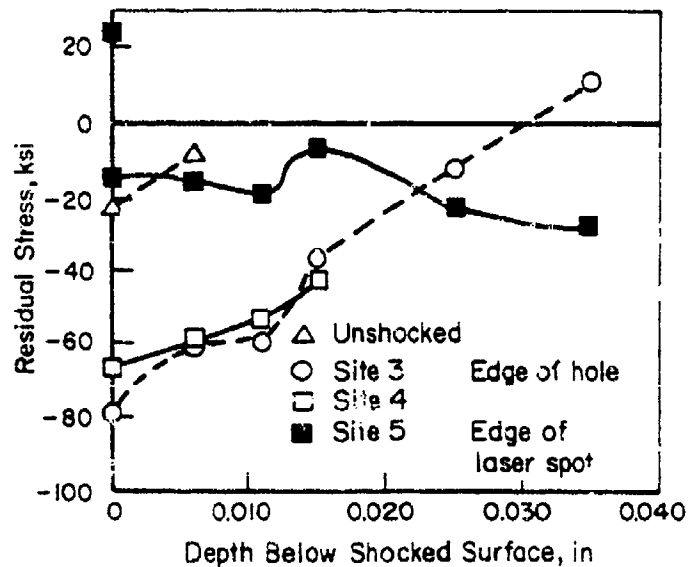
<sup>c</sup>This value is suspect.

<sup>d</sup>The unshocked measurements were taken at distances of 1.75 and 1.25 inches from the edge of the laser irradiated spot.

<sup>e</sup>These are three independent measurements on the same site with the specimen removed and replaced between each measurement.



a. Hole drilled before laser shocking



b. Hole drilled after laser shocking

Figure 17. In-depth residual stress distribution at the sites shown in Figure 16



shot peening. Site 4, just inside the edge of the laser-treated zone, shows that there exists a rather complex distribution of residual stresses at the perimeter of the shocked region which is unlike that at Site 3.

The sub-surface distribution of stresses is different when the hole is drilled after laser shocking (Figure 17b). Neither Site 3 nor Site 4 shows the stress maximum below the surface, although there may be a maxima between the surface and 0.005 inch below the surface. Instead, the compressive residual stress falls off continuously with depth and becomes tensile at about 0.030 inch below the surface. It is possible that the lack of the maximum in residual stress below the surface, like that in Figure 17a, was caused by stress relaxation occurring when the hole was drilled. However, on the basis of only two specimens, no definitive analysis of this effect can be made. Site 5, at the edge of the laser-treated region, again shows a rather complex stress distribution but remains compressive to 0.035 inch deep in contrast to the cyclic compressive-tensile variation shown at the similar position, Site 4, Figure 17a. The surface tensile stress data point included for Site 5 is the measurement made before drilling the hole.

It is possible that some of the variations observed with increasing depth at the sites on the edge of the laser-shocked zone are due to a small repositioning error occurring while setting the specimen up for successive measurements. At the edges of the shocked zone, where the stress gradients in the surface are very large, this factor could cause a significant variation from measurement to measurement.

Another point of interest is the variation in surface residual stresses across the laser-shocked region. This variation is shown in Figure 18 along the radius of the laser-shocked spot, both before and after drilling the hole. Radial stresses are also shown before drilling the hole. The surface stresses are relatively uniform across the spot and fall off rapidly at the edge of the shocked region. Thus, most of the laser-shocked surface is effectively placed in compression. The outside site actually shows a tensile residual stress before drilling the hole. After drilling, the surface stresses show essentially no change except for the outside site, Site 5 (the change in the outside stress could be a change due to repositioning the beam).

On the basis of these surface stresses and the fact that the specimens were shocked symmetrically on both surfaces at once, a rough estimate of the

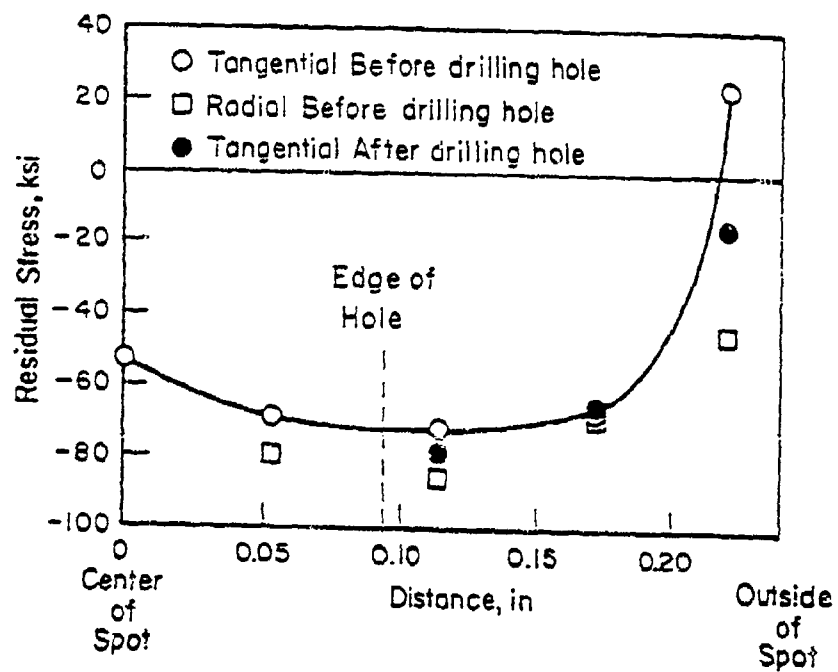


Figure 18. The distribution of surface residual stresses across the radius of the laser-shocked region

residual tensile stress distribution in the midthickness region of the specimens can be made. This was done as shown in Figure 19, where the measured stress distribution below the surface is plotted at both surfaces of the 0.25-inch-thick plate. In the midthickness region where the residual stresses were not measured, possible tensile stress distributions were dashed in to illustrate the possible magnitude of the tensile stresses. The dashed lines were drawn to balance the stresses by making the areas under the tensile and compressive portions of the curve equal.\* These dashed lines indicate that interior tensile stress levels might lie between 20 and 40 ksi at Site 3 for the hole drilled before shocking (Figure 19a) and somewhat lower, less than 20 ksi, at a similar site (Site 4) when the hole is drilled after shocking (Figure 19b). These figures are meant to serve only as illustrations to provide a perspective for the residual tensile stresses which might exist in the midthickness of the specimens laser shocked with a split beam.

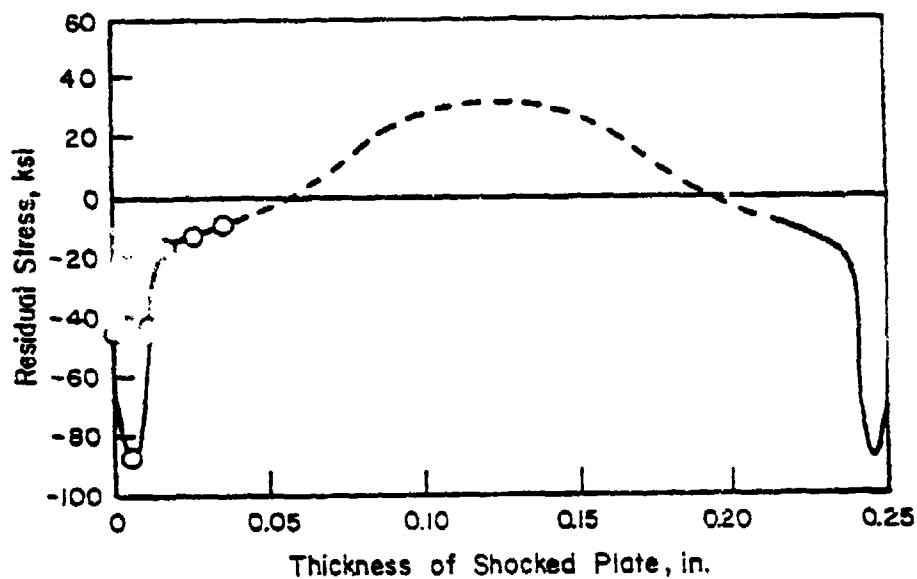
The residual stresses for Sites 6 and 7 reported in Table 6 are lower than comparative Sites 2 and 4, respectively (Figure 16b). This may indicate that the slight bumps that sometimes occur on the surfaces of laser-shocked zones may be indicators of areas of incomplete coupling whereby full shock pressures are not generated.

The highest residual compressive stresses of about 80 ksi are above the yield strength of 7075-T651 and are at the level of the ultimate tensile strength for this alloy.\*\* This indicates enough plastic deformation occurred during laser shocking to increase the flow stress of the surface layers to this level and prevent relaxation of these stresses to lower levels. It appears that the strain hardening induced by the laser shocking is quite effective, inhibiting relaxation of high residual stresses in the surface layers. Also, the compressive stresses extend for a significant distance below the surface, down to at least 0.035 inch for the drill before shock case and to 0.030 inch for the drilled after shock case. Funding limitations did not allow confirmation of these conclusions for the 2024 alloy.

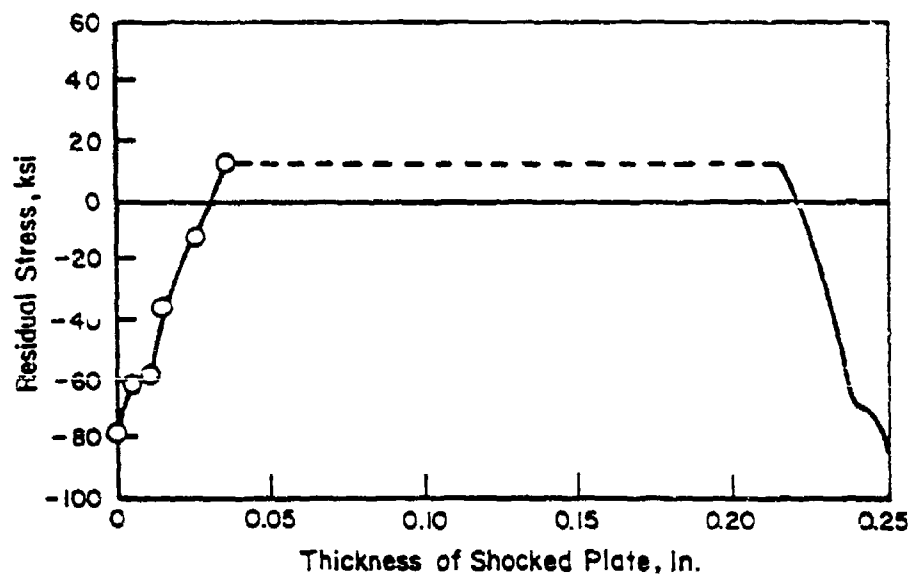
---

\* This will be approximately correct away from the edge of the hole and edge of the laser shocked region. Since the plastic deformation causing the residual stresses decreases with increasing depth below the surface, the residual stresses will balance through the thickness.

\*\* Tensile tests on two specimens from this same lot of material gave average room temperature tensile properties of 76.4 ksi, 0.2% offset yield strength, 82.3 ksi ultimate strength, and 21.0% of total elongation.



a. Hole drilled before shocking at Site 3



b. Hole drilled after shocking at Site 4

Figure 19. Possible tensile stress distribution in the mid-thickness region of the shocked specimens

### 3. Metallurgical Studies

#### a. Fracture Surfaces

The fracture surfaces of selected specimens were examined by scanning electron microscopy. These specimens were all crack propagation specimens selected from the initial phase of the program. The specimens selected and the rationale for selection are given in Table 7.

The results of these examinations showed that with few exceptions the crack initiation sites occurred along the hole in the central half to two-thirds of the specimen thickness. No failures occurred where the hole intersected the specimen surface. Thus, radiusing the hole edge would have no effect on the fatigue life.

The major findings of the failure surface investigation was the effect laser shocking had on the pattern of crack propagation. The appearance of the crack initiation and propagation regions in the laser-shocked zone is shown in Figure 20. A comparison of the "river-line" patterns on these micrographs shows that there are significant differences between the shocked and unshocked specimens.

These differences are best seen by the drawings presented in Figure 21. The solid lines on these drawings trace the flow of the river lines on the micrographs shown in Figure 20. Comparison of Figures 20a and 20b shows that the curvature of these lines is different for the shocked and unshocked fracture surfaces. Since these river lines are often presumed to be perpendicular to the crack front, crack-front contours can be drawn using these lines by drawing contours perpendicular to the solid lines. This is shown by the dashed lines in Figure 21.

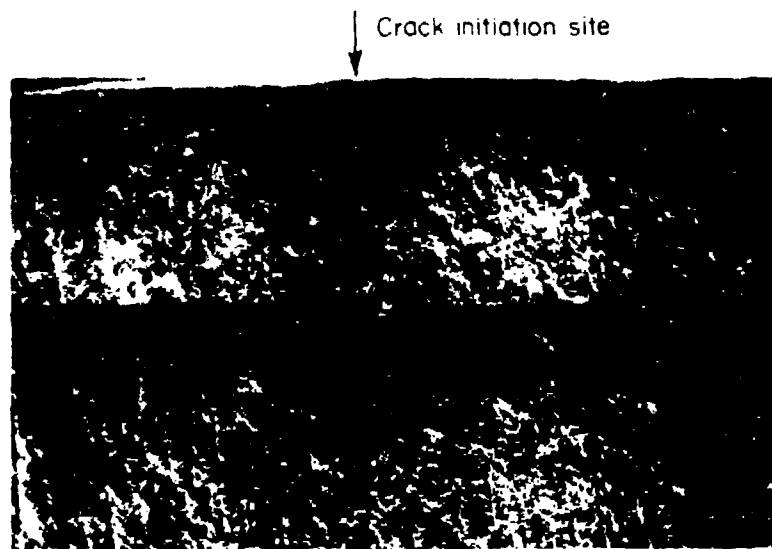
Comparison of the crack-front contours represented by the dashed lines in Figure 21 now shows the difference in crack propagation characteristics for the various laser shocking configurations. These show that for the unshocked specimen (Figure 21a), the crack front rapidly straightens out to propagate uniformly along the cross section of the specimen. However, for the specimen shocked by the split beam (Figure 21b), the crack is constrained to propagate in the midthickness region of the plate by the high residual compressive stresses near the surface of the specimen. This constraint

TABLE 7. FRACTURE SURFACES EXAMINED BY SCANNING ELECTRON MICROSCOPY

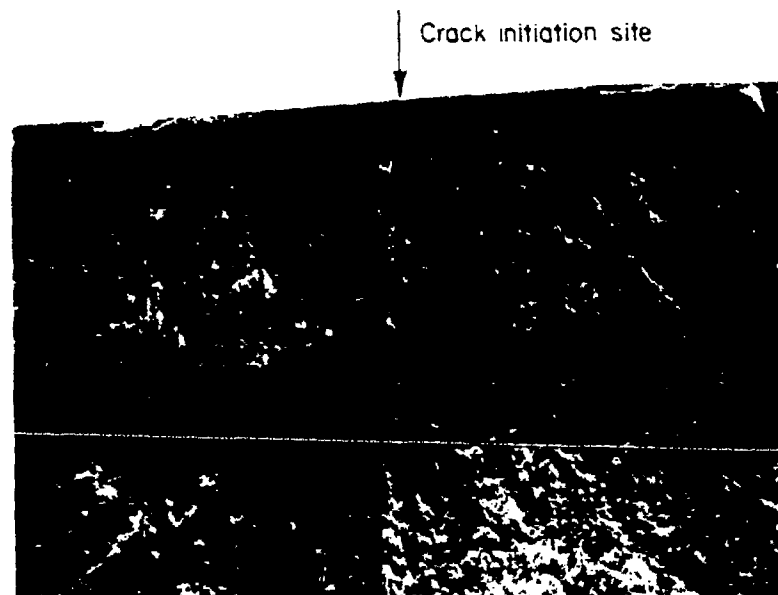
Specimen <sup>a</sup> Number	Special <sup>b</sup> Conditions	Fatigue Life, cycles	Rationale for Selection
1 (A)	Low power density, $\phi_1$ , Lowest stress, 13 ksi	193,220	Short life
2 (A)	$\phi_1$ , step up stress 13 to 14 ksi	2,265,000	Long life
3 (A)	$\phi_1$ , 14 ksi	497,580	Compare to 1 (A) and 2 (A)
7 (B)	Thin section, 0.125 inch	713,590	Special con- ditions
8 (B)	Radius hole edge	278,990	"
9 (B)	Duplicate of 8 (B)	123,950	"
10 (A)	Drill before shock	357,090	"
11 (A)	Duplicate of 10 (A)	237,290	"
14 (A)	Single side shock		"
15 (B)	Duplicate of 14 (A)	> 88,520	"
21 A (B)	Not shocked	261,450	"
22 (A)	Not shocked	89,390	"
42 (A)	Precracked	139,260	"
43 (A)	Precracked. 24 ksi	63,650	"

<sup>a</sup> The letter in parenthesis refers to the hole designation.

<sup>b</sup> All tests were made at a maximum stress of 15 ksi and are on 0.25-inch-thick specimens unless otherwise noted.

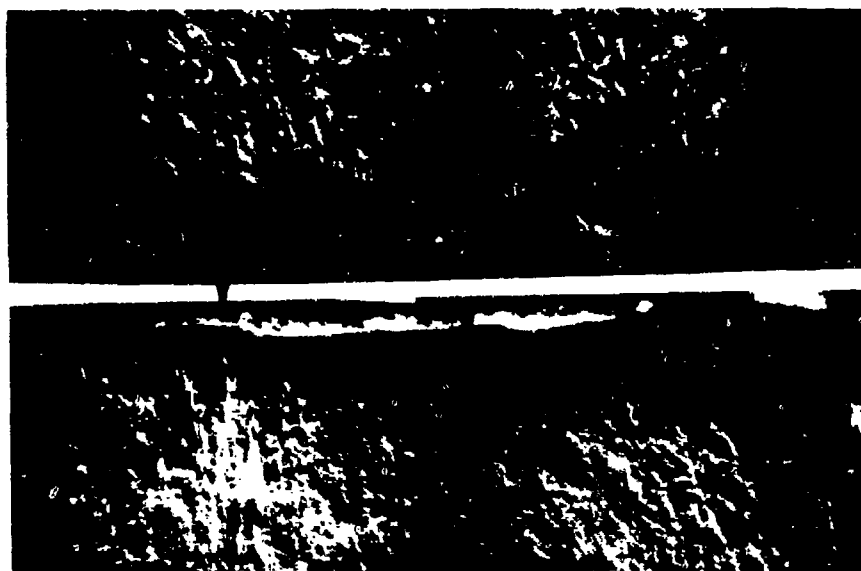


a. Unshocked, Specimen 21A

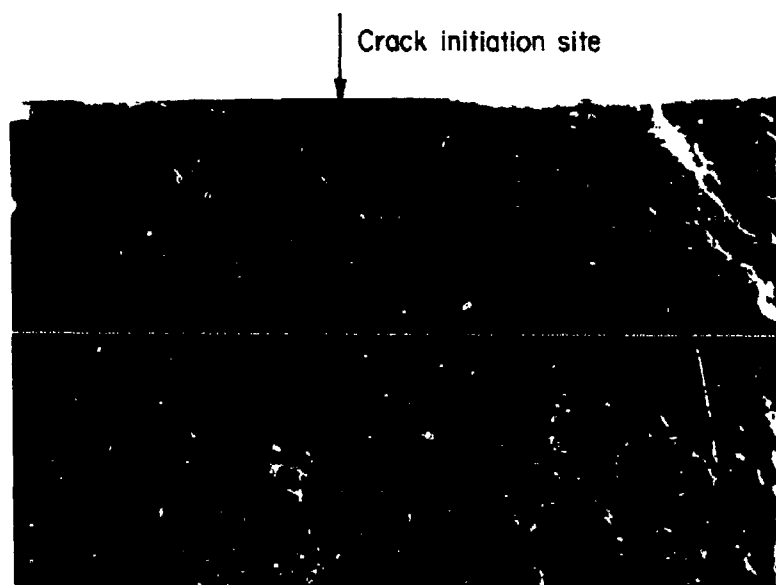


b. Shocked both sides, split beam, Specimen 8S

Figure 20. Fracture surfaces including the crack initiation sites and propagation regions through the laser shocked zone



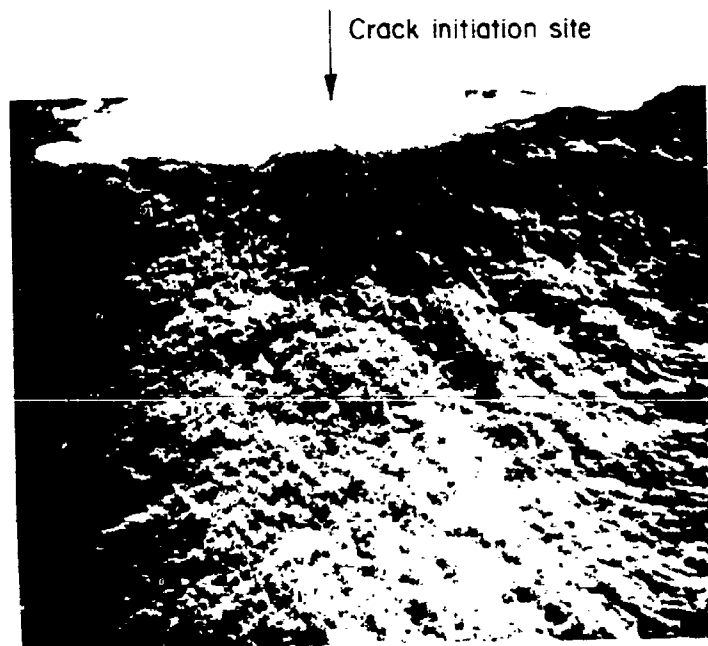
c. Shocked one side only, Specimen 14A, showing the pattern on both sides of the hole



d. Precracked and shocked both sides, Specimen 43A

Figure 20. (Continued)





e. Shocked both sides, thin section,  
0.125 inch

Figure 20. (Concluded)

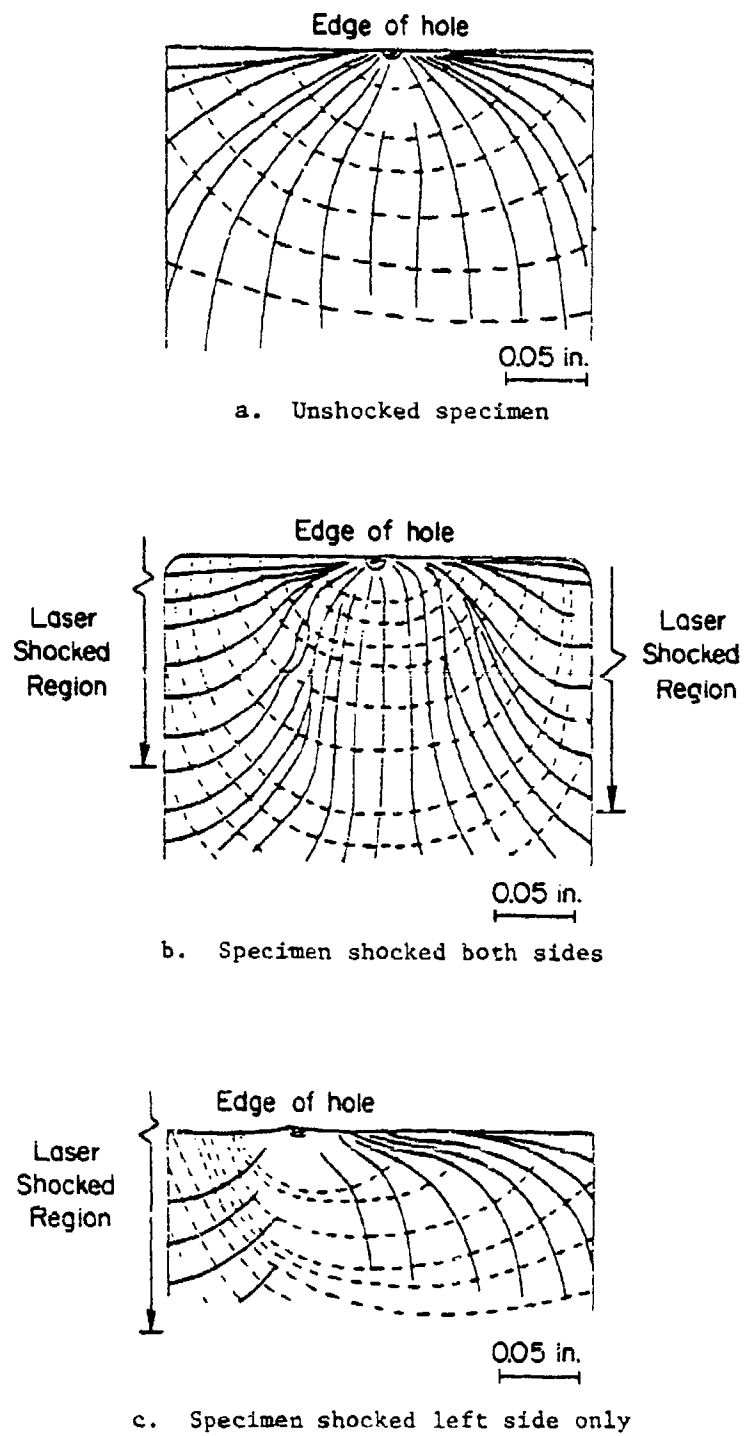
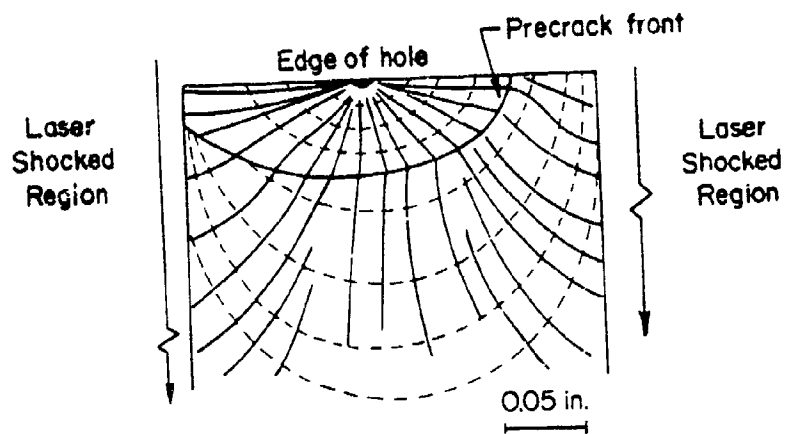
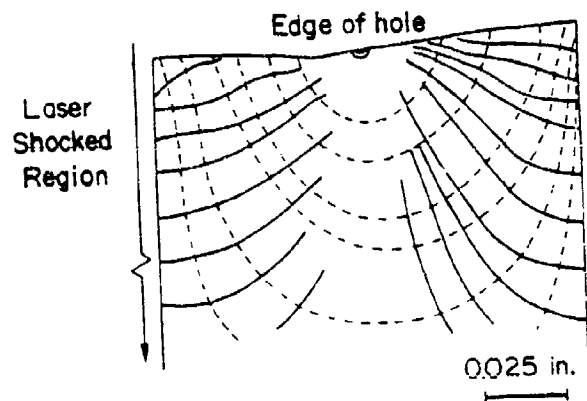


Figure 21. Fracture surface river line patterns and crack front contours



d. Precracked specimen  
shocked both sides



e. Thin (0.125 in. thick)  
specimen shocked both sides

Figure 21. (Concluded)

retards the crack propagation rate relative to the unshocked conditions by causing the crack to, in effect, "tunnel" through the laser-shocked zone. This pattern is also reflected in the specimens shocked on one side only (Figure 21c) where the shocked side shows the crack-propagation constraints (Figure 21b) and the unshocked side shows the straightening of the crack front (Figure 21c). The precracked specimen, Figure 21d also shows both aspects of crack propagation behavior. In the precrack propagation region (inside the solid contour line), the crack front was straightening out but after laser shock, the crack assumed the more elliptical shape representative of the laser-shocked specimens.

The effect of a thinner cross section is shown in Figure 21e where the cross section of Specimen 7B, 0.125-inch thick, is shown the same size as that of the 0.25-inch-thick specimens. Comparison shows that the compressive stress region occupies a larger proportion of the thickness in the thin section compared to the thick section and has a greater tendency to channel the crack within the midthickness region. The compressive stress region here is taken to be proportional to the region where the river lines are not parallel to the sides of the specimen. This effect could cause slower crack propagation in the thin sections and be the cause of the longer life noted for the thinner specimens compared to the 0.25-inch-thick specimens.

This investigation of the fracture surfaces of the crack propagation specimens then suggests the following behavior. Crack initiation tends to occur at the hole in the central portion of the through-thickness dimension. After initiation in laser-shocked specimens, the crack tunnels through the laser shocked zone for some distance before breaking through to the surface. It may, in some cases, tunnel completely through the laser-shocked zone before "popping" through to the surface. Although no definitive evidence for this was observed, observation of crack lengths during fatigue testing of shocked specimens often showed the cracks to suddenly become visible beyond the laser-shocked zone. It is not known whether they were surface connected earlier, but were held too tightly closed by the surface compressive stresses to be visible. The crack openings were always much less in the laser-treated zone than outside it, even after removal from the testing machine.

This sequence of events indicates it would be very difficult to identify the occurrence of crack initiation. The crack front may have

propagated a significant distance in the specimen before surface intersection occurs (Figures 21b and e) compared to the unshocked condition (Figure 21a). Thus, the cycles to crack initiation in the laser-shocked specimens must be viewed with caution.

These results, taken together with the residual stress measurements, show that crack propagation in the laser-shocked specimens is restrained by the surface residual compressive stresses, but may be aided by the residual tensile stresses in the midthickness region. Because of this, an optimization of the process may require balancing these two forces to minimize the crack propagation rate.

#### b. Microstructure

The microstructures developed by laser shocking and subsequent fatigue were examined in six crack propagation specimens by transmission electron microscopy. The specimens examined and the rationale for their selection are shown in Table 8.

Thin foils were prepared from the surface and the midthickness regions at the sides of the holes towards the ends of the specimen, i.e., the sides of the hole 90 degrees from the crack initiation sites. These sites were selected to minimize the effects of fatigue damage, to assess in the short-lived specimens 1(A) and 3(A) whether there was significant evidence of laser-shock-induced plastic strain.

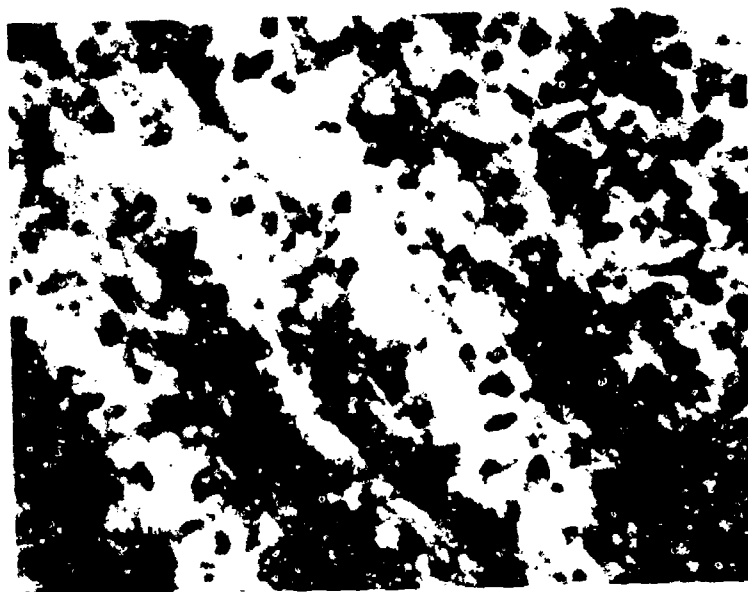
The result of this investigation was that evidence of strain hardening was seen in all the specimens examined, even in the unshocked specimen. Thus, much of the dislocation substructure seen in the specimens is actually fatigue-induced damage. The typical appearance of the dislocation structures is shown in Figure 22 for the shocked and unshocked conditions. Both show a heavy dislocation density which is not present in the unshocked condition before fatigue testing.

The dislocation structures of the laser-shocked and unshocked specimens appear so much alike after fatigue that it would not be possible to differentiate between them. Both conditions show regions of heavy shear bands and regions of more uniform but dense dislocation distribution. The presence in the unshocked specimens indicates these are developed during fatigue testing and not by laser shocking.

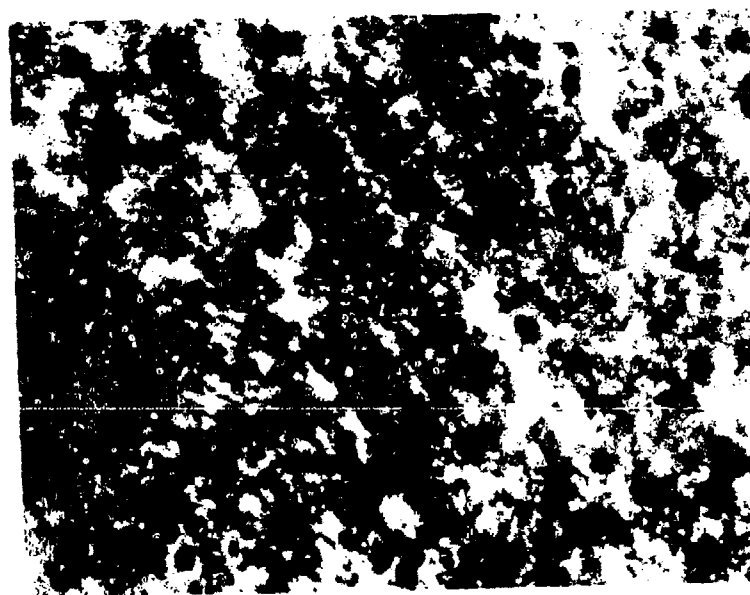
TABLE 8. SPECIMENS EXAMINED BY TRANSMISSION ELECTRON MICROSCOPY

Specimen Number	Condition <sup>a</sup>	Fatigue Life, cycles	Rationale for Selection
1 (A)	Split beam, $\phi_1$ , 13 ksi	193,220	Low shock pressure short life
2 (A)	Split beam, $\phi_1$ 13 to 13.5 to 14 ksi	2,265,000	Low shock pressure long life
3 (B)	Split beam, $\phi_1$ 14 ksi	497,580	Low shock pressure
2A (B)	Split beam, $\phi_*$ 15 ksi	102,000	High shock pressure
3A (A)	Split beam, $\phi_*$ 15 ksi	76,000	Duplicate of 2A (B)
21A (B)	Not shocked	261,450	Not shocked

<sup>a</sup>  $\phi$  indicates the power density level, re. Table A-5.



a. Unshocked specimen



b. Laser shocked specimen

Figure 22. Transmission electron micrographs of the micro-structure in specimens after failure

Thus, no judgment concerning the possible relative intensity of the laser shocking treatment to explain the difference in fatigue lives of Specimens 1, 2, and 3 can be made on the basis of the transmission electron microscopy results. Although the region for obtaining the thin foils was selected to minimize the obscuring effects of subsequent fatigue deformation, these effects were still sufficient to inhibit a clear differentiation between the shocked and unshocked conditions.

#### 4. Fatigue-Crack Initiation

Fatigue life consists of cycles to crack initiation and cycles of crack growth. Generally, cycles to crack initiation share a major portion of the total life. Test data verifies this point for the unshocked specimens. Detection of the time when crack initiation occurred for the shocked specimens was not possible due to the crack tunneling. It is expected from the tensile residual stress measurement found in the shocked specimen midthickness region that crack initiation occurs much earlier for the shocked condition. An analysis will be presented showing the tensile residual stress effect on crack initiation.

The presence of a tensile residual stress in the shocked specimens will act to increase the mean stress, thereby lowering the fatigue life. Making the assumption that crack initiation is a major portion of the life, one can conclude that crack initiation will occur much earlier in the shocked specimens. The fact that shocked specimens have as long or longer fatigue life than unshocked specimens indicates that the crack-growth rate in shocked specimens is reduced.

##### a. Residual Stress Effect on Mean Stress and Stress Amplitude

Study of the fracture surfaces of the laser-shocked specimens indicates that crack initiation and crack propagation appear to be influenced by the residual stresses produced from the laser shock process. Compressive residual stresses surrounding the initial flaw, and located at both surfaces, tended to confine crack initiation and initial crack growth to the midthickness region where tensile residual stresses are produced from the laser shock process. Since stress equilibrium must be satisfied, compressive residual stresses are equalized



by an appropriate distribution of tension residual stresses. The residual stresses that most affect crack initiation and crack propagation are those that are circumferential to the hole normal to the crack surface and at the point of highest stress concentration (which happens to be at the hole). An analysis of the effects of these residual stresses on crack initiation will be presented in this section.

Figure 23 presents a concentric laser shock spot around a circular hole. Figure 24 is an enlarged through-the-thickness slice of the "element" taken from the laser-treated region as shown in Figure 23. Near the surface, compressive stresses are shown similar to those measured in laser-shocked specimens (Figure 18). To balance the element in equilibrium, tensile stresses must be applied in the midthickness region. This occurs in both the circumferential and radial direction, with the radial stresses approaching zero at the hole surface.

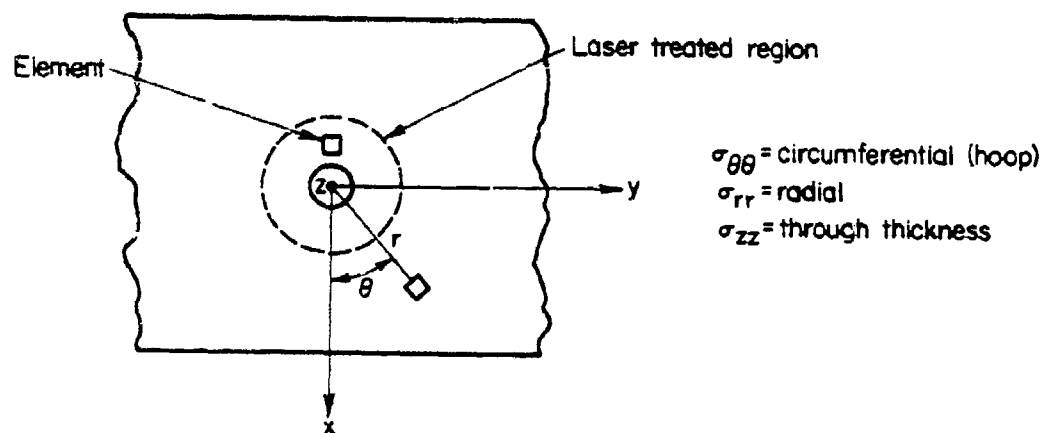


Figure 23. Concentric laser shock spot

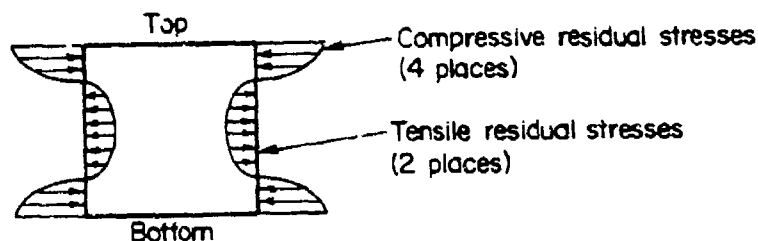


Figure 24. Internal residual hoop stress profile for an element in the laser-treated region

Not all compressive residual stresses are necessarily reacted by mid-thickness tensile stresses. Some of the compressive residual stresses in the circumferential direction may be balanced by tensile residual stresses outside the laser shock zone. If a cut is made in the  $x - z$  plane of Figure 23, the stress distribution could be similar to that shown on the cut edge sketched in Figure 25. This distribution is what causes the uncertainty in the measured in depth stress distribution at the edge of the laser shocked zone in Figures 17 and 18. These residual stresses contribute to the increase of the positive mean stress in the midthickness and the decrease in the negative mean stress near the surface during cyclic loading.

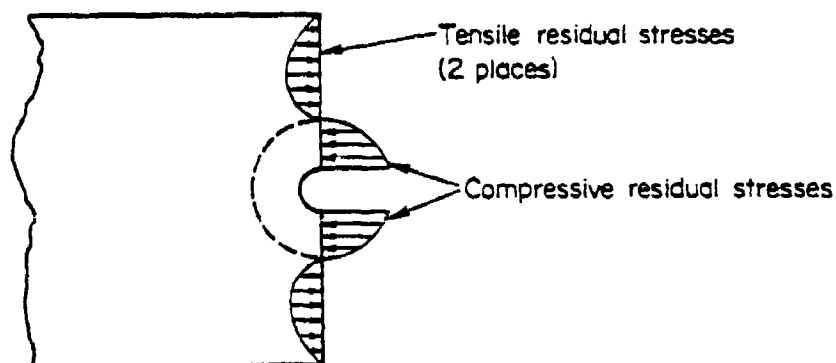
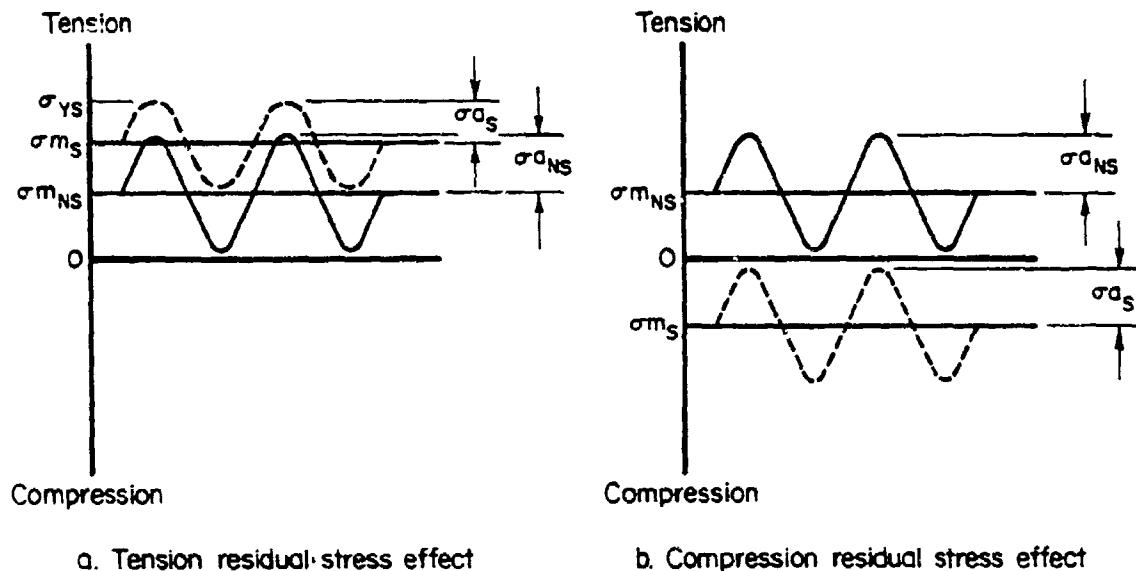


Figure 25. Elemental slice through the compressive residual hoop stress zone

The residual stress effect on the mean stress amplitude during stress cycling is presented in Figure 26. The solid curve is the applied stress and the dashed curve represents the combination of applied and residual stress. The tensile residual stress effect in Figure 26a shows both the increase in the mean stress and the possible decrease in the stress amplitude as the maximum stress approaches the yield stress. Inversely, the compressive residual stress in Figure 26b has the effect of lowering the mean stress with no influence on the stress amplitude until yielding occurs in the tensile residual stress zone. The compressive residual stress combined with the externally applied tensile stress may remain compressive.



$\sigma_{mNS}$  = mean stress of nonshocked condition  
 $\sigma_{mS}$  = mean stress of shocked condition  
 $\sigma_{aNS}$  = stress amplitude of nonshocked condition  
 $\sigma_{aS}$  = stress amplitude of shocked condition  
 $\sigma_{ys}$  = yield stress

Figure 26. Laser-shock effect on mean stress and stress amplitude

It can be deduced from the above discussion that those areas containing residual compressive stresses will require higher and/or more cyclic load applications to initiate a fatigue crack than an area containing no residual stresses. Conversely, one can expect crack initiations to occur sooner in those areas experiencing a tensile residual stress.

## 5. Fatigue Crack Propagation

Large improvements in the fatigue properties of the laser-treated 2024 aluminum alloy and the thinner (1/8 inch versus 1/4 inch thick) 7075 aluminum alloy were observed. The thicker 7075 alloy specimens showed only modest improvements in fatigue properties of about a factor of 2 to 3 over unshocked specimens or no improvement at all. It is believed that residual stresses introduced in the test specimens from laser shocking are responsible for the changes in fatigue properties. The presence of these residual stresses, in the laser-treated specimens, are confirmed by fracture surface observations and X-ray diffraction stress measurements. A theoretical analysis predicts that time to crack initiation in the shocked specimens is less than in the unshocked specimens. To account for the relative cycles to fracture in comparing the test results of the unshocked and shocked specimens, a slower crack growth rate in the shocked specimens is suspected.

A discussion of the crack propagation mechanism through the laser-shocked region and methods to improve fatigue properties beyond those observed will now be presented.

### a. Fracture Mechanics Analysis

As a result of the residual tension stress at the midthickness, analysis has indicated that crack initiation possibly occurs earlier in the shocked specimens than in the unshocked specimens. The likely mechanism responsible for the as-long or longer life in the shocked specimens is the slower stable fatigue-crack-growth rate. Linear elastic fracture mechanics provides a method for explaining the mechanism of fatigue-crack propagation.

Mathematical expressions utilizing empirically derived material constants have been developed to describe fatigue-crack growth. The rate of fatigue-crack propagation per cycle,  $da/dN$ , is primarily influenced by the stress-intensity factor range,  $\Delta K$  (where  $\Delta K = K_{\max} - K_{\min}$ ).

Stress intensities for various common geometries are available. An approximate solution <sup>(8)</sup> for a plate in tension with a finite width and central through notch is shown in Figure 27. This solution closely describes that of the unshocked specimens tested in this program (see Figures 2 through 5).

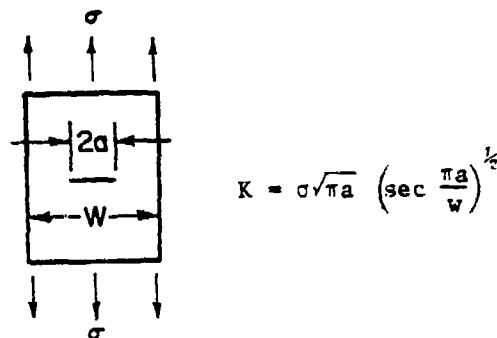


Figure 27. Stress-intensity solution for a center-notched panel of finite width

Complications arise in the shocked condition. No longer is the crack a through crack. The compressive residual stresses force the crack to "tunnel" through the midthickness region. A cross section taken through the specimen and showing the crack shape is shown in Figure 28. Due to the complex nature of the shocked specimen crack geometry and residual stress field, a rigorous solution will not be presented at this time. The following presentation is to discuss the approximate flaw shape mechanism arising from first order effects.

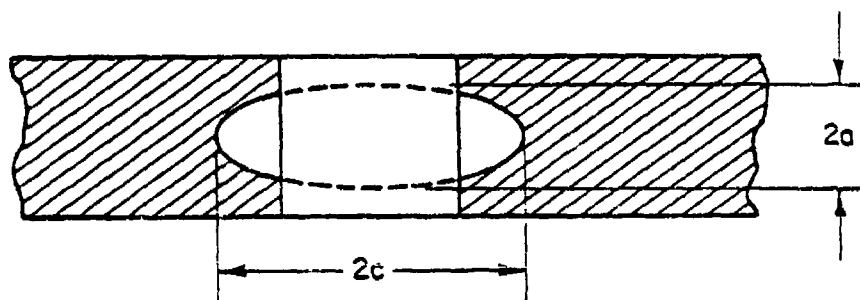


Figure 28. Crack shape in laser-shocked specimen

Assuming the flaw is idealized as an embedded elliptical crack, the effect on the stress intensity for a change in the crack aspect ratio,  $a/2c$ , may be observed. The stress-intensity solution for an embedded elliptical flaw was proposed by Irwin<sup>(9)</sup> and is illustrated in Figure 29. The major point of interest is for  $\theta = 0$  and  $\theta = \pi/2$ . The stress-intensity solution shown in

Figure 29 reduces to the form

$$K = \frac{\sigma \sqrt{\pi a^2/c}}{\phi} \text{ for } \theta = 0 \quad (1)$$

and

$$K = \frac{\sigma \sqrt{\pi a}}{\phi} \text{ for } \theta = \pi/2 \quad (2)$$

In a rigorous solution other factors should be added to the above expression to describe such effects as stress gradients and other geometry factors. For example, the stress in Figure 29 is the remote constant stress; whereas, in the laser-shocked specimens, there are locally varying stresses.

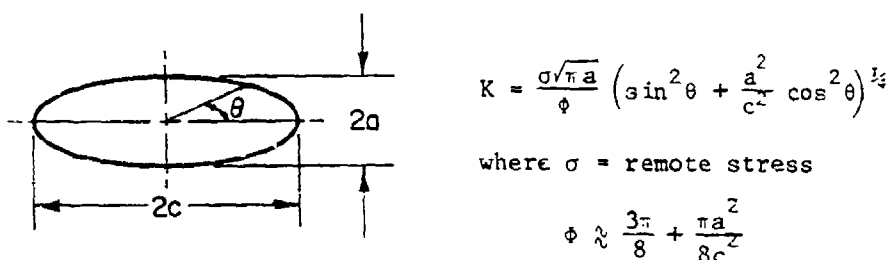


Figure 29. Embedded elliptical flaw stress-intensity solution

The effect of the embedded elliptical flaw aspect ratio,  $a/2c$ , is shown in Figure 30. In this figure the ratio  $K/\sigma\sqrt{\pi a}$  is plotted as a function of eccentricity  $2a/2c$ . For an aspect ratio of 1.0, the stress intensity is the same for  $\theta = 0$  and  $\theta = \pi/2$  (the ellipse becomes a circle). [But for decreasing aspect ratios ( $a/c$ ), the stress-intensity factor increases at  $\theta = \pi/2$  whereas it decreases at  $\theta = 0$ .]

Figure 21 presented sketches of actual crack front shapes developed during fatigue cycling. These show the crack extending in the midregion of the plate while the residual surface stresses retard crack growth near the plate surface. As the aspect ratio  $a/2c$  decreases with the crack extension, it is seen from Equation 1 or Figure 29 that the stress intensity factor for  $\theta = 0$  should decrease. Provided that the stress field is not significantly altered by the fatigue process, this would lead to a slowing of the crack extension or even crack arrest if  $K$  fell low enough.

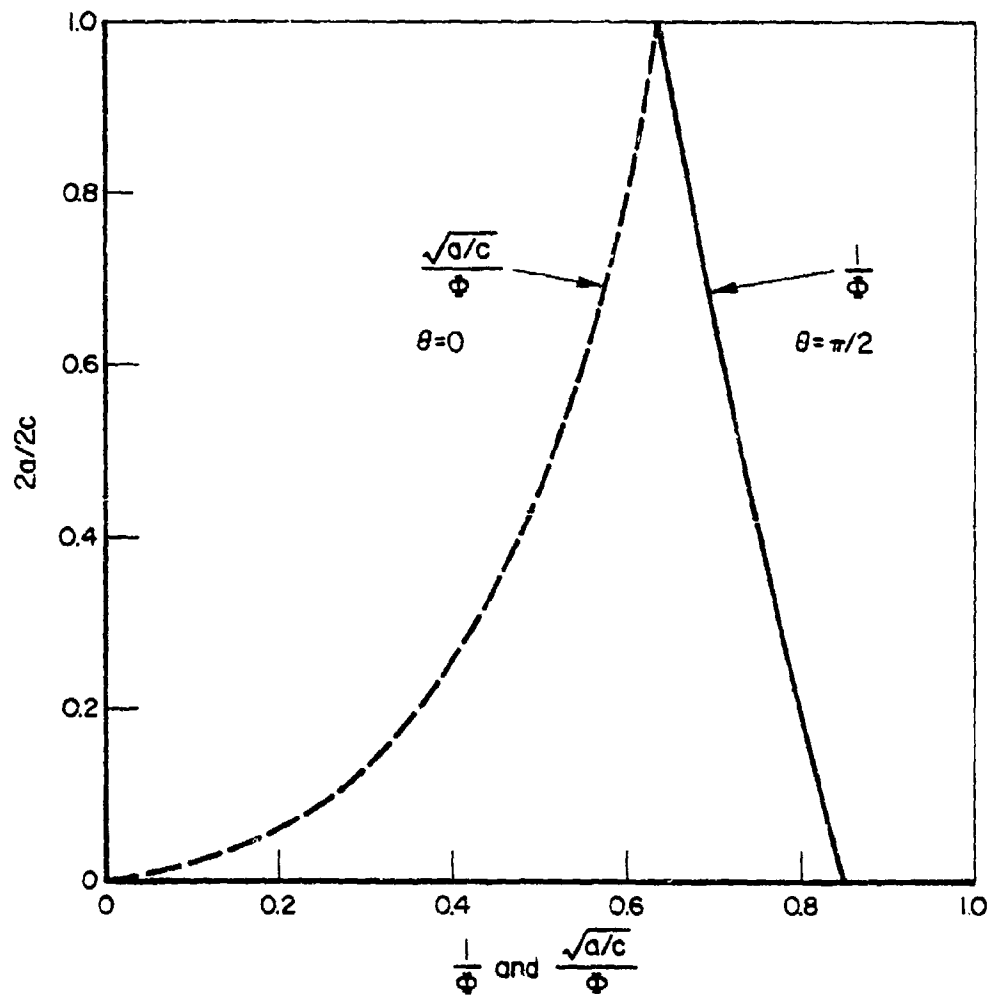


Figure 30. Embedded elliptical flaw aspect ratio effect

At the same time as the aspect ratio decreases, the stresses at the trailing edges of the crack near the surface will increase (Equation 2). However, crack growth to the surface is prevented as long as the compression residual stresses are sufficient. Eventually, as is seen in Figure 29, the stress intensity factor increases on the trailing edges of the crack to a point that it exceeds the local residual stresses by a sufficient amount to cause crack growth. The crack then will break through to the surface.

#### b. Summary of Analysis

This program has determined the probable laser shock mechanism affecting fatigue and fracture. Tensile residual stresses in the midthickness may cause cracks to initiate earlier and the compressive residual stresses force the crack to tunnel in the midthickness region. This restriction on crack shape effectively decreased the crack growth rate.

It is theoretically possible that a combination of laser spot size and penetration depth may be produced which gives an optimum in total fatigue life. By locally measuring striation spacing in a scanning electron microscope, or by cycling a specimen and periodically producing marker bands on the fracture surface by a change of cycling frequency, crack growth could be traced as a function of cycles as shown in Figure 31. Then the local stress-intensity solution for the shocked specimen can be estimated by using the known  $da/dN$  versus  $\Delta K$  plot as a calibration for the measured local  $da/dN$  values in the laser-shocked specimens.

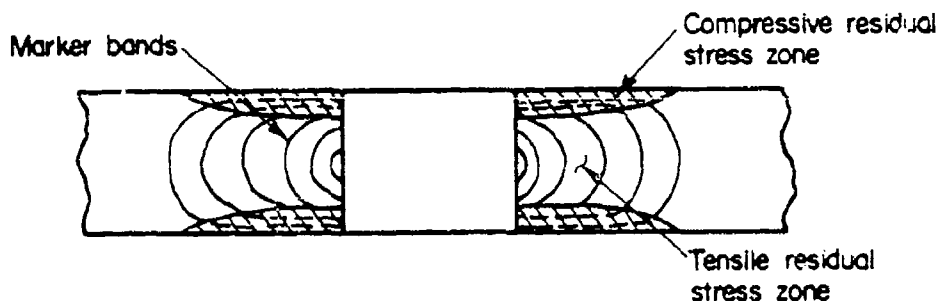


Figure 31. Crack-growth rate trace through use of marker bands



## 6. Summary of Results

A wide variety of test conditions were investigated in this program, both to identify major effects and to attempt to identify under what conditions laser shock conditioning would be most beneficial. As described earlier in this section, results were mixed. However, it appears possible to relate most of the observed fatigue behavior to the apparent residual stress state caused in the specimens by the laser shock. This residual stress is generated by the high intensity shock wave generated by the laser shot. The intensity is significantly above the dynamic flow stress of the aluminum and, hence, the aluminum is plastically deformed as the shock passes. After shock passage, the specimen is left in a complex state of residual stress in which the surface tends to be in compression while the interior probably is in tension. The magnitude and distribution of this residual stress state determines the fatigue life behavior of the specimen. However, if the amplitude of the fatigue cycle is sufficiently large that the combined load and residual stress exceeds yield over parts of the specimen, plastic flow will again occur in a direction that tends to break down the residual stress distribution and negate the crack retardation effects of the laser shocking.

It is clear that residual surface stresses can have a significant effect on fatigue. Compressive residual surface stresses as developed by shot peening, for example, can improve fatigue life. Tensile residual surface stresses such as those associated with welded joints are detrimental to fatigue life. Strain hardening which raises the ultimate strength and modifies the microstructure of the material would also influence the fatigue properties. In these laser shock experiments, we were not able to separate these two effects. However, the actual levels of the plastic strain are relatively low, normally a few percent at the peak pressures used in this program. Therefore, strain hardening is probably much less significant than the residual stresses in their effect on fatigue properties after laser shocking.

Significant differences in fatigue response were observed between the 7075 and 2024 alloys. The 2024 alloys showed a substantial fatigue life improvement at 15 ksi after laser shocking, whereas 7075 showed some improvement only in certain cases. Such a difference could result from the different strengths and behavior of the two alloys. The lower yield strength of 2024

compared to that of 7075 could have created a difference in the magnitude and distribution of the residual stress between the two alloys, with apparently more favorable effects in the 2024 specimens. Since the residual stresses were measured only in the 7075 specimens, a direct comparison of the different residual stresses between the two alloys cannot be made.

Another difference noted was that the 7075 specimens showed a benefit from laser shocking in the 40 ksi maximum stress flight-by-flight spectrum (Figure 11) but showed little or no benefit at the 15 and 17 ksi constant stress amplitudes. This could easily be attributed to the lower average stress level for the 40 ksi maximum stress flight-by-flight spectrum.

The precracked specimen results suggest that laser shocking does decrease the crack propagation rate. This is particularly clear in the 2024 specimens (Figure 12), but is also indicated in the 7075 specimens. For the 7075 alloys, the cycles to 0.45 inch crack length after laser shocking are greater than the crack propagation cycles in the unshocked specimens over the same distance for nearly all precracked conditions investigated (Figures 9, 10, 11, and 12).

It is suspected that crack initiation may have occurred earlier in shocked specimens compared to unshocked specimens because of tensile residual stresses along the hole surface in the midthickness region of the hole. In this case perhaps most of the total cycles to reach 0.45 inch were used in propagating the crack even in the non-precracked specimens. It would appear, however, that the crack propagation cycles are greater in the precracked specimens with larger laser-shocked zone than in the non-precracked specimens. How much of this decrease in apparent crack propagation rate can be attributed to the larger laser shocked zone ahead of the crack in the precracked specimens (Figure 6) and how much to the presence of the laser-shocked zone alone should be investigated further. Because of this apparent effect, an investigation should be made specifically of the effect of the length of the laser-shocked zone ahead of the crack. It is believed that a minimum laser-shocked zone length could be defined below which significant relaxation of the residual stresses by the hole surface and edge of the laser-shocked zone would occur. Laser-shocked zones greater than this length would be necessary to get an appreciable interaction of the crack front with the residual stress field. It is possible that a larger laser-shocked zone could increase the stress levels at which the fatigue

life is increased. This is because a residual stress field extending further from the hole may not be as susceptible to relaxation of these stresses by plastic deformation at maximum stress amplitude.

Based on these results, it is clearly necessary to further develop the requisite laser shock processing methods to control the magnitude and distribution of the residual stresses in a controlled manner. It should be possible to tailor the residual stress field developed by the process to obtain maximum benefit from inhibiting both crack initiation and propagation. For example, the surface of the hole could be put in compression to inhibit crack initiation, along with a compressive stress on the plate surface to inhibit crack propagation. There are many other alternative modifications to the laser-processing conditions to provide similar modifications of the residual stress fields which remain to be investigated.

The results of the low-load transfer, fastened joint specimens also show that the benefits of laser shocking decrease as the stress levels increase as expected from a residual stress viewpoint. Earlier work at Battelle on one and one-half dogbone, medium-load transfer, fastened joint specimens tested at 14 ksi constant stress amplitude showed orders of magnitude improvement in fretting fatigue life. This benefit was no longer present at 16.8 ksi. Examination of the fracture surfaces of these early specimens indicated that the failure mechanism of the shocked and unshocked specimens was the same. It is suggested that in the shocked specimens, the residual surface compressive stresses inhibited the surface cracks developed during fretting to propagate into the specimens. While this is effective at lower stress levels, at higher stress levels the residual stresses will be nullified and possibly removed locally by stress concentration induced yielding. The benefit of laser shocking will then decrease at higher stress levels.

## APPENDIX A

### 1. Detailed Listing of Test Results

#### a. Introduction

The experimental program was designed to investigate the effect of three different laser conditions on fatigue properties. In the initial phase of the program, screening tests were run at two different laser conditions. These conditions were designated  $\phi_1$  and  $\phi_2$ , where  $\phi_2$  was a more intense laser environment than  $\phi_1$ . Based on these tests, the one condition demonstrating the greatest improvement in fatigue properties was selected for further tests. This condition, which turned out to be  $\phi_2$ , was relabeled  $\phi_*$  for the remainder of the program. In the final stages of the program, tests also were run at a more intense laser condition ( $\phi_3$ ) than  $\phi_*$ .

In the early portion of the program, each laser test condition was defined solely in terms of laser power density, e.g.,  $\phi_1$ ,  $\phi_*$ , and  $\phi_3$  were given in W/cm<sup>2</sup>. Later in the program, it was determined that a more meaningful way to define the laser condition was the time integral of laser power density, which is the laser power density multiplied by the duration of the laser pulse. This parameter (energy density) is given in joules per cm<sup>2</sup>. The data presented in the following sections of this Appendix give both the laser power density and energy density to which each specimen was exposed as well as the duration of the laser pulse.

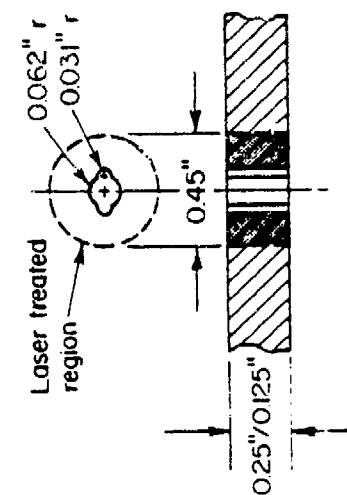
Examination of these data shows that the duration of the laser pulse varied by about a factor of two during the course of the program. This change in laser output conditions is due to variations in system performance. As seen from these data, change in pulse width affects laser power density but not laser energy density which is controlled by energy in the laser beam and size of the laser spot at the specimen surface.

The effect of this variation in laser system performance on laser-shock processing data is not fully understood at this time; however, it probably does not significantly impact the observed changes in fatigue properties because the reduction in pulse width which increases peak laser power density and peak shock pressure also leads to shorter duration pressure pulses, e.g., Appendix B of this report. Data generated on this program tend to confirm this hypothesis.

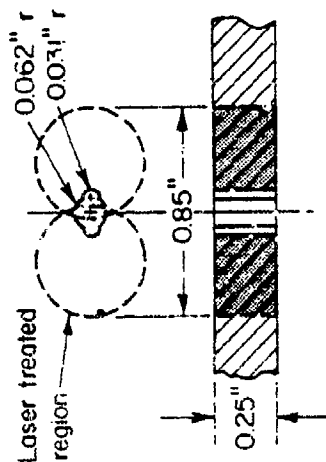
b. Test Parameter Details

Tables A-1 through A-4 present the test conditions for all of the specimens used in this program. Test Matrix I was used to develop insights concerning the variables of laser shocking. Test Matrix II provided data for differing materials, stress states, and hole quality conditions. Test Matrix III defines the tests for fastened joint specimens and Test Matrix IV deals with increased laser power and plastic overlay tests.

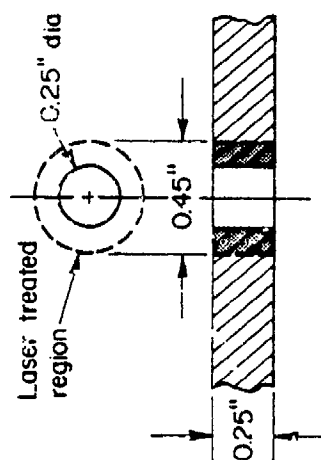
Figure A-1 details the different laser shock configurations used in the program. Tables A-5 through A-8 detail the laser environment for each test specimen. In those cases where more than one laser shot was taken to treat a specimen, the specified laser condition is the average value.



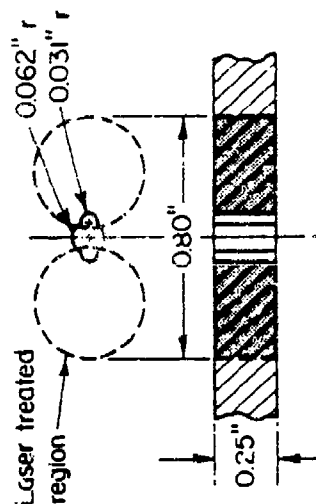
a. Crack propagation specimen with a 0.45" diameter centered laser spot.



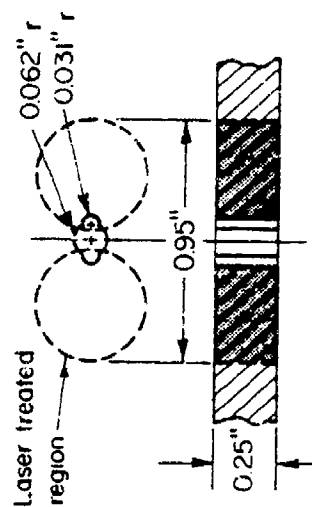
b. Crack propagation specimen with precrack and two 0.45" diameter off-centered laser spots.



c. Low-load transfer fastened joint specimen with a 0.45" diameter centered laser spot.



d. Crack propagation specimen with two 0.37" diameter off-centered laser spots.



e. Crack propagation specimen with two 0.45" diameter off-centered laser spots.

Figure A-1. Laser spot configurations

TABLE A-1. TEST MATRIX I - INVESTIGATION OF SHOCK PARAMETERS

Specimen Number	Sheet Thickness, t	Laser Parameter	Shock Both Sides of Specimen?	Special Conditions	Reason
1	0.25	$\phi_1$	Yes	None	Define working stress that will propagate cracks
2, 3, 2*, 3*	0.25	$\phi_1$	Yes	None	Baseline
4, 5	0.25	$\phi_2$	Yes	None	Evaluate effect of increased laser power density
6, 7	0.125	$\phi_2$	Yes	None	Determine if there is a thickness effect
8, 9	0.25	$\phi_*$	Yes	Radius Hole Edge	Evaluate through-thickness effect with optimum shock parameter
10, 11	0.25	$\phi_*$	Yes	Drill Before Shock	Evaluate drill sequence effects
12, 13	0.25	$\phi_*$	Yes	Drill Before Shock and Radius Hole Edge	Evaluate through thickness and drill sequence effects
14, 15	0.25	$\phi_*$	No	Drill Before Shock	Evaluate effect of shocking one side only (thickness effect)
16, 17	0.125	$\phi_*$	No	Drill Before Shock	Confirm Experiments 14 and 15 (thickness effects)
18, 19	0.125	$\phi_*$	No	Drill After Shock	Confirm thickness and drill sequence effects
20, 21	0.125	$\phi_*$	No	Use Back-up Plate on Back Side	To determine if back-up plate will reflect shock wave

Note 1.  $\phi_*$  is optimum laser power density -- selected after Experiment Number 7.

Note 2. All specimens to be made of 7075-T651 aluminum alloy.

Note 3. Specimen 1 was tested at a maximum stress of 13 ksi. Specimens 2 and 3 were tested at a maximum stress of 14 ksi, 2\*, 3\* and all of the following specimens were tested at a maximum stress of 15 ksi.

TABLE A-2. TEST MATRIX II - BASELINE CRACK INITIATION/GROWTH DATA MATRIX

Specimen Number	Sheet Thickness, t	Laser Parameter	Shock Both Sides of Specimen?	Special Conditions	Reason
20A, 21A, 22	0.25	No Shock	--	Constant Amplitude 7075-T651 ( $\sigma_1$ )	Baseline
23, 24 <sup>a</sup>	0.25	$\phi_*$	Yes	Constant Amplitude 7075-T651 ( $\sigma_1$ )	Direct comparison of laser shock effect
25, 26	0.25	$\phi_*$	Yes	Constant Amplitude 7075-T651 ( $\sigma_2$ )	Evaluate stress effect
25*, 26*	0.25	No Shock	--	Constant Amplitude 7075-T651 ( $\sigma_2$ )	Baseline
27, 28	0.25	$\phi_*$	Yes	Constant Amplitude 7075-T651 ( $\sigma_3$ )	Evaluate stress effect
27*, 28*	0.25	No Shock	--	Constant Amplitude 7075-T651 ( $\sigma_3$ )	Baseline
29, 30	0.25	No Shock	--	Constant Amplitude 2024-T3 ( $\sigma_1$ )	Baseline
31, 32	0.25	$\phi_*$	Yes	Constant Amplitude 2024-T3 ( $\sigma_1$ )	Direct comparison of laser shock effect
33, 34	0.25	$\phi_*$	Yes	Constant Amplitude 2024-T3 ( $\sigma_3$ )	Evaluate stress effect
35, 36	0.25	No Shock	--	Flight/Flight 7075-T651 ( $\sigma_4$ Mean)	Baseline
37-38	0.25	$\phi_*$	Yes	Flight/Flight 7075-T651 ( $\sigma_4$ Mean)	Direct comparison of shock effect

<sup>a</sup>Specimens 4 and 5 are the same as Specimens 23 and 24.



TABLE A-2. (Concluded)

Specimen Number	Sheet Thickness, t	Laser Parameter	Shock Both Sides of Specimen	Special Conditions	Reason
39,40	0.25	$\phi^*$	Yes	Flight/Flight 7075-T651 ( $\sigma_5$ Mean)	Evaluate mean stress effect
41,42	0.25	$\phi^*$	Yes	Constant Amplitude Precrack 7075-T651 ( $\sigma_1$ )	Direct comparison to Experiments 20-24 for repair capability
43,44	0.25	No Shock	Yes	Constant Amplitude Precrack 7075-T651 ( $\sigma_3$ )	Direct comparison to Experiments 27 and 28 for repair capability
45,46	0.25	$\phi^*$	Yes	Flight/Flight Precrack 7075-T651 ( $\sigma_4$ Mean)	Direct comparison to Experiments 35-38 for repair capability
47,48	0.25	$\phi^*$	Yes	Flight/Flight Precrack 7075-T651 ( $\sigma_5$ Mean)	Direct comparison to Experiments 39-40 for stress effect
49,50	0.25	$\phi^*$	Yes	Constant Amplitude Precrack 2024-T3 ( $\sigma_1$ )	Direct comparison to Experiments 29-32 for repair capability
51,52	0.25	$\phi^*$	Yes	Constant Amplitude Precrack 2024-T3 ( $\sigma_3$ )	Direct comparison to Experiments 33-34 for repair capability

TABLE A-3. TEST MATRIX III - LOW-LOAD TRANSFER  
FASTENED JOINT FATIGUE EXPERIMENTS

Specimen Number	Laser Shocked	Hole Condition	Stress
53-59	No	As Drilled/Reamed	$\sigma_4$ (40 ksi) <sup>a</sup>
60-62	No	Flawed	$\sigma_4$ (40 ksi) <sup>a</sup>
63-69	Yes	As Drilled/Reamed	$\sigma_4$ (40 ksi) <sup>a</sup>
70-72	Yes	Flawed	$\sigma_4$ (40 ksi) <sup>a</sup>
101-102	No	As Drilled/Reamed	$\sigma_6$ (27 ksi) <sup>b</sup>
103-104			
7-973, 7-975 7-926A	Yes	As Drilled/Reamed	$\sigma_6$ (27 ksi) <sup>b</sup>

<sup>a</sup>FALSTAFF Flight 130 modified variable amplitude.

<sup>b</sup>40 ksi FALSTAFF Flight 130 modified, proportionally reduced to 27 ksi maximum.

NOTE: All specimens are 7075-T651 aluminum.

TABLE A-4. TEST MATRIX IV - HIGH INTENSITY AND  
PLASTIC OVERLAY EXPERIMENTS

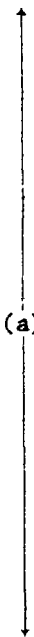
Specimen Number	Laser Power Density	Overlay	Test Conditions
3-EXT, 4-EXT	$\phi_3^a$	Water	15 ksi Constant Amplitude
1-EXT, 2-EXT	$\phi_3$	Water	15 ksi Constant Amplitude (Drilled Before Laser Shocking)
9-EXT, 10-EXT	$\phi_3$	Water	15 ksi Constant Amplitude (Precrack)
5-EXT, 6-EXT	$\phi_3$	Water	17 ksi Constant Amplitude
7-EXT, 8-EXT	$\phi_1$	Plastic	15 ksi Constant Amplitude
11-EXT, 12-EXT	$\phi_*^b$	Plastic	15 ksi Constant Amplitude

$^a\phi_3 > \phi_*$ .

$^b$ Tests conducted to compare with  $\phi_*$ -Water Overlay Experiments

NOTE: Material 7075-T651 aluminum.

TABLE A-5. INVESTIGATION OF SHOCK PARAMETERS (CRACK INITIATION/GROWTH SPECIMENS)

Specimen number	Flaw number	Laser environment			Laser shock <sup>a</sup> configuration
		Energy density (J/cm <sup>2</sup> )	Pulse width (nsec)	Power density $\phi$ , 10 <sup>9</sup> W/cm <sup>2</sup>	
1	A & B	57.5	21.3	$\phi_1$ , 2.7	
2	A & B	57.5	21.3	$\phi_1$ , 2.7	
3	A & B	57.5	21.3	$\phi_1$ , 2.7	
2*	A & B	49.9	17.2	$\phi_1$ , 2.9	
3*	A & B	49.9	17.2	$\phi_1$ , 2.9	
4	A & B	115.0	21.3	$\phi_2$ , 5.4	
5	A & B	110.8	21.3	$\phi_2$ , 5.2	
6	A & B	115.0	21.3	$\phi_2$ , 5.4	
7	A & B	112.9	21.3	$\phi_2$ , 5.3	
8	A & B	100.4	19.3	$\phi_*$ , 5.2	
9	A & B	108.1	19.3	$\phi_*$ , 5.6	
10	A & B	104.2	19.3	$\phi_*$ , 5.4	
11	A & B	104.2	19.3	$\phi_*$ , 5.4	
12	A & B	104.2	19.3	$\phi_*$ , 5.4	
13	A & B	102.3	19.3	$\phi_*$ , 5.3	
14	A & B	104.2	19.3	$\phi_*$ , 5.4	
15	A & B	102.3	19.3	$\phi_*$ , 5.3	
16	A & B	102.3	19.3	$\phi_*$ , 5.3	
17	A & B	104.2	19.3	$\phi_*$ , 5.4	
18	A & B	108.1	19.3	$\phi_*$ , 5.6	
19	A & B	106.2	19.3	$\phi_*$ , 5.5	
20	A & B	108.1	19.3	$\phi_*$ , 5.6	
21	A & B	108.1	19.3	$\phi_*$ , 5.6	

<sup>a</sup>See Figure A-1.

TABLE A-6. BASELINE<sup>a</sup> CRACK INITIATION/GROWTH DATA MATRIX

Specimen number	Flaw number	Laser environment			Laser shock <sup>a</sup> configuration
		Energy density (J/cm <sup>2</sup> )	Pulse width (nsec)	Power density $\phi$ , 10 <sup>9</sup> W/cm <sup>2</sup>	
23	A & B	94.6	17.2	$\phi_*$ , 5.5	(a)
24	A & B	109.2	14.0	$\phi_*$ , 7.8	
25	A & B	99.8	17.2	$\phi_*$ , 5.8	
26	A & B	106.6	17.2	$\phi_*$ , 6.2	
27	A & B	101.5	17.2	$\phi_*$ , 5.9	
28	A & B	103.2	17.2	$\phi_*$ , 6.0	
31	A & B	101.5	17.2	$\phi_*$ , 5.9	
32	A & B	104.9	17.2	$\phi_*$ , 6.1	
33	A & B	101.5	17.2	$\phi_*$ , 5.9	
34	A & B	99.8	17.2	$\phi_*$ , 5.8	
37	A & B	103.2	17.2	$\phi_*$ , 6.0	
38	A & B	94.6	17.2	$\phi_*$ , 5.5	
39	A & B	98.0	17.2	$\phi_*$ , 5.7	
40	A & B	101.5	17.2	$\phi_*$ , 5.9	
41	A	101.4	16.9	$\phi_*$ , 6.0	(b)
42	A	111.5	16.9	$\phi_*$ , 6.6	
43	A	103.9	15.5	$\phi_*$ , 6.7	
44	A	105.4	15.5	$\phi_*$ , 6.8	
45	A	106.5	16.9	$\phi_*$ , 6.3	
46	A	108.2	16.9	$\phi_*$ , 6.4	
47	A	104.8	16.9	$\phi_*$ , 6.2	
48	A	109.9	16.9	$\phi_*$ , 6.5	
49	A	103.1	16.9	$\phi_*$ , 6.1	
50	A	106.5	16.9	$\phi_*$ , 6.3	
51	A	103.1	16.9	$\phi_*$ , 6.1	
52	B	106.5	16.9	$\phi_*$ , 6.3	

<sup>a</sup>See Figure A-1.

TABLE A-7. FASTENED JOINT FATIGUE SPECIMENS

Specimen number	Hole condition	Laser environment			Laser shock <sup>a</sup> configuration
		Energy density (J/cm <sup>2</sup> )	Pulse width (nsec)	Power density $\phi$ , 10 <sup>9</sup> W/cm <sup>2</sup>	
63	As Drilled	96.8	12.9	$\phi_*$ , 7.5	(c)
64	As Drilled	94.1	21.9	$\phi_*$ , 4.3	
65	As Drilled	101.9	12.9	$\phi_*$ , 7.9	
66	As Drilled	102.6	12.9	$\phi_*$ , 8.0	
67	As Drilled	101.9	12.9	$\phi_*$ , 7.9	
68	As Drilled	96.8	12.9	$\phi_*$ , 7.5	
69	As Drilled	100.0	12.9	$\phi_*$ , 7.8	
70	Flawed	94.1	21.9	$\phi_*$ , 4.3	
71	Flawed	94.1	21.9	$\phi_*$ , 4.3	
72	Flawed	94.1	21.9	$\phi_*$ , 4.3	
103 <sup>b</sup>	As Drilled	153.3	23.6	$\phi_3$ , 6.5	
104	As Drilled	145.4	23.6	$\phi_3$ , 6.2	
7-973 <sup>c</sup>	As Drilled	73.2	14.0	--, 5.2	
7-975	As Drilled	73.2	14.0	--, 5.2	
7-976	As Drilled	71.3	14.0	--, 5.1	

<sup>a</sup>See Figure A-1.

<sup>b</sup>Specimens 103 and 104 were prepared and laser shocked at Battelle.

<sup>c</sup>Specimens 7-973, 7-975, and 7-976 were supplied by the Air Force and laser shocked at Battelle.

TABLE A-8. CRACK INITIATION/GROWTH AND RESIDUAL STRESS SPECIMENS  
(PROGRAM EXTENSION)

Specimen number	Type of test and condition	Laser environment			Laser shock <sup>a</sup> configuration
		Energy density (J/cm <sup>2</sup> )	Pulse width (nsec)	Power density $\phi$ , 10 <sup>9</sup> W/cm <sup>2</sup>	
1-Ext	Crack Initiation/ Growth Water Overlay	145.3	19.9	$\phi_3$ , 7.3	(d)
2-Ext	Crack Initiation/ Growth Water Overlay	153.2	19.9	$\phi_3$ , 7.7	
3-Ext	Crack Initiation/ Growth Water Overlay	159.6	21.0	$\phi_3$ , 7.6	
4-Ext	Crack Initiation/ Growth Water Overlay	149.1	21.0	$\phi_3$ , 7.1	
5-Ext	Crack Initiation/ Growth Water Overlay	163.8	21.0	$\phi_3$ , 7.8	
6-Ext	Crack Initiation/ Growth Water Overlay	149.1	21.0	$\phi_3$ , 7.1	
7-Ext	Crack Initiation/ Growth Plastic Overlay	144.9	21.0	$\phi_3$ , 6.9	
8-Ext	Crack Initiation/ Growth Plastic Overlay	152.8	23.5	$\phi_3$ , 6.5	
9-Ext	Crack Initiation/ Growth Water Overlay	152.8	23.5	$\phi_3$ , 6.5	
10-Ext	Crack Initiation/ Growth Water Overlay	150.4	23.5	$\phi_3$ , 6.4	
11-Ext	Crack Initiation/ Growth Plastic Overlay	103.1	23.5	$\phi_*$ , 4.4	
12-Ext	Crack Initiation/ Growth Plastic Overlay	100.7	23.5	$\phi_*$ , 4.3	(e)
1-Residual	Residual Stress	101.0	19.9	$\phi_*$ , 5.0	
2-Residual	Residual Stress	101.0	19.9	$\phi_*$ , 5.1	

<sup>a</sup>See Figure A-1.

### c. Fatigue Test Results

Fatigue test results investigating the effects of laser shocking are presented in the following tables and figures. Tables A-9, A-10, A-12, and Figures A-2, A-3, A-4, A-5, and A-8 contain crack-growth milestones for the fatigue-crack-growth experiments. Tables A-11 and Figures A-6 and A-7 contain fatigue results for the low-load transfer fastened-joint experiments.

Crack-growth measurements were made visually on both front and back surfaces with the aid of a 10X traveling microscope. Direct comparison of shocked and unshocked cycles to grow a certain crack length is not possible due to the tunneling characteristics of the shocked specimen crack. Direct comparison of shocked and unshocked experiments should be directed to cycles to failure. Tabular data is presented as cycles to grow to 0.25 inch (slightly larger than the characteristic flaw size), cycles to grow to 0.45 inch (the characteristic diameter of a single laser spot), cycles to failure, and cycles for growth from 0.25 to 0.45 inch.

Fatigue results for the low-load transfer fastened-joint experiments are in load spectrum passes to failure. The failure mode describing the location of crack initiation is also indicated.

Crack-growth data for the crack propagation experiments will be provided upon request.



TABLE A-9. INVESTIGATION OF SHOCK PARAMETERS FATIGUE TEST RESULTS  
MATRIX I

Experiment Number	Flaw	Cycles to Grow Crack				Comment
		To 0.25 inch	To 0.45 inch	To Failure	From 0.25 to 0.45 inch	
1	A	--	165,000	193,220	--	
	B	>193,220	--	--	--	
2	A	>2,171,000	2,179,000	--	8,000	1
	B	2,265,000	--	--	--	
3*	A	127,000	140,000	--	13,000	1
	B	>497,500	--	--	--	
2*	A	93,000	--	--	--	
	B	75,000	85,000	102,100	10,000	
3	A	61,000	76,000	91,700	15,000	
	B	72,000	85,000	>91,700	13,000	2
4	A	<405,000	405,000	>407,000	--	3
	B	>1,045,550	--	--	--	3
5	A	>2,500,000	--	--	--	
	B	839,000	847,000	--	8,000	
6	A	>1,800,000	--	--	--	
	B	>1,800,000	--	--	--	
7	A	>2,503,590	--	--	--	
	B	<680,000	691,000	713,590	>11,000	
8	A	2,508,990	--	--	--	
	B	260,000	264,000	278,990	>4,000	
9	A	110,000	113,500	>123,950	3,500	2
	B	100,000	106,000	123,950	6,000	
10	A	328,000	334,000	357,090	6,000	
	B	396,000	403,000	423,580	7,000	
11	A	209,000	213,500	237,290	4,500	
	B	<254,600	255,000	276,890	--	
12	A	290,000	293,000	313,840	3,000	
	B	<529,000	529,000	547,720	--	
13	A	236,000	242,000	254,090	6,000	
	B	112,000	113,500	127,570	1,500	
14	A	51,000	57,000	>70,940	6,000	2
	B	51,000	57,000	70,940	6,000	
15	A	56,000	69,000	88,520	13,000	2
	B	65,000	78,000	>88,520	13,000	
16	A	164,000	182,000	198,220	18,000	
	B	76,000	119,000	139,435	43,000	
17	A	58,000	--	>83,800	--	2
	B	34,000	59,000	83,800	25,000	
18	A	149,000	181,000	204,180	32,000	
	B	1,000,180	--	--	--	

TABLE A-9. (Concluded)

Experiment Number	Flaw	Cycles to Grow Crack				Comment
		To 0.25 inch	To 0.45 inch	To Failure	From 0.25 to 0.45 inch	
19	A	235,000	254,000	277,260	19,000	2
	B	154,000	181,000	205,510	27,000	
20	A	170,000	212,000	242,910	42,000	
	B	186,000	225,000	> 242,910	39,000	
21	A	238,000	240,000	254,490	2,000	
	B	>1,400,000	--	--	--	

## COMMENTS:

1. Crack tip drilled and mandrelized to stop crack growth after crack approached laser shock perimeter.
2. Flaw was not cycled to failure.
3. Specimen ran 4,725,000 cycles at 14 ksi and no crack was initiated.

TABLE A-10. BASELINE CRACK INITIATION/GROWTH DATA MATRIX TEST RESULTS MATRIX II

Specimen Number	Flaw	Cycles to Grow Crack				Comment
		To 0.25 inch	To 0.45 inch	To Failure	From 0.25 to 0.45 inch	
20A	A	131,000	138,000	155,730	7,000	1
	B	64,000	80,000	--	16,000	3
21A	A	>261,450	--	--	--	
	B	223,000	240,000	261,450	17,000	
22	A	57,000	67,000	89,390	10,000	
	B	>89,390	--	--	--	3
23	A	142,000	148,000	176,290	6,000	
	B	460,000	462,000	474,720	2,000	
24	A	>197,050	--	--	--	?
	B	170,000	178,000	197,050	8,000	
25	A	63,500	73,000	87,230	9,500	
	B	97,000	100,000	109,270	3,000	
26	A	109,000	113,000	126,010	4,000	
	B	88,000	93,000	104,700	5,000	
25*		--	--	302,520	--	7
26*		70,000	76,000	87,330	6,000	
27	A	29,000	32,500	>34,300	3,500	3
	B	25,000	29,500	34,300	4,500	
28	A	29,500	--	--	--	3
	B	22,000	27,000	31,250	5,000	
27*		11,000	13,000	16,310	2,000	
28*		10,000	12,000	15,230	2,000	
29	A	130,000	138,000	>145,150	8,000	3
	B	108,000	118,000	145,150	10,000	
30	A	100,000	124,000	>135,640	24,000	3
	B	96,000	109,000	135,640	13,000	
31	A	838,000	847,000	877,550	9,000	
	B	1,057,000	1,062,000	1,085,790	5,000	
32	A	780,000	797,000	844,130	17,000	
	B	637,000	642,000	692,810	15,000	
33	A	45,000	56,500	>57,090	11,500	3
	B	39,000	48,000	57,090	9,000	
34	A	48,000	57,000	>57,180	9,000	3
	B	40,000	51,000	57,180	11,000	
41	A	40,000 (80,000)	116,000	142,340	36,000	2
	B	--	--	--	--	4
42	A	40,600 (80,000)	113,000	139,260	33,000	2
	B	--	--	--	--	4
43	A	44,500 (49,000)	55,000	63,650	6,000	2
	B	--	--	--	--	4
44	A	52,500 (56,000)	63,000	69,690	7,000	2
	B	--	--	--	--	4
49	A	80,000 (144,000)	>620,110	--	605,710	2,3,6
	B	--	--	--	--	5,6
50	A	--	--	--	--	4
	B	74,000 (200,000)	860,000	927,470	660,000	2

TABLE A-10. (Concluded)

Specimen Number	Flaw	Cycles to Grow Crack				Comment
		To 0.25 inch	To 0.45 inch	To Failure	From 0.25 to 0.45 inch	
51	A	86,000 (95,000)	109,000	125,070	14,000	2
	B	--	--	--		4
52	A	--	--	--		4
	B	77,500 (83,000)	93,000	107,570	10,000	2

Spectrum Passes to Grow Crack

35	A	130	173	>202	43	3
	B	125	170	>202	45	3
36	A	113	160	>183	47	3
	B	114	155	>183	41	3
37	A	249	340	>380	91	3
	B	250	345	>380	95	3
38	A	215	310	>354	95	3
	B	230	335	>354	105	3
39	A	530	622	>622	92	3
	B	410	530	>622	120	3
40	A	440	565	>623	125	3
	B	432	532	>623	100	3
45	A	(45)	155	>243	110	2,3
	B	--	--	--	--	3,4
46	A	(129)	240	>352	111	2
	B	--	--	--	--	3,4
47	A	(160)	342	>509	182	2,3
	B	--	--	--	--	3,4
48	A	(235)	390	>574	155	2,3
	B	--	--	--	--	3,4

## COMMENTS:

1. Crack tip drilled and mandrelized to stop crack growth after crack approached laser shock perimeter.
2. Specimen was precracked then shocked. Cycles or passes to initiation is for unshocked condition. Parenthesis value is for growth to 0.25 inch.
3. Flaw was not cycled to failure.
4. Flaw was unshocked.
5. Adhesive doublers were bonded across the flaw.
6. Specimen failed through unshocked flaw.
7. Specimen did not fail through initial flaw.

TABLE A-11. FASTENED JOINT SPECIMEN FATIGUE TEST RESULTS MATRIX III

Specimen Number	Shocked?	Hole Condition	Maximum Stress (ksi)	Passes To Failure	Failure Mode
53	No	As Drilled	40.0	2,951	a
53*	"	"	"	1,239	a
54	"	"	"	1,645	a
55	"	"	"	3,226	a
56	"	"	"	1,535	a
57	"	"	"	980	a
58	"	"	"	2,443	a
59	"	"	"	1,425	c
60	No	Flawed	40.0	1,553	a
60**	"	"	"	2,311	a
61	"	"	"	1,978	b
62	"	"	"	2,607	a
63	Yes	As Drilled	40.0	3,106	a
64	"	"	"	1,557	a
65	"	"	"	3,106	c
66	"	"	"	2,408	b
67	"	"	"	2,461	c
68	"	"	"	3,293	b
69	"	"	"	2,858	b
70	Yes	Flawed	40.0	768	a
71	"	"	"	2,652	a
72	"	"	"	2,248	a
101	No	As Drilled	27.0	5,811	a
102	"	"	"	9,979	a
103	Yes	As Drilled	27.0	17,982	c
104	"	"	"	24,860	a
7-973	"	"	"	26,784	a
7-975	"	"	"	6,799 <sup>(a)</sup>	c
7-926A	"	"	"	28,774	a

## Failure modes:

- a Crack initiated at hole.
- b Crack initiated at test section edge.
- c Crack initiated at test section surface.

(a) Failed in gross section away from fastener hole.

TABLE A-12. CRACK INITIATION/GROWTH TEST RESULTS  
(PROGRAM EXTENSION) MATRIX IV

Specimen Number	Cycles to Grow Crack			
	To 0.25 inch	To 0.45 inch	To Failure	From 0.25 to 0.45 inch
1-EXT	90,000	106,000	130,880	16,000
2-EXT	65,000	94,000	113,930	29,000
3-EXT	160,000	174,000	193,800	14,000
4-EXT	80,000	104,000	132,360	24,000
5-EXT	29,000	43,000	64,070	14,000
6-EXT	36,000	48,000	72,900	12,000
7-EXT	200,000	215,000	233,550	15,000
8-EXT	124,000	135,000	154,000	11,000
9-EXT	1,145,000	1,162,000	1,186,900	17,000
10-EXT	739,000	779,000	802,230	40,000
11-EXT	61,000	72,000	91,160	11,000
12-EXT	>1,000,000	--	--	--

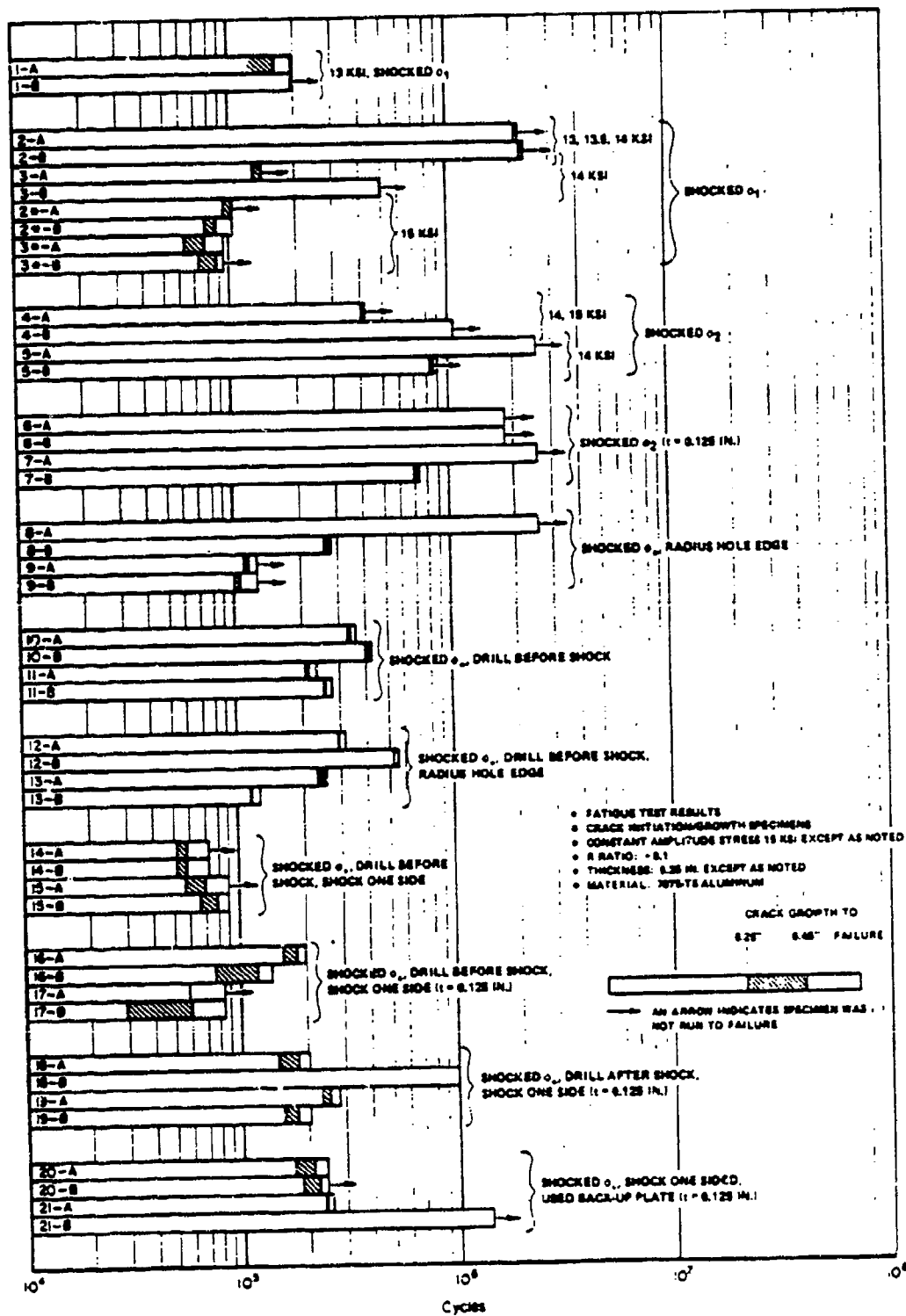


Figure A-2. Matrix I fatigue test results

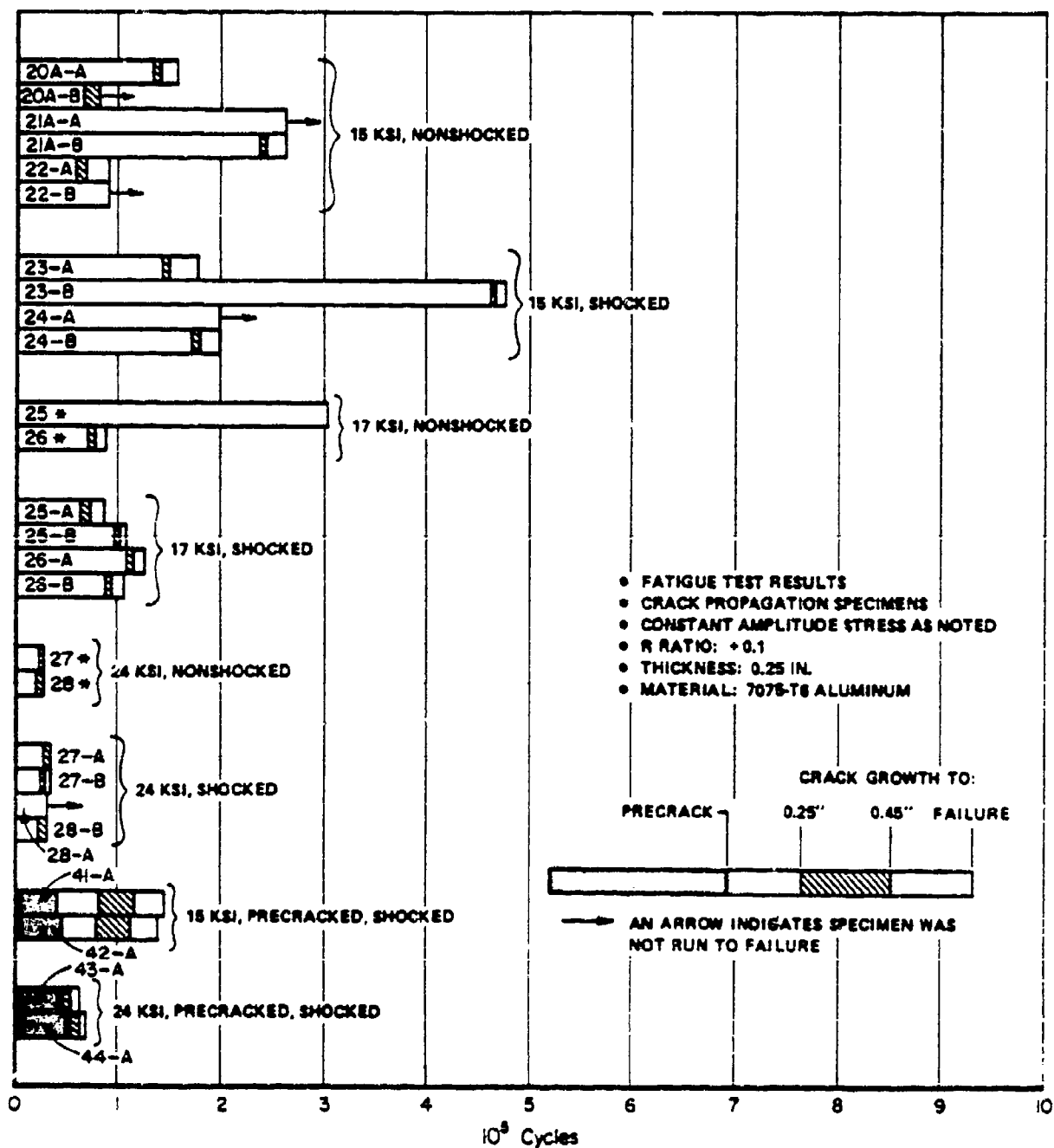


Figure A-3. Matrix II fatigue test results 7075-T6 aluminum specimens



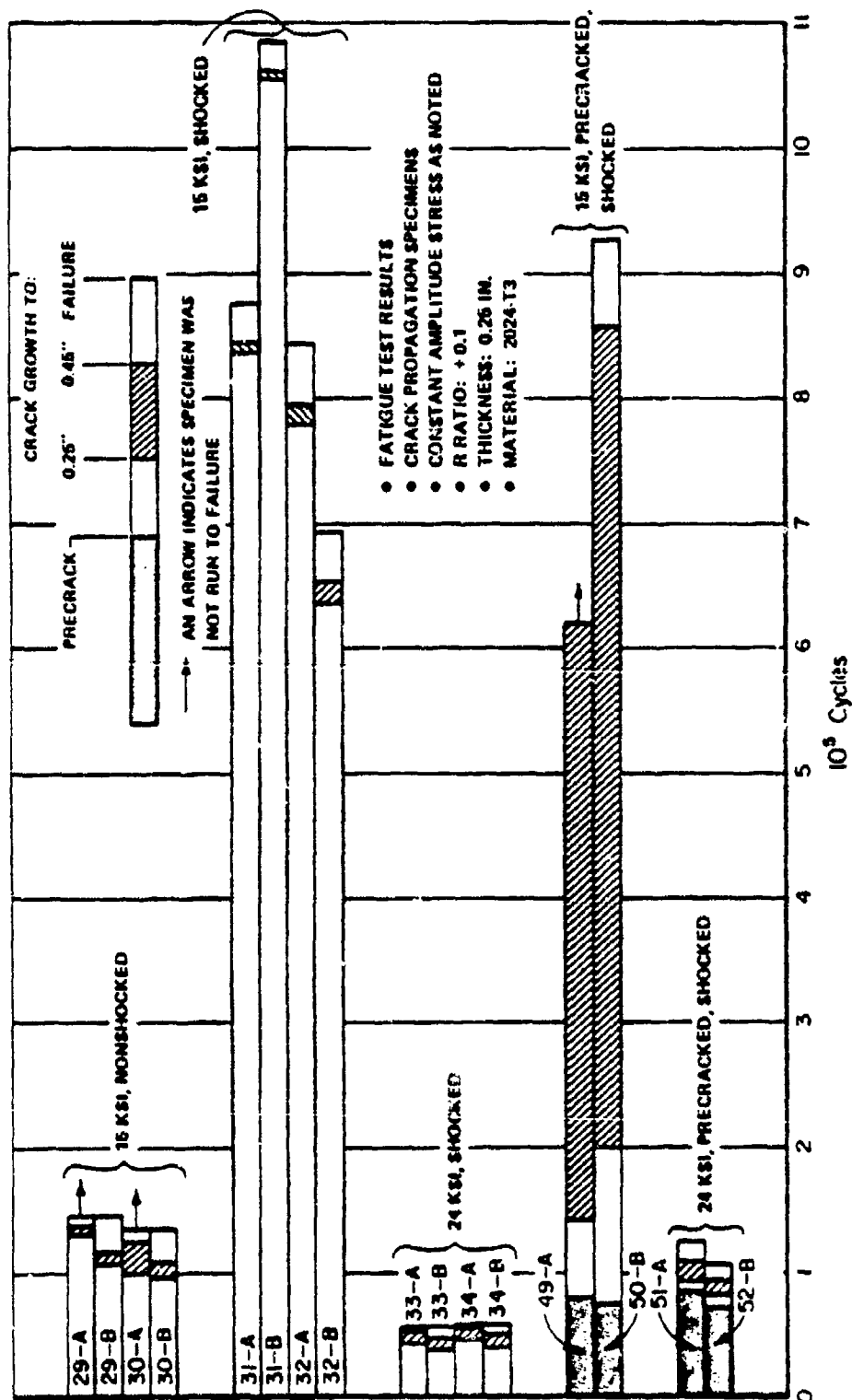


Figure A-4. Matrix II fatigue test results 2024-T3 aluminum specimens

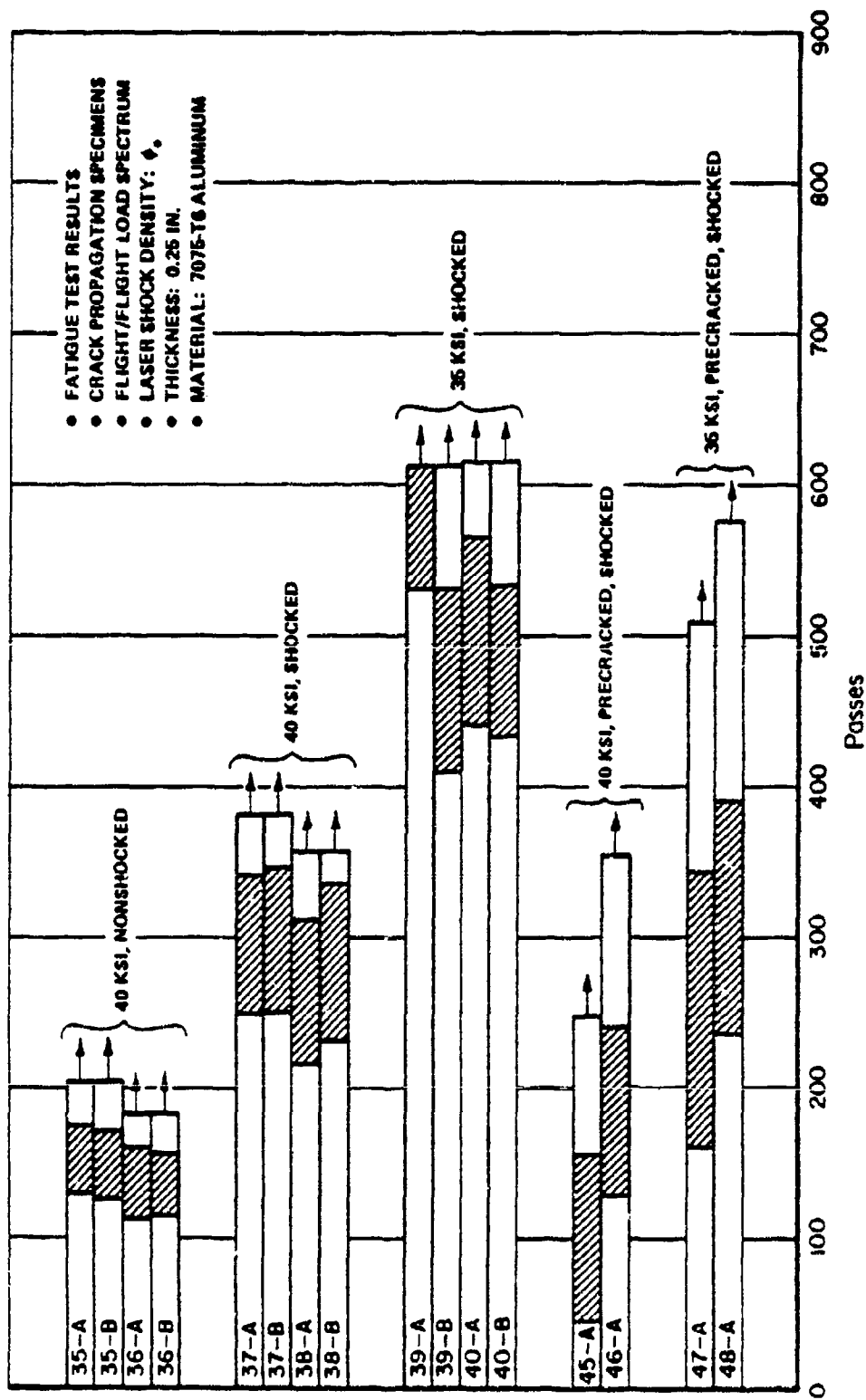


Figure A-5. Matrix II fatigue test results flight/flight load spectrum

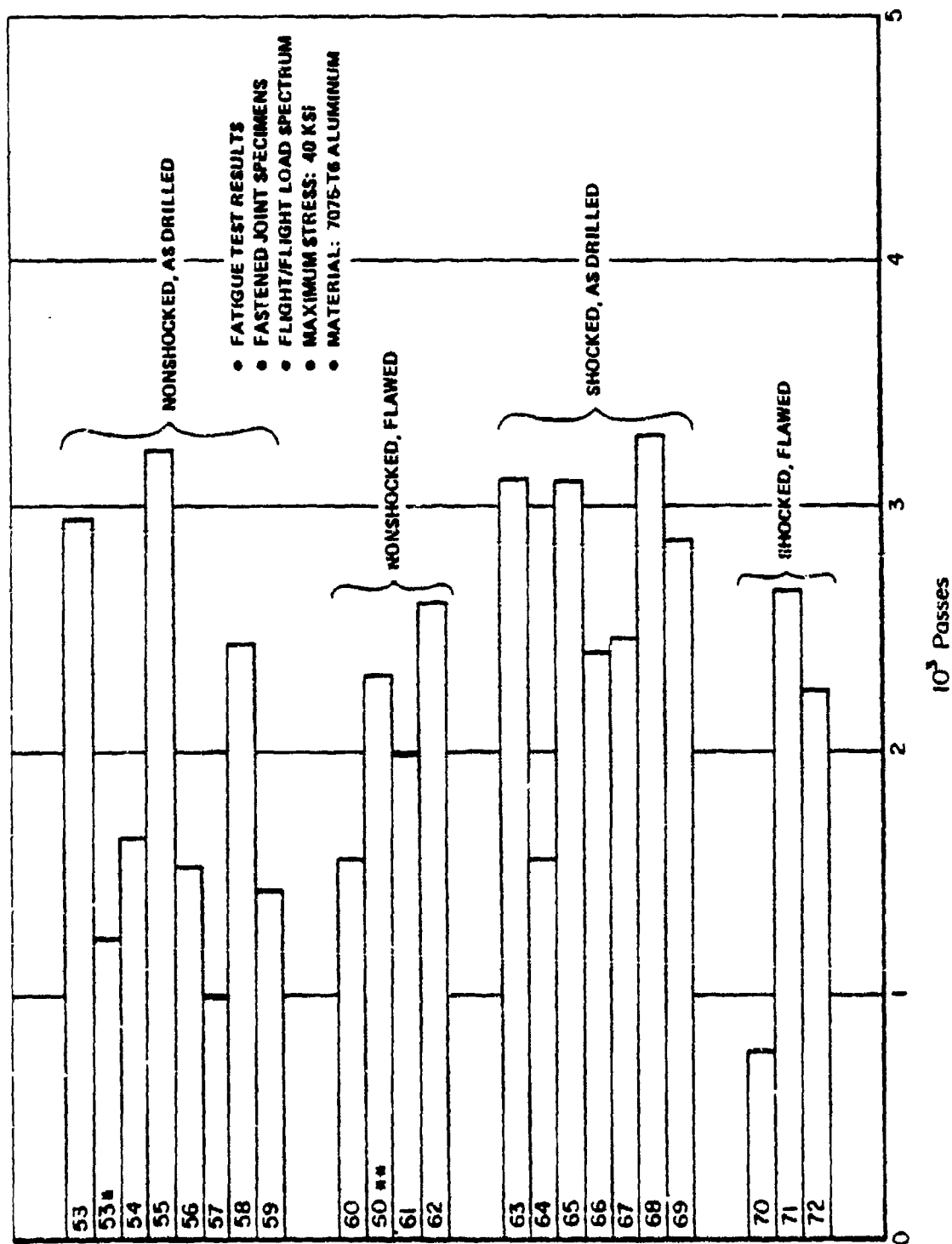


Figure A-6. Matrix III fatigue test results 40 ksi flight/flight load spectrum

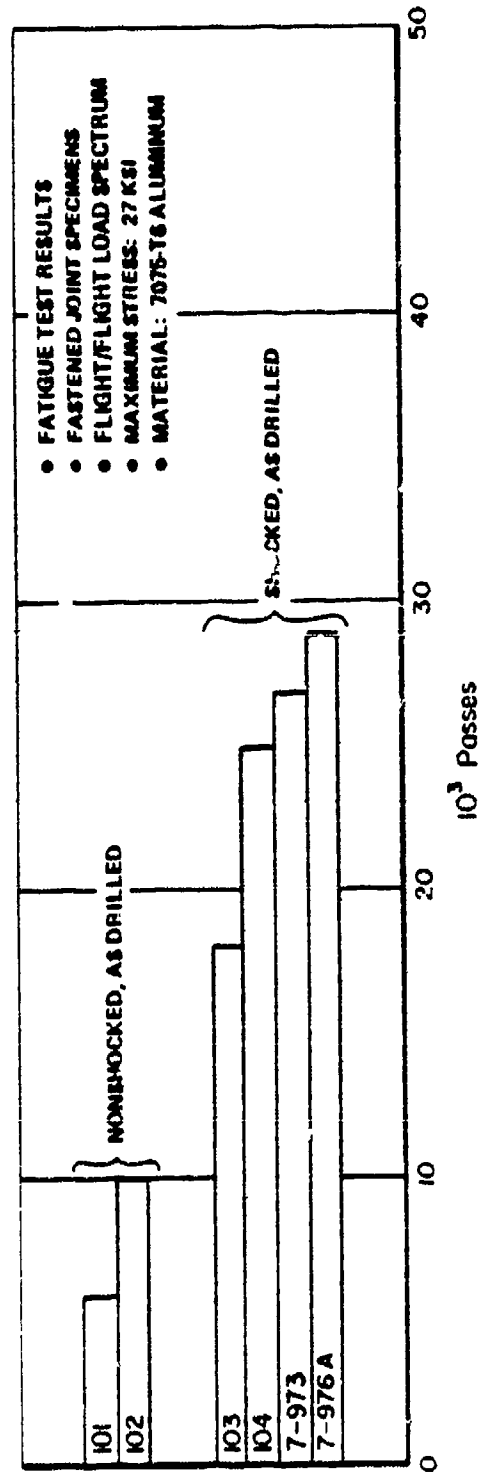


Figure A-7 Matrix III fatigue test results 27 ksi flight/flight load spectrum

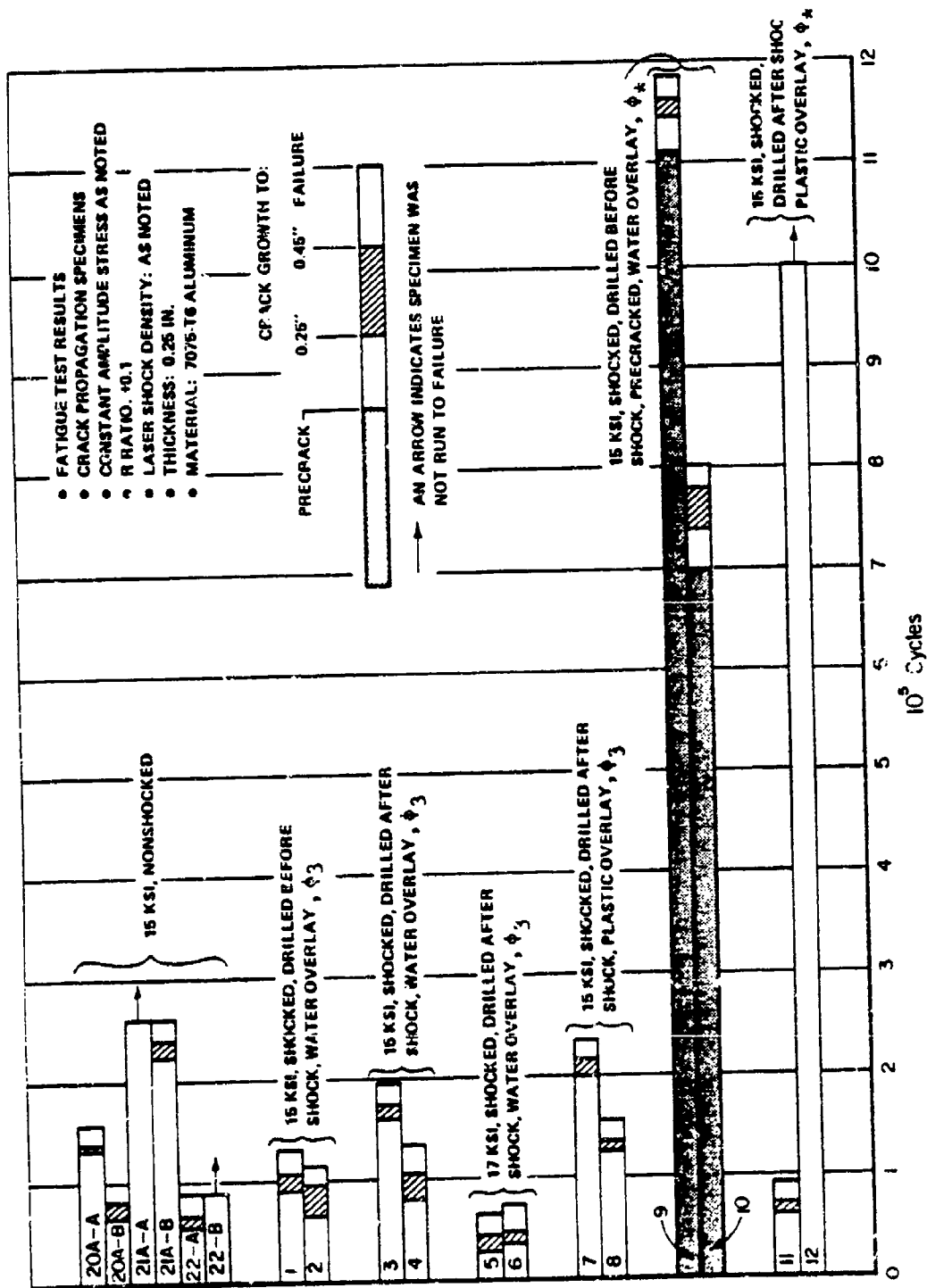


Figure A-8 Matrix IV fatigue test results

## APPENDIX B

### 1. Pulsed Laser Technology

#### a. Introduction

Laser-shock processing uses the radiation emitted by a high-power pulsed laser to generate a short-duration (less than one millionth of a second), high-amplitude pressure pulse at the surfaces of the material. It changes the metal's microstructure and stress state which is the source of the observed improvements in material properties.

Generation of the high-amplitude stress waves needed to improve fatigue properties in aluminum alloys requires covering the surfaces to be laser shocked with a material which is transparent to the laser light. A layer of water approximately 1 mm in thickness or plastic tape with a clear polyester backing was used for this purpose. A thin layer of black paint also was added to the surface to enhance absorption of the laser radiation and protect the metal surface from melting and vaporization (reference Figure 1). The pressure environment generated by this combination of surface overlay materials has been characterized in past studies.<sup>(10)</sup> Peak pressures generated at the surface of aluminum targets as a function of the incident laser power density and transparent overlays are shown in Figure B-1. Results for water and quartz are based on experimental measurements given in Reference 10. Peak pressures given for plastic overlays are based on an interpolation between water and quartz overlays where differences in acoustic impedance of the overlay materials are taken into account. The shape of the pressure pulse at the target surface approximates the shape of the laser pulse during its rise to peak power. Thereafter, the pressure pulse tends to decay in amplitude at a slower rate than the laser pulse. This behavior is illustrated in Figure B-2 which compares the measured time history of the laser pulse with the measured and predicted pressure pulse for the case of a transparent water overlay on aluminum.

#### b. Experimental Setup

Battelle's CGE VD 640 high-power neodymium-glass laser was used in all of the laser shock experiments. This system, which consists of a Q-switched

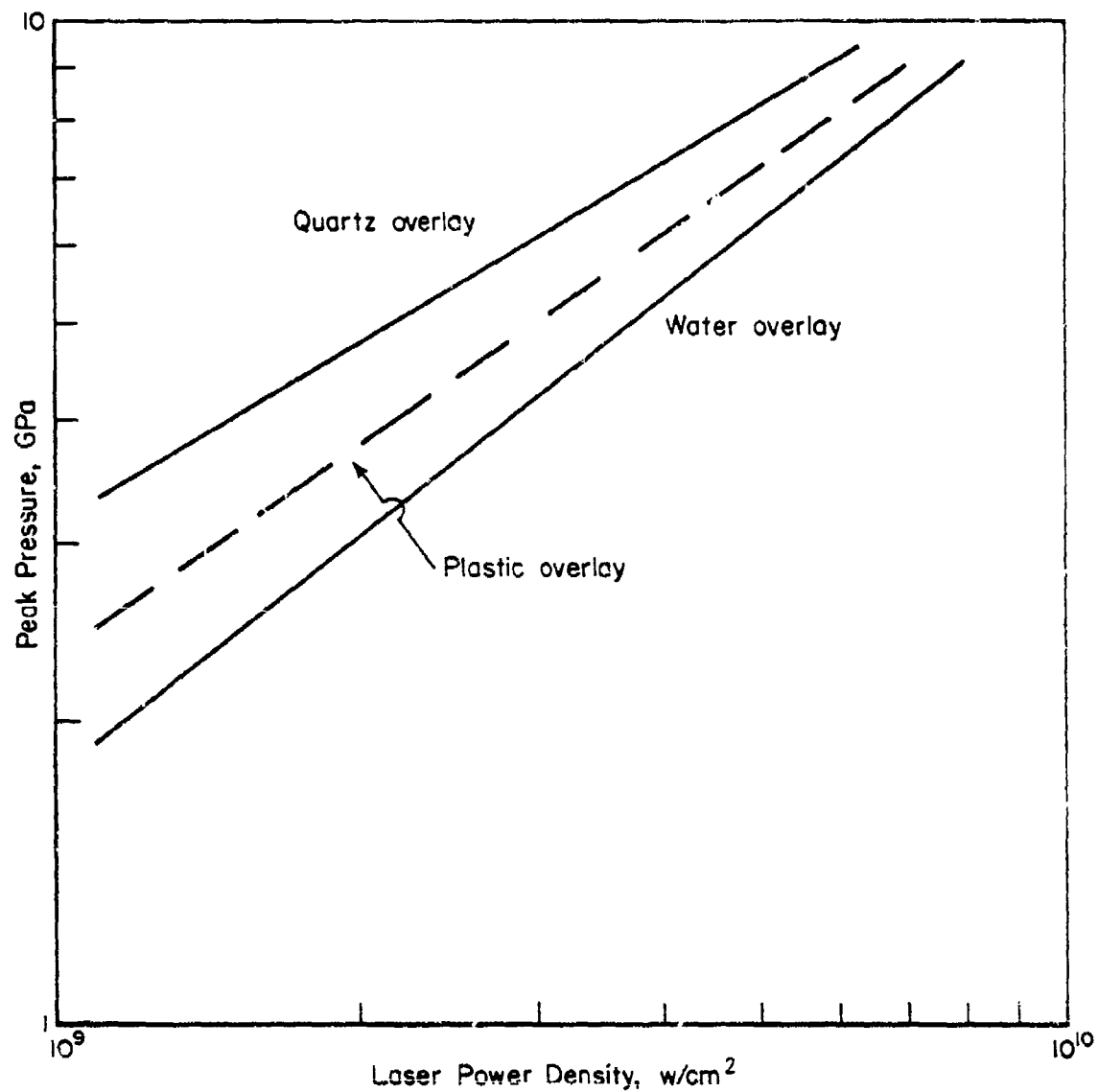


Figure B-1. Peak pressures for different overlays and laser power density conditions

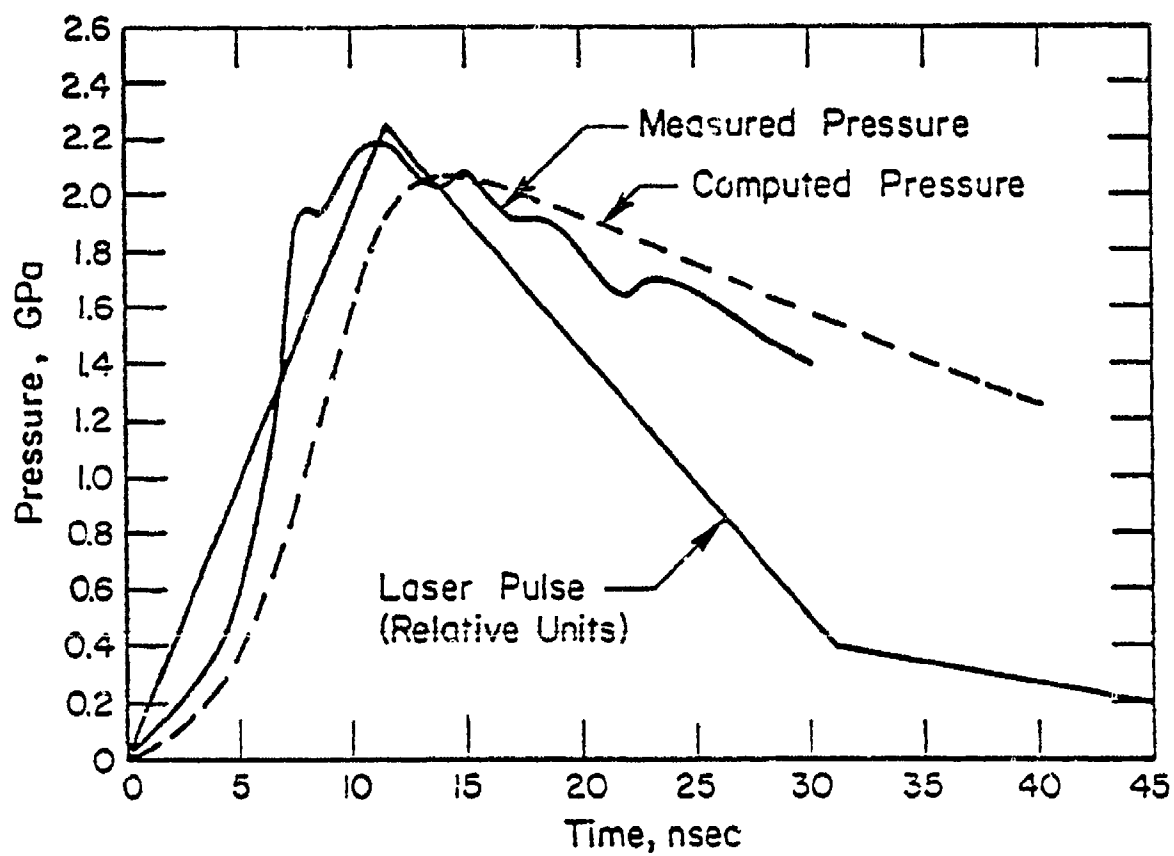


Figure B-2. Comparison of computed and measured pressures water overlay - aluminum target



laser oscillator followed by six amplifier stages, delivers about 200 joules of laser energy onto a target surface in a laser pulse having a full width at half maximum of approximately 20 nanoseconds. The laser setup and the system used in the water overlay experiments are shown in Figure B-3. As seen from Figure B-3, laser shocking of a single surface is accomplished by removing the beam splitter.

The plastic overlay experiments employed the same laser setup shown in Figure B-3. The tape was bonded to the surface of the specimen over the region to be laser shocked and the specimen was positioned at the same location occupied by the water overlay specimens.

### c. Experimental Conditions

A 100 cm (39.4 inch) focal length converging lens was used to focus the laser beam to the desired spot size at the specimen surface. The size of the laser spot on the target was determined by directing a colinear neodymium-YAG laser beam through the amplifier chain and measuring the spot size with an infrared viewer. Laser power densities were defined in terms of average values over these spot sizes. Laser energy incident on fatigue specimens was determined by first measuring the energy at the irradiation site with CGE carbon calorimeters. On-line photodiode detectors which monitor the output of the laser during each shot were then calibrated against these measurements.

The shape of the laser pulse emitted by the sixth amplifier was monitored during each shot by using a beam splitter to direct a small amount of laser energy to a photodiode whose output was displayed on a fast oscilloscope. The peak laser power densities used to correlate pressure measurement results were determined by dividing the calculated average laser energy densities by the measured laser pulse full width at half maximum.

A single spot diameter of 0.45 inch (1.15 cm) was used in all of the laser shock processing experiments conducted during the initial phase of the program. Studies to determine the effect of reducing the laser input conditions (pressure environment) on change in fatigue properties were achieved by placing a three-db filter in the laser beam. This reduced the laser energy incident on the specimen surface by a factor of two. With the

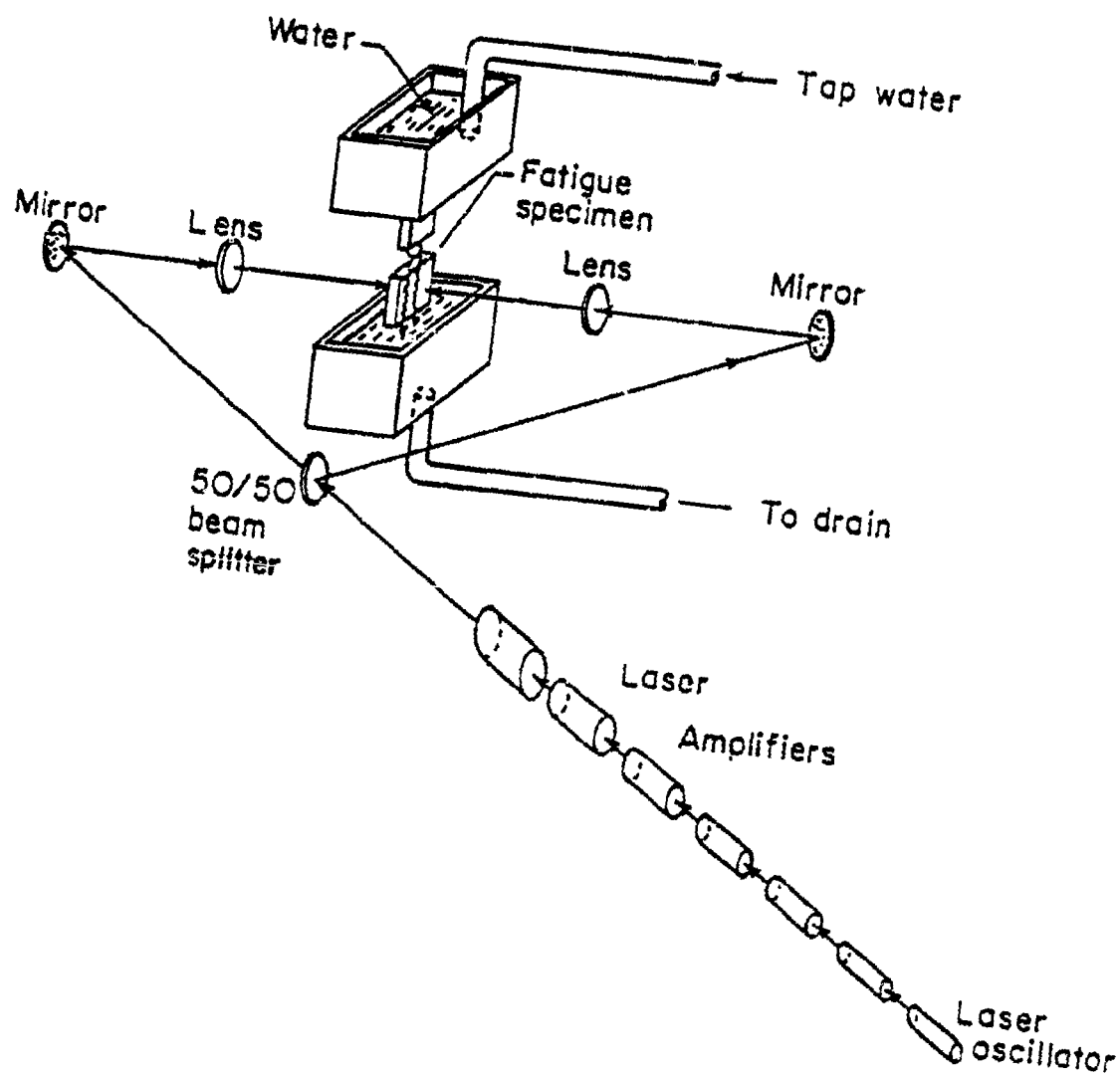


Figure B-3. Laser setup and water flow system

exception of the precracked specimens, the laser spot used in the initial phase of the program was concentric with the fastener hole region. In the precracked specimen experiments, the two laser shots shown in Figure 3 were used to treat the fastener hole region.

To achieve the more intense laser environment required in the latter portion of the program, it was necessary to reduce the size of the laser spot at the specimen surface from 0.45 inch in diameter to 0.37 inch (0.95 cm) in diameter. Because of the concomitant reduction in area of laser-treated material, a shock geometry similar to that shown in Figure 3 was used for all of the higher intensity laser shock experiments. This allowed significantly more material around the fastener hole region where the fatigue crack initiates and propagates to be treated than possible by laser shocking concentrically around the fastener hole.

In the experiments run with plastic overlays, the laser shock configuration shown in Figure 3 also was employed even for the lower intensity laser shots. This was done for comparison purposes.

In addition to the fatigue specimen, two 7075-T6 aluminum plates were laser shocked using the split beam setup. These specimens, which were used for residual stress measurements, were shocked under conditions similar to those used in the initial phase of the program, e.g., laser-treated zone concentric to fastener region.

Laser conditions for all of the shocked specimens are given in Appendix A.

## 2. Laser Shock Processing Systems

### a. Introduction

An iodine and a neodymium-glass laser, which are considered to be the best candidates for first generation implementation of the laser shock process for treatment of metal joints in aircraft structure, were investigated. The lasers were designed to operate in a pulsed 30-nanosecond mode with an output energy per pulse of 200 joules and a pulse repetition rate of 0.1 Hz to 1.0 Hz. These parameters are based on results of the laser shock processing program and reflect the system properties needed to substantially improve the fatigue properties of fastener regions in aircraft under production conditions.

The small-signal gain of each amplifier stage is given by

$$G = [\exp(\rho_{out}) - 1] / [\exp(\rho_{in}) - 1] \quad , \quad (B-1)$$

where  $\rho_{out}$  and  $\rho_{in}$  are the degrees of saturation at the output and input apertures and are given by

$$\rho_{out} = e_{out} / e_s \quad , \quad (B-2)$$

$$\rho_{in} = e_{in} / e_s \quad . \quad (B-3)$$

$e_{out}$  and  $e_{in}$  ( $J/cm^2$ ) are the output and input energy densities of the amplifier, and  $e_s$  ( $J/cm^2$ ) is the saturation energy density, defined as the energy per  $cm^2$  that is required to reduce the inversion by a factor of  $e$ . Its value is given by

$$e_s = \frac{a}{b} \frac{h\nu_{laser}}{\sigma_{max}} \quad , \quad (B-4)$$

where  $\sigma_{max}$  is the maximum value of the stimulated emission cross section as a function of line frequency,  $a$  and  $b$  are quantum mechanical correction factors, and  $h\nu_{laser}$  is the output frequency of the laser.

The small-signal gain and small-signal gain coefficient are related to the gain length  $l(cm)$  by

$$G = \exp(g_0 l) \quad . \quad (B-5)$$

The small signal-gain coefficient is given by

$$g_0 = \sigma_{max} \Delta_n \quad , \quad (B-6)$$

where  $\Delta_n$  is the inversion density. The inversion density is a function of the lasting medium and pump conditions.

The above equations form the basis for amplifier design. In addition, several design constraints exist which must be observed while optimizing the system performance. For example, to avoid optical damage at the output surface of each amplifier, the output energy must be less than the damage threshold appropriate for the given laser pulse width. Parasitic self-oscillations and amplified spontaneous emission place constraints on the gain of each amplifier stage and require the use of isolation schemes between stages.

Both laser systems are based on an oscillator-amplifier concept to achieve the large energy output per pulse needed in shock processing applications and use flashlamps to pump the lasant material. A neodymium-glass laser of this design was used in the experimental part of this program. This research facility is not designed to operate in an industrial environment and cannot be pulsed at the high repetition rates, e.g., 0.1 Hz to 1.0 Hz, required for production application; however, the essential features of this laser can be used in the design of a production system. The atomic iodine laser operates at an output wavelength of 1.315  $\mu\text{m}$  which is slightly longer than the 1.06  $\mu\text{m}$  wavelength of the neodymium-glass laser. The iodine lasing system has been under intensive study for a number of years, especially in West Germany and the USSR. The objective of that research has been the development of a laser driver for inertial confinement fusion where energetic, high-repetition-rate pulses of subnanosecond duration are necessary. It is important to note that iodine laser systems capable of achieving the pulse-width (30 nanoseconds) and energy per pulse (200 joules) required for the present application have been built; although systems satisfying the requisite pulse-repetition frequency (0.1 to 1.0 Hz) have not been built, their engineering is relatively straightforward. Unlike the neodymium-glass laser, waste heat removal which limits the pulse-repetition frequency is facilitated by recirculating the gas mixture in a closed-cycle system containing the necessary heat exchangers. This closed-cycle system may also have provisions for rejuvenation of the lasant material and, thus, the cost of consumables is minimized.

#### b. Amplifier Design Theory

The design relationships for each amplifier stage in a neodymium-glass laser and the iodine photodissociation laser can be derived from the appropriate rate equations. Starting with the stipulated output conditions, the amplifier stages are designed in an iterative fashion back to a given oscillator output energy. Although all of the design criteria have been satisfied by the proposed laser systems, these systems are not fully optimized and further work will be necessary to completely refine the design and characterize their performance.

### c. Pumping Considerations

Flashlamp selection and driver circuitry design must take into consideration two opposing requirements - maximum possible light output in the spectral region that can be absorbed by the material and maximum life expectancy. This situation arises because flashlamps must be driven in a high-current density mode of discharge to give significant spectral output, but this tends to increase the probability for flashlamp explosion and decrease the life expectancy. The single-shot explosion energy is given by

$$E_{xp} = K \ell D T^{1/2}, \quad (B-7)$$

where  $K$  is the explosion energy parameter ( $J \text{ cm}^{-2} \text{ sec}^{-1/2}$ ),  $\ell$  is the flashlamp arc length,  $D$  is the bore diameter, and

$$T = \sqrt{LC} \approx \frac{1}{3} t_p, \quad (B-8)$$

for critically damped driver circuits where  $L$  is the circuit inductance,  $C$  is the circuit capacitance, and  $t_p$  is the duration of the flashlamp pulse.

To achieve a flashlamp life expectancy of about  $10^6$  shots or greater requires that the flashlamp operating discharge energy not exceed 20 percent of the explosion energy. This criterion was used in design of the flashlamp parameters.

The driver circuitry equations are given as follows:

$$C = \left( \frac{2E_o \alpha^4 T^2}{\zeta} \right)^{1/3}, \quad (B-9)$$

$$L = \frac{T^2}{C}, \quad (B-10)$$

$$V = \left( \frac{2E_o}{C} \right)^{1/3}, \quad (B-11)$$

where  $E_o$  is the flashlamp discharge energy ( $E_o = 0.20 E_{xp}$  for a  $10^6$  - shot life expectancy),  $\alpha$  is the discharge damping factor ( $\alpha = 0.8$  for critically damped), and  $\zeta$  is the flashlamp impedance parameter.

The above equations were used to design the flashlamp and driver circuits for the laser systems.

#### d. Flow Systems

A major consideration in the design of a neodymium-glass laser is heating of the laser rods from absorption of pump radiation. Heating of the laser material leads to a nonuniform temperature of the rod which results in distortion of the laser beam due to nonlinear variation of the index of refraction and in the extreme case, fracture of the rod itself. Therefore, cooling of the laser rods by a system such as flowing water is required.

Disposal of waste heat in the case of iodine laser is simpler because it is a gas laser and the lasing chemicals can be cycled through a heat exchanger. An additional consideration in the design of an iodine laser is replenishment of the I<sub>2</sub> lasing chemical and removal of R<sub>2</sub> and I<sub>2</sub> secondary reaction by-products from the laser gas mixture.

#### e. System Designs

Laser shock processing systems were designed on the basis of the design equations and constraints given in the preceding sections. For the neodymium-glass laser design, information already existed for the system components, and it only required integration of these components into a system after proper consideration was given to cooling of the laser heads.

A design for a neodymium-glass laser system capable of producing 30 nanosecond, 200 joule pulses at a repetition rate of 0.1 Hz is shown in Figure B-4, and the associated operational parameters are given in Table B-1. Higher pulse rates are not possible with this design because of heating of the glass laser rods. A face-pumped slab laser rather than the cylindrical design shown in Figure B-1 probably could be pulsed at a higher repetition rate; however, design of this type of laser will require additional study. Even at a pulse repetition rate of 0.1 Hz, temperature-induced changes in the index of refraction of cylindrical rods probably will require the use of phosphate glass rather than silicate glass.

A design for an iodine laser system capable of producing 30 nanosecond, 200 joule pulses at a repetition rate of 1.0 Hz is given in Figure B-5, and the associated operational parameters are given in Table B-2. It is assumed that the oscillator is capable of delivering an energy of 0.1 joule.

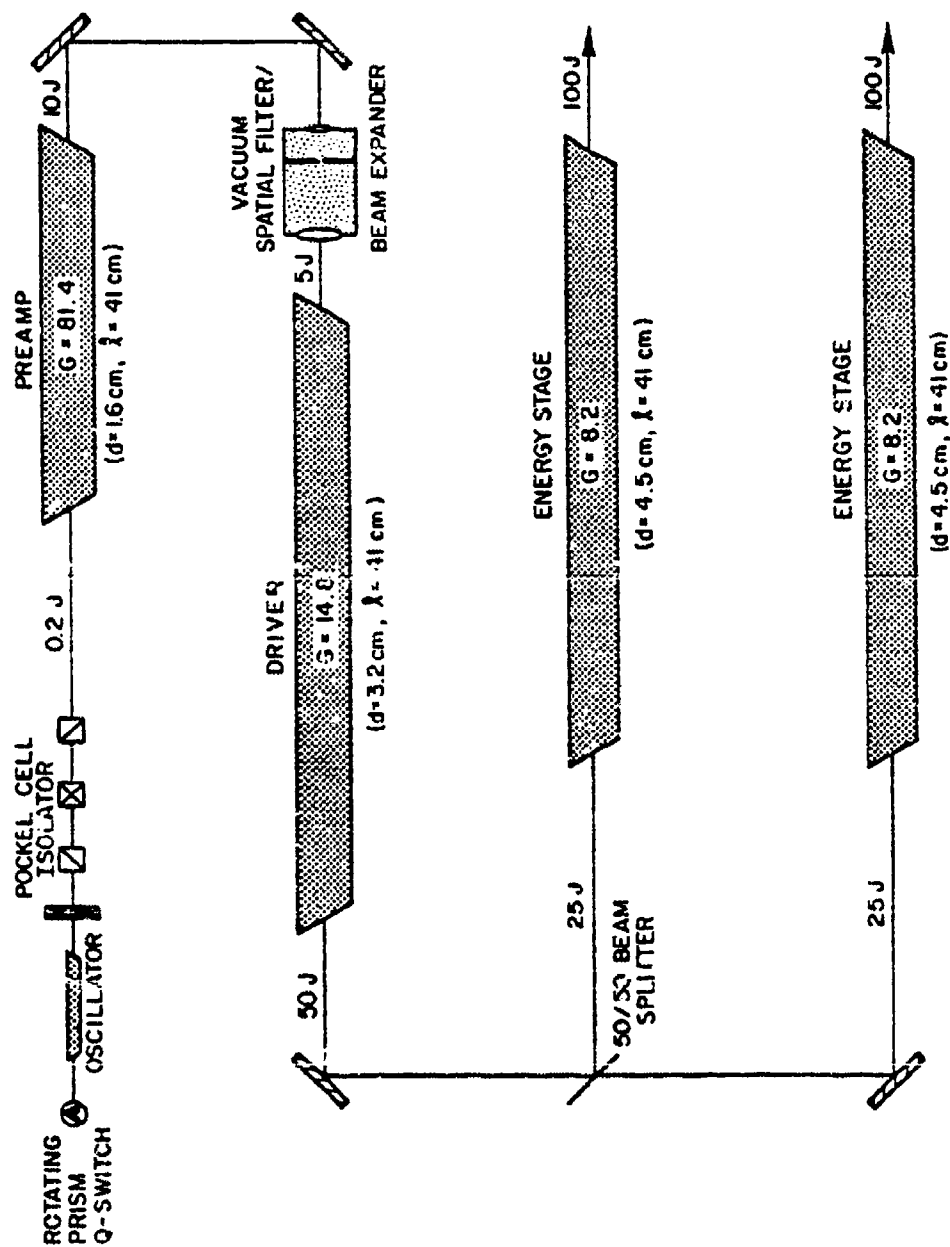


Figure B-4. 30-nsec, 200-J neodymium-glass laser system



TABLE B-1. OPERATIONAL PARAMETERS FOR A 3-D-NANOSECOND-PULSEWIDTH,  
200-J OUTPUT ENERGY ND-GLASS LASER SYSTEM

Parameter	Preamplifier Stage	Driver Stage	Energy Stage
Input Energy (J)	0.2	5	19
Output Energy (J)	10	50	100
Energy Amplification, A	50	10	5.3
Diameter d, (cm)	1.6	3.2	4.5
Length L, (cm)	41	41	41
Input Energy Density, $e_{in}$ ( $J/cm^2$ )	0.09	0.62	1.2
Output Energy Density, $E_{out}$ ( $J/cm^2$ )	5	6.2	6.3
Saturation Energy Densities, ( $J/cm^2$ )	6.2	6.2	6.2
Small Signal Gain, G	31.4	14.8	8.2
Small Signal Gain Coefficient, $g_0$ ( $cm^{-1}$ )	0.107	0.066	0.051
Stored Energy Density, $e_{st}$ ( $J/cm^3$ )	0.67	0.41	0.31
Number of Flashlamps	2	4	4
Capacitor Bank Energy, $E_{cap}$ (kJ)	14	24	24

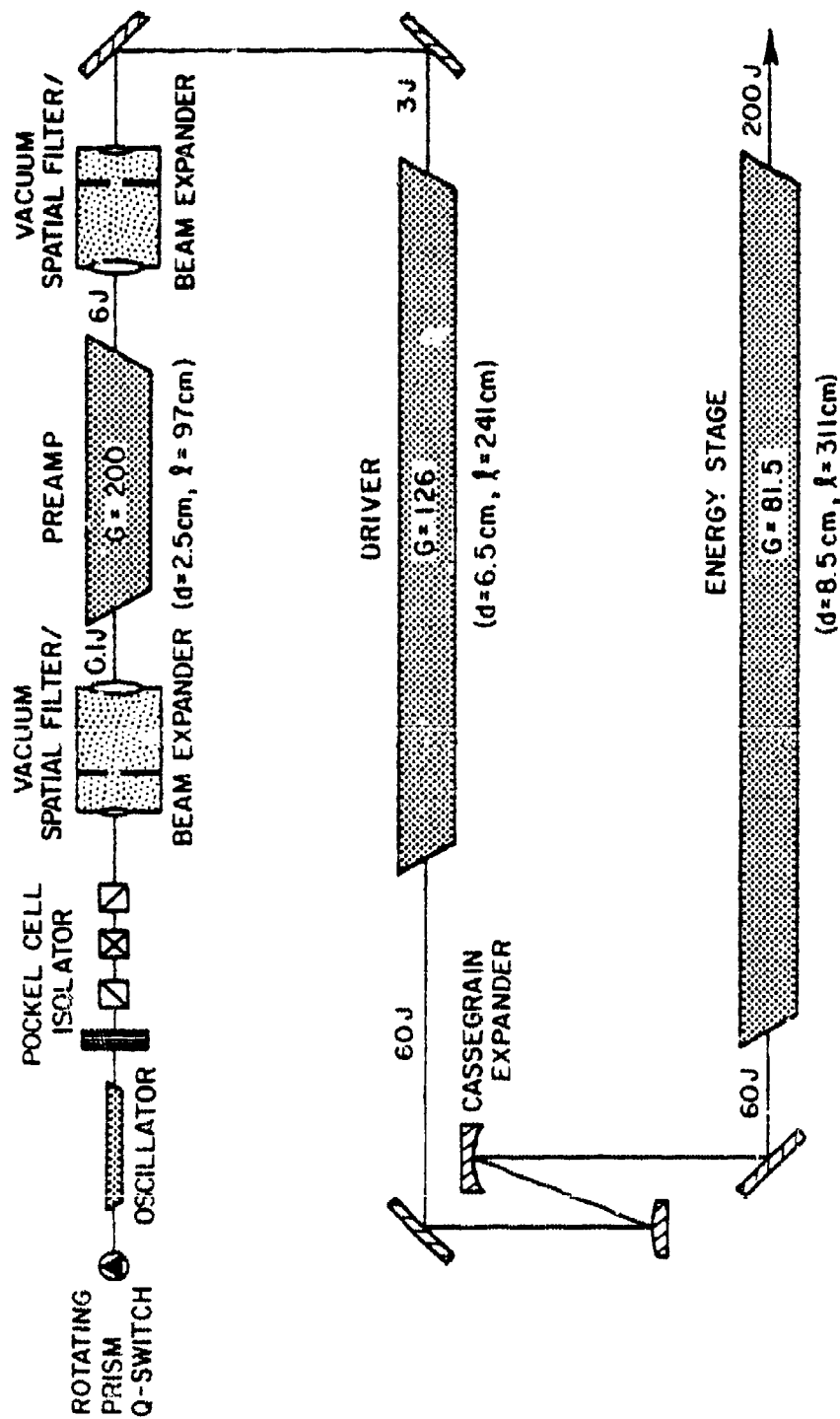


Figure B-5. 30-nsec, 200-J iodine laser system

TABLE B-2. OPERATIONAL PARAMETERS FOR A 30-NOANOSECOND-PULSEWIDTH,  
200-J OUTPUT ENERGY IODINE PHOTODISSOCIATION LASER  
SYSTEM

Parameter	Preamp Stage	Driver Stage	Energy Stage
Input Energy, $E_{in}$ (J)	0.1	3.0	60
Output Energy, $E_{out}$ (J)	1.0	60	200
Energy Amplification, A	10	20	3.33
Diameter, d (cm)	2.5	6.5	8.5
Length, $l$ (cm)	97	241	311
Input Energy Density, $e_{in}$ ( $J/cm^2$ )	0.0204	0.0704	1.06
Output Energy Density, $e_{out}$ ( $J/cm^2$ )	1.22	1.81	3.53
Saturation Energy Density, $e_s$ ( $J/cm^2$ )	0.584	0.584	0.584
Small-Signal Gain, G	200	126	81.5
Small-Signal Gain Coefficient, $g_0$ ( $cm^{-1}$ )	$5.44 \times 10^{-2}$	$2.01 \times 10^{-2}$	$1.42 \times 10^{-2}$
Number of flashlamps placed radially around the laser tube, $N_{amps}$	4	10	12
Total number of Flashlamps, $N_{total}$	8	50	84
Capacitor Bank Energy, $E_{cap}$ (kJ)	2.93	18.30	30.74

at the input aperture of the preamplifier stage. While a number of design interactions were performed to arrive at this system and all design constraints are satisfied, this particular design may not be fully optimized.

#### f. Cost Analysis

Cost estimates for the neodymium-glass and iodine laser hardware were obtained from manufacturers' information where possible and estimated for these components which must be custom built.

A conservative design philosophy was adopted for both systems to allow a large number of laser shots to be taken before part replacement and maintenance were required. For the neodymium-glass laser, lifetime of the laser rods probably is subject to greatest uncertainty. Probably the one item which is subject to greatest uncertainty in the case of the iodine laser is the cost of the chemical regeneration system. Therefore, cost estimates were made for systems with and without chemical regeneration capability. The cost-per-shot analyses for the glass and iodine laser are given in Tables B-3 and B-4.

#### g. Diagnostics and Beam Transport

Regular monitoring of the laser system is required to ensure its operation at the prescribed energy and pulse width conditions. Photodiode detectors placed at the oscillator and each amplifier provide a good method of measuring the shape of the laser pulse. Calibration of these detectors against carbon calorimeter measurements also provide on-line measurements of the energy output of each stage of the laser system. Data generated by these detectors and measurements of flashlamp operating parameters can be fed into a minicomputer for real-time evaluation of system performance. For safety reasons and protection from the surrounding shop floor environment, the laser needs to be packaged in a protective enclosure and the output of the last amplifier directed to the vicinity of the workpiece in a conduit arrangement. A schematic of this setup is shown in Figure B-6. The gas flow shown in Figure B-6 may be required to protect the focusing optic from dust and debris. Another option to protect the lens assembly from target blowoff material might involve impingement of the laser beam at an oblique angle to

TABLE B-3. NEODYMIUM-GLASS LASER COST-PER-SHOT ANALYSIS

Replacement Component or Cost Factor	No. of Units	Unit Cost	Total Cost	(MTBF) <sup>-1</sup>	Cost/ Shot
Flash lamps	10	\$150	\$1,500	10 <sup>6</sup>	\$0.002
Capacitors and Switchgear	100 kJ	\$1000/kJ	\$100,000	5 x 10 <sup>6</sup>	\$0.020
Laser Glass	5	--	\$13,700	5 x 10 <sup>5</sup>	\$0.027
Electricity	92 kJ/shot	\$1.39 x 10 <sup>-5</sup> /kJ <sup>a</sup>	--	--	\$0.001
Depreciation <sup>b</sup>	1	\$234,650	\$234,650	2.6 x 10 <sup>6c</sup>	\$0.090
Maintenance and Operation <sup>d</sup>	64 technician hours	\$25/hr	\$1,600	1.73 x 10 <sup>5</sup>	\$0.09
					\$0.23

<sup>a</sup>Based on a conservative power cost of \$0.050/kwh.<sup>b</sup>Three (3) year straight-line depreciation with no salvage value.<sup>c</sup>System lifetime number of shots based on a 3-year life and an operational duty factor based on 50 weeks per year, 6 days per week, 8 hours per day, and a 0.1-Hz repetition frequency.<sup>d</sup>Maintenance and operations personnel per week of operation.

TABLE B-4. IODINE LASER COST PER SHOT ANALYSIS

Replacement Component or Cost Factor	No. Units	Unit Cost	Total Cost	(MTBF) <sup>-1</sup>	Cost/Shot
Flashlamps	144	\$140	\$ 20,200	$1.0 \times 10^6$	\$0.020
Capacitors and Switchgear	52.70 kJ	\$2,500/kJ	\$131,800	$6.2 \times 10^6$	\$0.021
Lazant:					
I-C <sub>3</sub> F <sub>7</sub> I	$1.06 \times 10^{-3}$ moles/shot	\$300/mole	---	---	\$0.320 (w/o regeneration)
t-C <sub>4</sub> F <sub>9</sub> I	$8.80 \times 10^{-5}$ moles/shot	\$475/mole	---	---	\$0.042 (w/o regeneration)
CF <sub>3</sub> I	0	\$245/mole	---	---	0 (w/ regeneration)
Electricity	66.0 kJ/shot 71.7 kJ/shot	$\$1.39 \times 10^{-5}/\text{kJ}^a$ $\$1.39 \times 10^{-5}/\text{kJ}^a$	---	---	\$0.001 (w/o regeneration) \$0.001 (w/ regeneration)
Depreciation <sup>b</sup>	1 1	\$296,500 \$346,500	\$296,500 \$346,500	$2.59 \times 10^7$ <sup>c</sup> $2.59 \times 10^7$ <sup>c</sup>	\$0.011 (w/o regeneration) \$0.013 (w/ regeneration)
Maintenance and Operation <sup>d</sup>	64 technician/hrs 72 technician/hrs	\$25/hr \$25/hr	\$1,600 \$1,800	$1.73 \times 10^5$ $1.73 \times 10^5$	\$0.009 (w/o regeneration) \$0.010 (w/ regeneration)
					\$0.382 (I-C <sub>3</sub> F <sub>7</sub> I) w/o regeneration \$0.104 (t-C <sub>4</sub> F <sub>9</sub> I) w/o regeneration \$0.065 (CF <sub>3</sub> I) w/ regeneration

<sup>a</sup>Based on a conservative power cost of \$0.050/kwh.<sup>b</sup>Three (3) year straight-line depreciation with no salvage value.<sup>c</sup>System lifetime number of shots based on a 3-year life and an operational duty factor based on 50 weeks per year, 6 days per week, 8 hours per day and a 1.0-Hz for Iodine Laser repetition frequency.<sup>d</sup>Maintenance and operations personnel per week of operation.

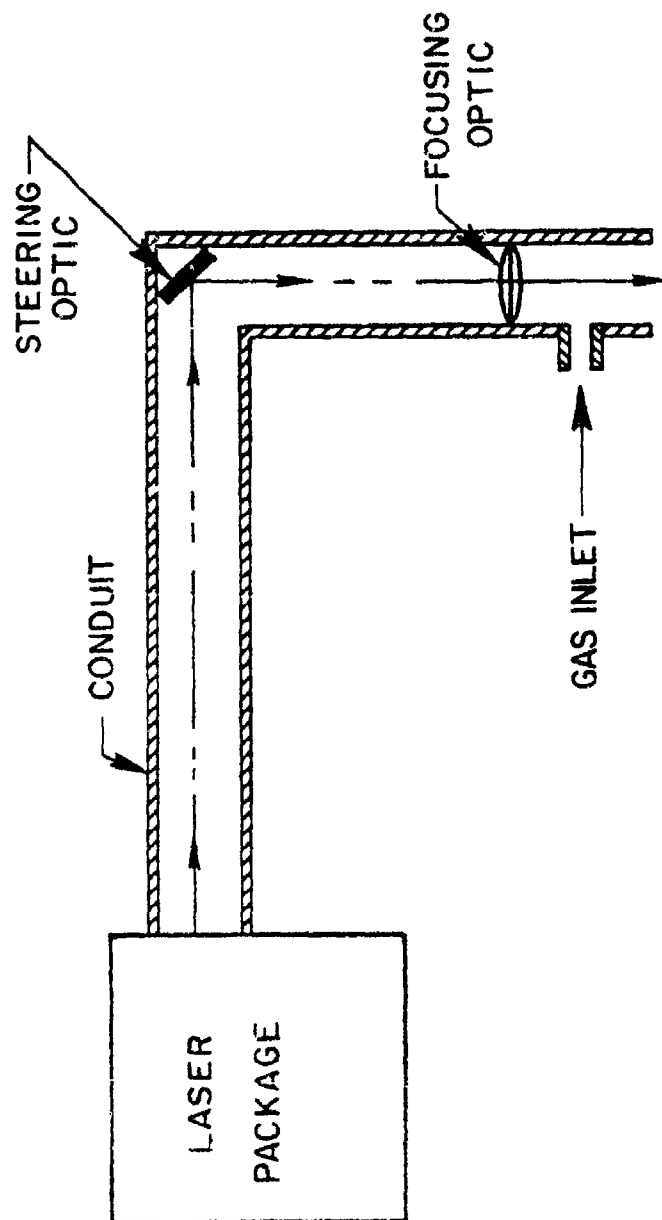


Figure B-6. Beam transport system

the target surface, e.g., the blowoff material will be ejected approximately normal to the surface.

### 3. Environmental Assessment

#### a. Introduction

Implementation of a laser system and its integration into a manufacturing plant requires an assessment of the laser's impact on the environment both at the work site and surrounding area. This evaluation must consider the effects of system operation and interaction of the laser beam with the target. The following environmental assessment includes an evaluation of ozone production from flashlamp discharge, waste chemicals from operation of an iodine laser, material vaporized in laser/target interactions, and noise pollution from interaction of the laser beam with the target.

#### b. Ozone Production

Ozone is produced whenever flashlamps, which are used to pump the laser medium, are discharged. Ozone limits for occupational exposure have been established by the Occupational Safety and Health Administration (OSHA). The threshold limit value which refers to time-weighted concentrations for an 8-hour workday and a 40-hour workweek is 0.1 ppm.

The amount of ozone produced by the neodymium-glass laser from discharge of the flashlamps was measured during laser shock treatment of the aluminum fatigue specimens. This system has a much lower pulse repetition rate than the projected production system, but the laser energy emitted per pulse is approximately the same. Therefore, results of these measurements can be scaled to a production system.

A Mast ozone meter was used to measure the ozone production. This sensor consists of positive displacement air and solution pumps, and coulometric ozone sensor utilizing potassium iodide reagent. Readings were taken during successive laser shots at various distances from the enclosures surrounding the flashlamps and laser rods. Readings a few feet from the enclosures did not exceed about 0.01 ppm. The concentration at which the



odor of ozone becomes noticeable is 0.01 to 0.02 ppm. A slight odor was detected in the monitoring region, thus confirming the meter readings. Readings taken adjacent to the flashlamp enclosure near a vent portal produced ozone concentrations up to 1 ppm.\* These readings provide a measure of the ozone expelled to the surrounding room from the flashlamp enclosure.

The total amount of ozone produced per shot by the laser system was determined to be about 3 ppm. This ozone concentration was contained in a volume of approximately  $2 \times 10^4 \text{ cm}^3$  (the total volume of the flashlamp enclosures). Production laser systems are expected to be pulsed at repetition rates ranging from 0.1 pulse per second up to 1 pulse per second.

Using these numbers, ozone concentrations as a function of time over an 8-hour day were calculated for the case of complete confinement within the flashlamp enclosures and for the case where the ozone is allowed to uniformly mix in a room volume of  $1.4 \times 10^9 \text{ cm}^3$  (100 ft. x 50 ft. x 10 ft). These calculations have neglected to take into account ozone depletion due to chemical reactions with the surrounding environment.

The ozone concentrations are shown in Figures B-7 and B-8. These concentrations can be compared to Figure B-9 which gives maximum concentrations versus time.\*\* Comparison of Figures B-7 and B-8 with Figure B-9 show that the ozone contraction exceeds the 0.1 ppm limit shortly after laser startup except for the lowest pulse repetition rate and uniform dilution situation. In the case where the ozone is confined to the flashlamp enclosures, severe exposure could occur for people located near the laser amplifiers who breathe the effluent gas. In fact, irritation to the eyes and nose will occur at much lower concentrations and therefore, methods to ventilate the ozone or eliminate its production will need to be considered in the design and construction of a production laser system.

Of these two options, elimination of ozone production appears to be a better solution to the problem. This can be done by covering the flashlamps with a gas different from air. Nitrogen is a good choice. This gas

---

\* Largest amplifier in the laser chain.

\*\* These concentrations were established by the American Council of Governmental Industrial Hygienists. The 0.1 ppm limit for continuous exposure (8-hour day) corresponds to the OSHA value.

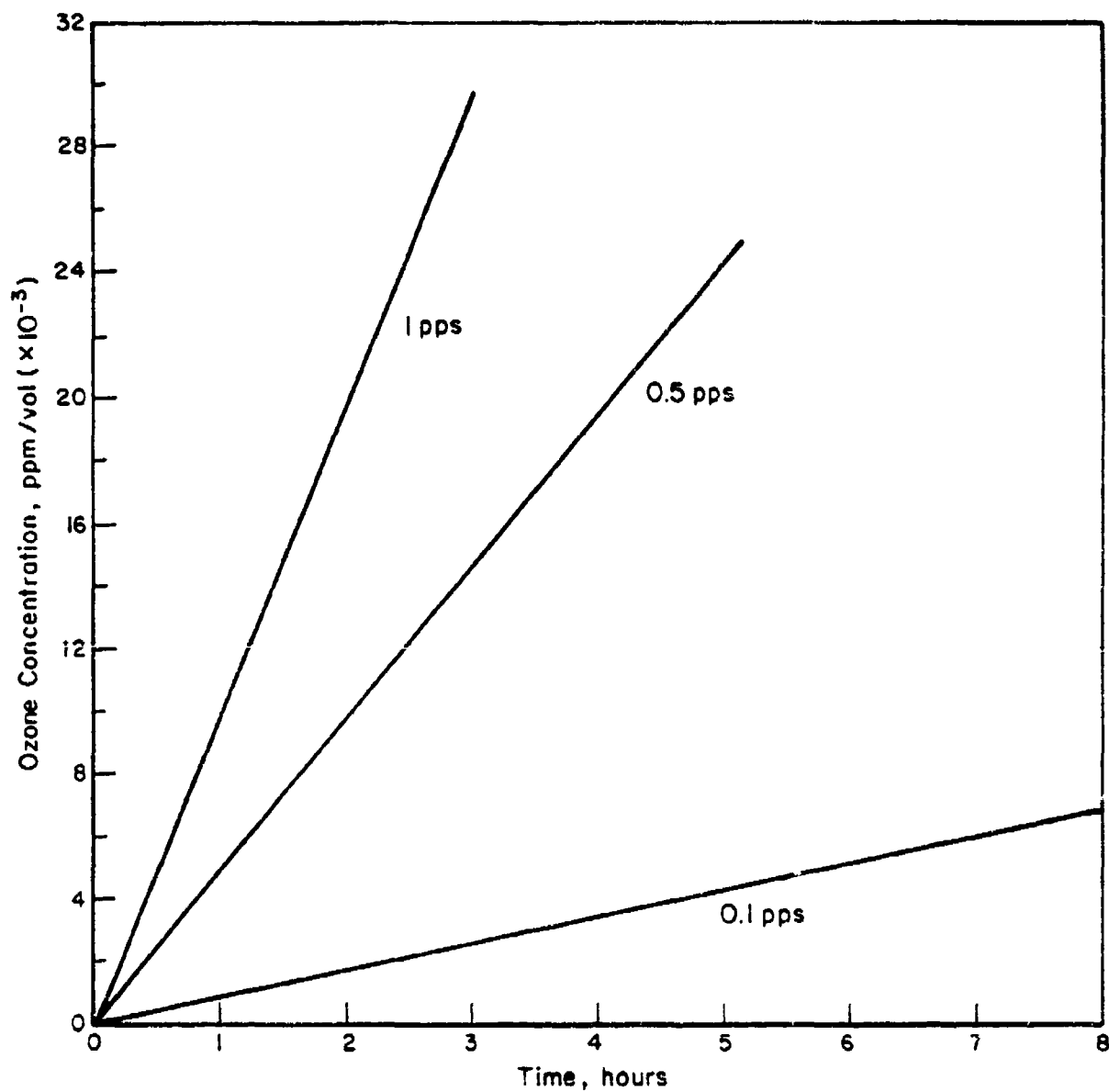


Figure B-7. Ozone concentration as a function of laser repetition rate (ozone confined to flashlamp enclosures)

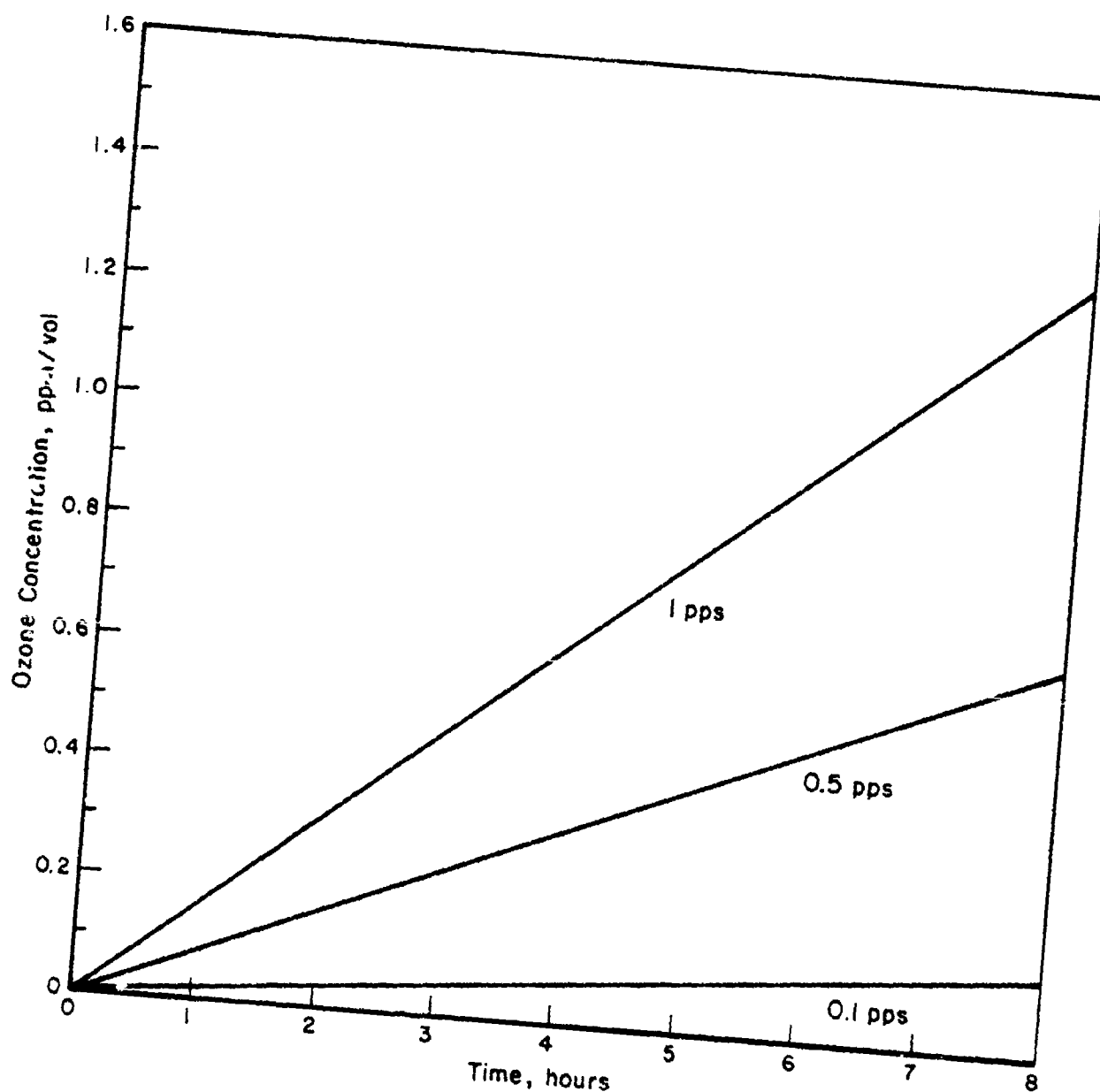


Figure B-8. Ozone concentration as a function of laser repetition rate  
(uniform dilution in 100 ft. x 50 ft. x 10 ft. volume)

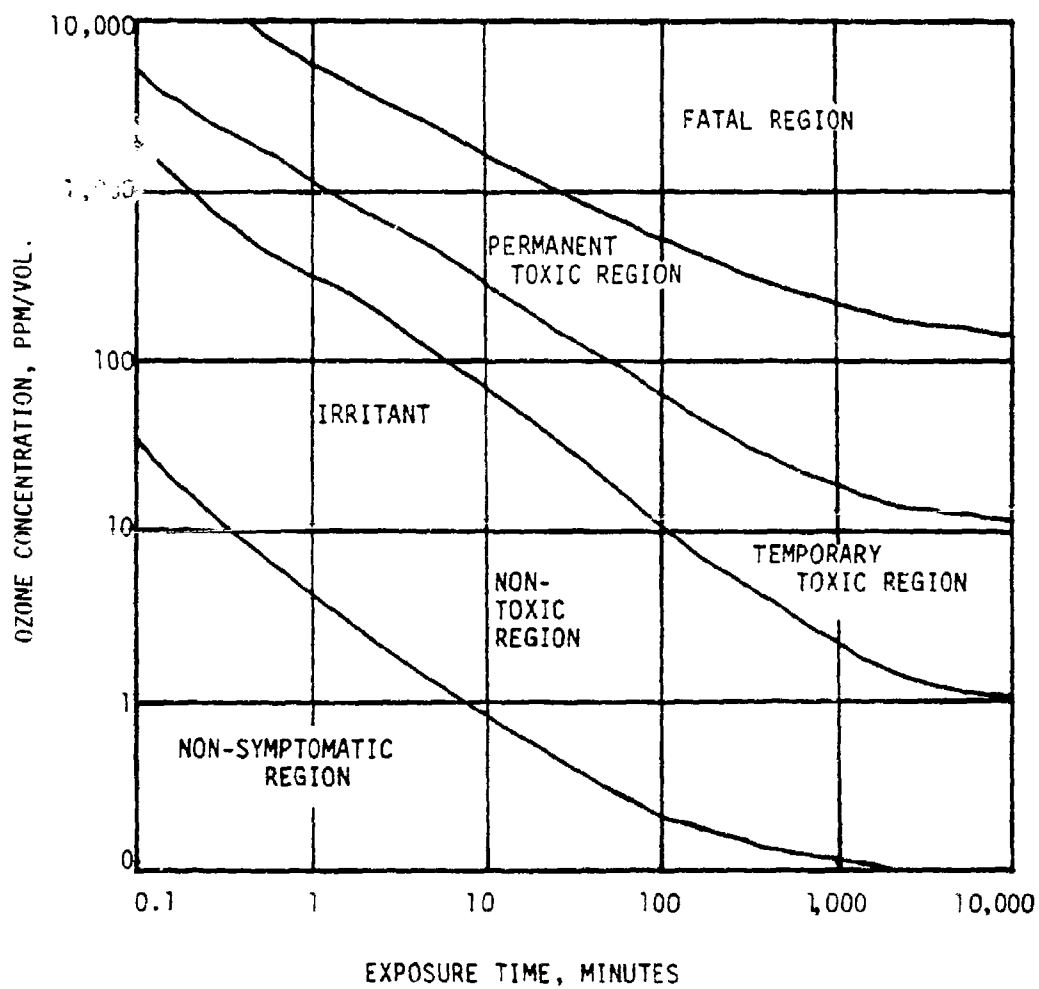


Figure B-9. Toxicity of ozone

could be flowed over the flashlamps at a slight positive pressure. Such a gas flow may be required in any case for flashlamp cooling.

c. Iodine Laser Chemical Wastes

Secondary by-products must be disposed of if a non-regenerative system is chosen. Conceivably, they could be sold rather than simply thrown away. Molecular iodine ( $I_2$ ) is a solid at room temperature and is non-volatile and noncorrosive. Unless ingested, it is nontoxic. The perfluoroalkanes ( $R_2$ ), such as perfluorohexane ( $C_6F_{14}$ ) or perfluorooctane ( $C_8F_{18}$ ), are inert liquids at room temperature and are nonflammable and noncorrosive. Unless significant vapor pressures are present in a poorly ventilated area, they are also nontoxic. Accumulating and storing such chemicals should not present any difficult safety problems. Also, the inventory of  $RI$ ,  $R_2$ , and  $I_2$  in the laser system is low, so that if the system is accidentally vented to the atmosphere, then the danger of excessive occupational dosages is small for properly ventilated working areas.

d. Vaporized Target Material

Target material will be vaporized when the laser beam interacts with the surface of the part being laser-shock processed. In this program and anticipated future production situations, the laser-shocked surfaces will be covered with a thin film of black paint. This paint is typically sprayed onto the surface to a thickness ranging from 8  $\mu m$  to 12  $\mu m$ . Experiments have shown that a few laser shots, e.g. 3, are needed to completely vaporize this coating thickness. Therefore, on the average, approximately 3.3  $\mu m$  of paint is vaporized in a single laser shot. The diameter of the laser-treated region in a typical production situation is expected to be about 0.5 inch. Therefore, the volume of paint vaporized in a single laser shot is  $4.3 \times 10^{-4} \text{ cm}^3$ . Since two surfaces may be shocked in a single treatment, the volume of paint may be twice this value. In terms of mass of vaporized material ( $\sim 0.5 \text{ gm/cm}^3$ ), this amounts to  $4.3 \times 10^{-4} \text{ gm}$ . The number of vaporized molecules can be found by multiplying by Avodadro's number divided by the molecular weight. Unfortunately, the vaporized material is a

complicated mixture of chemicals with an unknown molecular weight. A major fraction of the vaporized material, however, will appear as different types of hydrocarbons whose molecular weight is not expected to be much greater than 10. If this number is used, the number of molecules of vaporized material per laser shot is  $2.5 \times 10^{19}$ .

Consider two situations, one where the vaporized material is confined to the adjacent area around the interaction zone, e.g., a volume of about 3 ft. x 3 ft. x 3 ft. or  $7.6 \times 10^5 \text{ cm}^3$ , and the other where the vaporized material is uniformly dispersed in the room volume (100 ft. x 50 ft. x 10 ft. =  $1.4 \times 10^9 \text{ cm}^3$ ). For these two cases, the number of molecules of vaporized material produced per  $\text{cm}^3$  per laser shot is  $3.3 \times 10^{13}$  and  $1.8 \times 10^{10}$  respectively. The concentration of vaporized material in ppm is found by dividing these numbers by the number of molecular of air per  $\text{cm}^3$ . The resultant concentrations are 82.5 and 0.045 ppm per laser shot.

The threshold limit value (TLV) of the vaporized paint is based on the assumption that the vaporized products are moderately toxic. The TLV for moderately toxic materials fall in the range from 100 ppm to 500 ppm. The buildup in concentration of the vaporized products as a function of time is shown in Figures B-10 and B-11 for different laser shot repetition rates.

As seen from these curves, a worker stationed near the laser interaction zone could be exposed to toxic levels of vaporized material after as little as a few laser shots. Of course, significant diffusion of the vaporized products away from the interaction zone will occur as a function of time; however, prolonged exposure, e.g., greater than several minutes, by a worker located near the experimental site would not be advisable without proper ventilation or use of a protective device.

Proper ventilation appears to offer the best solution to the problem. In a manufacturing setup, the laser beam probably will be directed to the vicinity of the workpiece in a conduit-type enclosure to avoid worker interaction with the beam. This could be combined with a hood arrangement to exhaust the vapors formed during the laser shock treatment.

#### e. Noise Pollution

Significant increases in background noise levels are produced from interaction of the laser beam with the target surface. A decibel meter

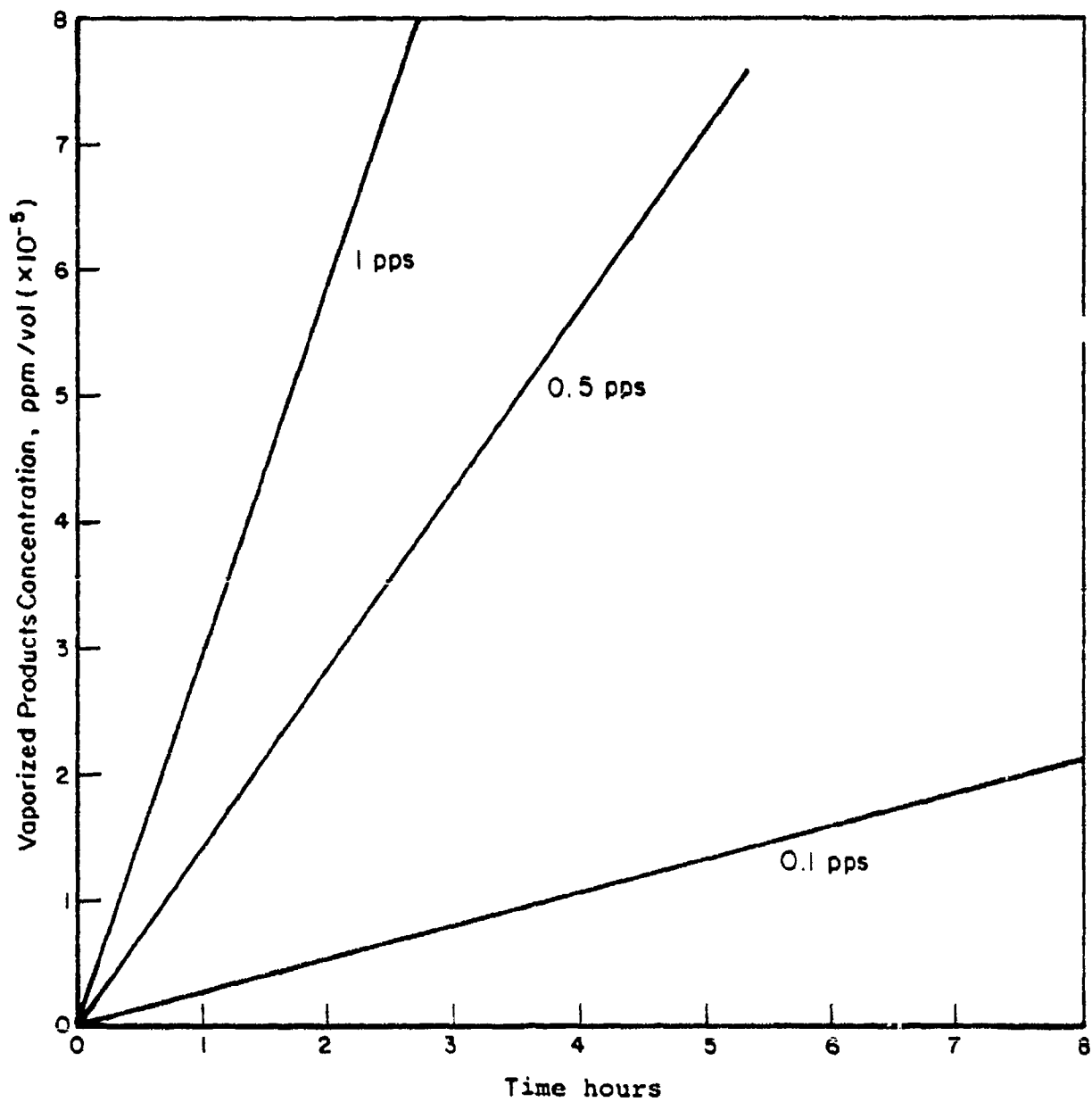


Figure B-10. Concentration of vaporized products as a function of laser repetition rate (material confined to interaction zone)

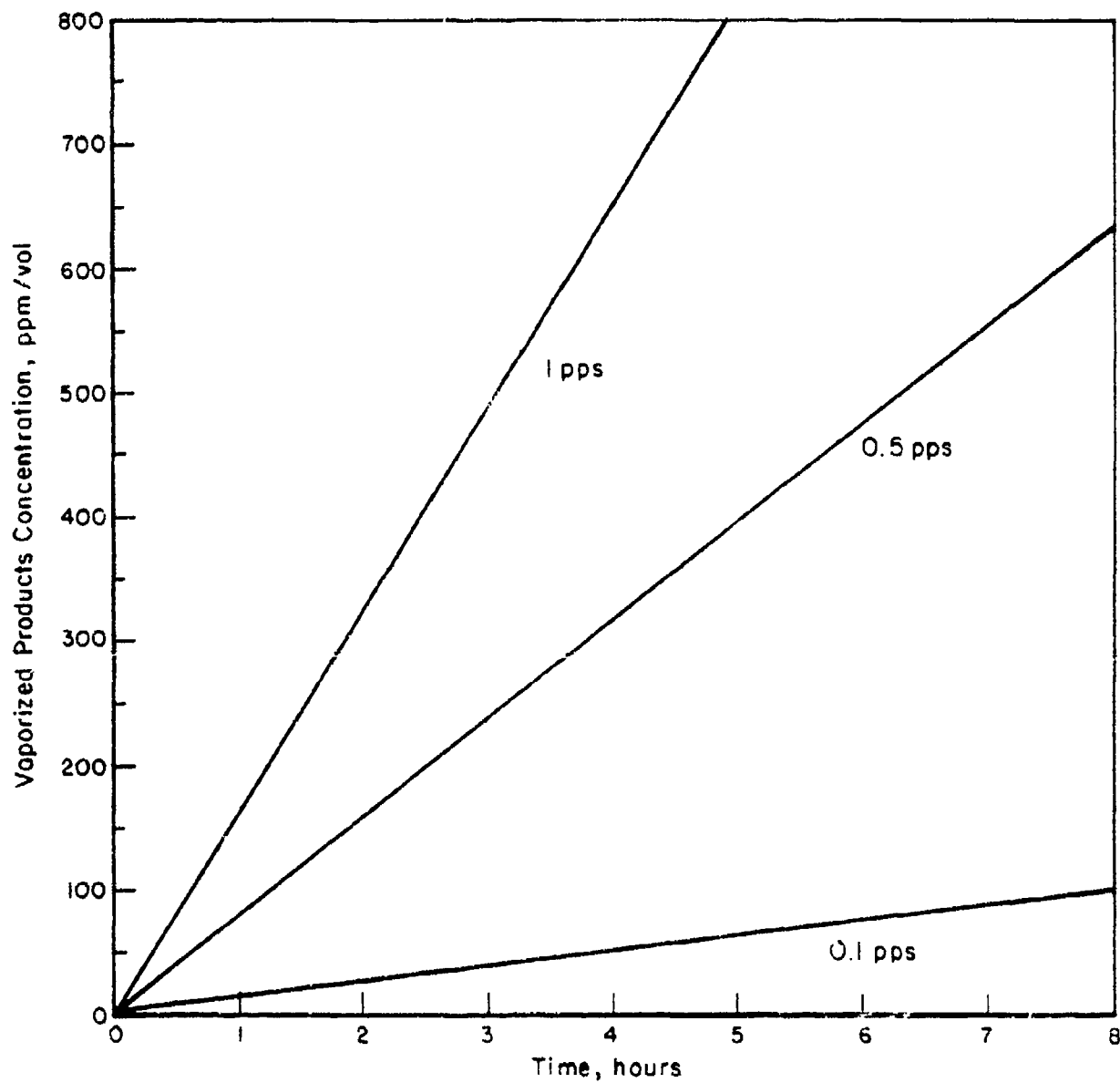


Figure B-11. Concentration of vaporized products as a function of laser repetition rate (uniform dilution in room)



was used to measure the impulsive increases in noise levels produced at various distances from the interaction site. Maximum decibel readings ranging from 100 db to 110 db were measured approximately two feet away from the source. These measurements were made without any intervening obstacles between the source and detector.

The threshold limit values for impulsive sources of sound vary according to the number of impacts per day. The maximum number of laser pulses per second for a production system probably will not exceed 1 pps for an 8-hour day; this gives 28,800 laser pulses or sound impacts per day. Based on data provided by the American Conference of Governmental Industrial Hygienists, the TLV for these number of impacts approaches the 110 db reading taken near the laser target. For this reason, some type of sound mitigating device probably will need to be incorporated in the design and construction of a production laser system. Such a device could be combined with the system that will be used to vent the harmful vapors formed during laser interaction with the workpiece. For example, the hood arrangement which is located adjacent to the target surface could contain sound-absorbing materials.

# REFERENCES

1. Fairand, B. P., Wilcox, B. A., Gallaher, W. J. and Williams, D. N., J. Appl. Phys., 43, 3893 (1972).
2. Fairand, B. P., Clauer, A. H., Jung, R. G. and Wilcox, B. A., Appl. Phys. Lett., 25, 431 (1974).
3. Clauer, A. H., Fairand, B. P. and Wilcox, B. A., Met. Trans. A., 8A, 1871 (1977).
4. Clauer, A. H., Fairand, B. P. and Wilcox, B. A., Met. Trans. A., 8A, 119 (1977).
5. Potter, J. M., Stewart, R. P. and Adams, F. D., "Evaluation of Fatigue Rated Fastener Systems; Constant Amplitude Fatigue Test Results", AFFDL TM 77-75-FBE, November, 1977.
6. "Residual Stress Measurements by X-Ray Diffraction", X-Ray Division of the SAE Fatigue Design and Evaluation Committee, Society of Automotive Engineers, Inc., SAE J784a, New York (1971).
7. Prevey, P. S., "A Method of Determining the Elastic Properties of Alloys in Selected Crystallographic Directions for X-ray Analysis", Vol. 20, pp 345-354 (1977).
8. Broek, David, "Elementary Engineering Fracture Mechanics", Noordhoff International Publishing, p 76 (1974).
9. Irwin, G. R., "The Crack Extension Force for a Part-Through Crack in a Plate", Trans. ASME, J. Appl. Mech., pp 651-654 (1962).
10. Fairand, B. P. and Clauer, A. H., J. Appl. Phys., 50, 1497 (1979).